An Assessment of CONTAIN 2.0:
A Focus on Containment Thermal Hydraulics (Including Hydrogen Distributions)

Jack Tills[1], Allen Notafrancesco[2], and Ken Murata[3]

July 2002

Office of
Nuclear Regulatory Research

SAFETY MARGINS AND SYSTEM ANALYSIS BRANCH

[1] Jack Tills & Associates, Inc.

[2] USNRC, Office of Nuclear Regulatory Research

[3] Sandia National Laboratories, Modeling and Analysis Department, Org. 6421

SMSAB-02-02

An Assessment of CONTAIN 2.0: A Focus on Containment Thermal Hydraulics (Including Hydrogen Distributions)

Jack Tills[1], Allen Notafrancesco[2], and Ken Murata[3]

July 2002

[1] Jack Tills & Associates, Inc.

[2] USNRC, Office of Nuclear Regulatory Research

[3] Sandia National Laboratories, Modeling and Analysis Department, Org. 6421

An Assessment of CONTAIN 2.0:
A Focus on Containment Thermal Hydraulics
(Including Hydrogen Distributions)

1 Introduction

2 Phenomena

2.1 Containment Phenomena Identification

2.1.1 Components

2.1.2 Processes

2.1.3 Phenomena

2.1.3.1 Phenomena Identification for the Atmosphere Component

2.1.3.2 Phenomena Identification for the Structure Component

2.1.3.3 Phenomena Identification for the Pool Component

2.2 Containment Phenomena Ranking

2.2.1 Accident Scenario and Phase Definition

2.2.2 Ranking Criteria

2.2.3 Ranking Components and Phenomena Importance

2.2.4 Phenomena Identification and Ranking Table (PIRT)

2.2.5 Implications of Rankings

3 Code Assessment Activities [Reference Studies]

3.1 Background

3.2 Facility and Test Scaling

3.2.1 Geometric Scaling

3.2.2 Blowdown Rate Scaling

3.3.3 Spray Injection Scaling

3.3 Reference Calculations

3.3.1 Separate Effects

3.3.1.1 Wisconsin Flat Plate Condensation Tests

3.3.1.2 Phebus Test FPT0

3.3.1.3 JAERI Pressure Suppression Spray Tests

3.3.2 Integral Effects (Thermal Hydraulics and Hydrogen Distributions)

3.3.2.1 HDR Tests

3.3.2.1.1 V44 [ISP-16]

3.3.2.1.2 T31.5 [ISP-23]

3.3.2.1.3 T31.5 (Project HDR Benchmark)

3.3.2.1.4 E11.2 [ISP-29]

3.3.2.1.5 E11.4 (Project HDR Benchmark)

3.3.2.6 CVTR

3.3.2.6.1 Test #3 (no sprays)

3.3.2.6.2 Tests #4 and #5 (sprays)

3.3.2.7 NUPEC Tests
3.3.2.7.1 M-7-1 [ISP-35] and M-8-2
(Hydrogen distribution with sprays)
3.3.2.7.2 M-4-3 and M-8-1
(Hydrogen distribution without sprays)

4 Code Assessment Activities [Sensitivity Studies]
4.1 Separate Effects
4.1.1 Wisconsin Flat Plate Condensation Tests
4.1.2 Phebus Test FPT0
4.1.3 JAERI Pressure Suppression Spray Tests
4.2 Integral Effects
4.2.1 HDR Tests
4.2.1.1 HDR Test V44 [ISP-16]
4.2.1.1.1 Maximum Pressure
4.2.1.1.2 Subcompartment Analysis
4.2.1.2 HDR Test T31.5 [ISP-23]
4.2.1.2.1 Maximum Pressure
4.2.1.2.2 Subcompartment Analysis
4.2.1.3 HDR Test T31.5 (Project HDR Benchmark)
4.2.1.4 HDR Test E11.2 [ISP-29]
4.2.1.5 HDR Test E11.4 (Project HDR Benchmark)
4.2.2 CVTR Test #3
4.2.3 NUPEC Tests
4.2.3.1 M-8-1 (mid-elevation injection, no sprays)
4.2.3.2 M-7-1 (mid-elevation injection, with sprays)

5 Summary of Findings and Conclusions
5.1 Phenomena
5.2 Reference Calculations
5.3 Sensitivity Calculations
5.4 User Guidelines and Implications for Plant Analyses

6 References

Appendix A: Listings of Reference CONTAIN Input Files

[Electronic Storage Disk]

Acknowledgment

Thanks to Dr. K. Campe (USNRC/NRR) for his helpful suggestions and editorial comments on the report manuscript.

1 Introduction

This report documents work carried out to assess the CONTAIN 2.0 code for predicting thermal hydraulic conditions and hydrogen distributions within a reactor containment building during a postulated accident event. The information provided is for code validation purposes which is separate from other efforts that focus on code quality assurance and verification through the use of standard test problems.

The CONTAIN code is a thermal hydraulics code that is based on the lumped parameter formulation for the integrated analysis of containment phenomena. CONTAIN was developed at Sandia National Laboratories (SNL) under the sponsorship of the United States Nuclear Regulatory Commission (USNRC) and is documented in a recently released code manual [Mur97]. To the extent practical, CONTAIN is an ex-vessel systems level code which has been developed using a physics-based modeling approach consistent within a lumped parameter framework. Accordingly, user-defined parameters are minimized, however, the code does include optional settings that allow the user to perform sensitivity studies of key models.

It should be noted that an extensive peer review of the CONTAIN code has been completed [Boy95], and the findings of that review were extremely positive. The review by six technical experts found that the CONTAIN code was very close to fulfilling all of its design objectives that enable the code to be used for its targeted applications. These applications include support for containment-related experiments, light water and advanced light water reactor plant analysis, and other issue resolutions related to containment integrity during postulated accident events, such as hydrogen combustion. In this regard, the peer reviewers determined that the code has modeling detail for key important phenomena anticipated to be present in plant accidents, provides reasonable predictions of containment transients, applies to various accident sequences for pressurized water reactors (PWR) and boiling water reactors (BWR), performs in a robust, portable, and fast running manner, and follows accepted quality assurance (QA) standards for NRC codes. This achievement was highlighted as a "significant accomplishment" for the code project.

The assessment presented in this report is based on relevant containment thermal hydraulic and hydrogen distribution experimental programs which include both separate and integral effects testing. Overall, the report demonstrates the adequacy of CONTAIN to predict pressure and regional temperature (and gas concentrations) response in a containment during accident conditions. This report complements earlier code assessments through the use of the latest code version, and by the inclusion of a number of new assessments.

To help focus this effort, containment phenomena are discussed in Section 2 using a Phenomena Identification and Ranking Table (PIRT) formalism. In this section, general accident sequences for beyond design (limited degraded core events which produces copious amounts of hydrogen)

and design basis accidents (typically a selective large pipe break inside containment) are discussed, and the criteria for ranking phenomena are outlined. The PIRT methodology is used here in a generic sense to categorize containment related phenomena.

Topics concerning code assessment are presented in Section 3, where analytical simulation models are described. Specific models for phenomena ranked as highly important are covered in subsequent validation discussions that concentrate on issues of applicability and reliability related to code modeling and performance. In this section, separate effects and integral effects experiments are cross-referenced to the highly ranked phenomena defined in Section 2, showing the completeness of the experiments with respect to measurement requirements and usefulness for evaluating the performance of the CONTAIN code. Integral testing facilities are described in this section and the scaling aspects of the facilities and test procedures are reviewed. The main body of the section provides a detailed discussion of reference input decks and model results for each of the 20 experiments on which assessments are based. In all cases, key model results are compared to experimental measurements.

Since there are uncertainties associated with every analytical simulation of a facility and experiment, Section 4 provides sensitivity case studies for selected tests analyzed previously with referenced inputs. These sensitivity cases are used to investigate the effects of uncertainties arising from code models, user knowledge, and experimental boundary conditions. The studies are helpful in establishing an in-depth understanding of the variability and integral aspects of process modeling in the simulation of containment accidents. Section 5 summarizes the findings of the reference and sensitivity studies, and provides some concluding remarks regarding implications for full plant analyses. Finally, listings of all the reference input decks are provided in Appendix A for archival purposes and to give users guidance on constructing various types of CONTAIN input.

2 Phenomena

An assessment of containment thermal hydraulic modeling is required to assure that codes like the CONTAIN code can be applied in an accurate, and also, conservative manner for confirmative safety analyses. Such an assessment relies heavily on experimental programs to investigate a spectrum of possible accident progressions and containment behavior. The purpose of a phenomena listing and ranking in this context is to provide guidance to the assessment so that the most important phenomena associated with events that may lead to conditions (pressure, temperature, and hydrogen concentration) beyond design or regulatory limits are adequately and appropriately considered, and to assure that the experimental programs have provided the necessary data on which to base the assessment. With an emphasis on containment, the accident types considered are those low-probability accidents that include design basis accidents (DBAs) and those beyond DBAs where some core damage is assumed resulting in generation and release of hydrogen. In such accidents, the design limits and the potential for a combustion event become two of the criteria for judging the integrity of the containment. This section reviews phenomena important to the assessment of containment loads and hydrogen distribution during critical times where design and regulatory limits are nearly approached. The discussion is abbreviated yet focused on those phenomena that need to be understood (experiments) and predicted (codes) in order to assess the severity of containment loadings. Although the general discussion is applicable to all types of containments (PWR and BWR, or the more recent advanced light water reactor (ALWR) types), emphasis is placed on the most common type, the large dry PWR containment.

Postulated accidents are impractical to test in full-scale containments. Therefore, computer codes must be used to evaluate loads and containment function. To assure the validity of these codes, the NRC has adopted an evaluation methodology to demonstrate code scalability, accuracy, and uncertainty [Boy90]. One feature in this evaluation method is the concept of a PIRT (phenomena identification and ranking table). The PIRT functions both as a resource management tool and as a formal procedural method that prioritizes engineering tasks. All PIRTs have a common basis which is to address plant behavior in the context of identifying the relative importance of systems, components, processes and phenomena driving the plant performance. We have adopted the PIRT-like formalism here as an organizational tool to help us present our state of knowledge and code assessment for the more important containment phenomena affecting thermal hydraulics and gas/vapor distribution. This section presents a general containment phenomena identification table that applies for most plant types. The PIRT discussed, however, is **illustrative** with the ranking of phenomena limited to one of the more common types of containments, the PWR large dry containment. Many of the table results are transferable to other plant types though with limited modifications.

The conceptual use of the PIRT, adapted from Wil96, is shown in Figure 2.1. Although containment performance is the historical basis for the PIRT development, there are three adjunct

functions that reflect how we can make use of the methodology in our code assessment effort. The adjunct objectives are to provide guidance is establishing the requirements in:

1) Separate and Integral Effects (SET, IET) experimental programs, where the objective is to help insure the experimental data fully reflect what may be expected in the containment,

2) Code development and improvement, where the objective is to help insure the code is capable of modeling the containment behavior, and

3) Code uncertainty quantification, where the objective is to help insure the various contributors to uncertainty are identified and treated in a manner appropriate to their importance to containment behavior and, thus, to the overall uncertainty.

The accomplishment of each objective is addressed in this report. Beginning with the first objective, a table listing important phenomena represented and measured in various experimental programs is given in Section 3. Those experiments are included here as the database for code assessment, which according to the second objective – the assessment focuses mainly on high importance phenomenon. Finally, critical uncertainties derived from experimental and analytical experiences are considered in Section 4.

In this section, the phenomena identification table for a containment is presented in detail and then extended to include ranking. The ranking criteria are derived from the basic regulatory requirements that limit maximum pressure, temperature, and hydrogen concentration. The process of ranking is by expert judgment and engineering experience. Most of the experience has been obtained in observation of experiments, in studies performed to analyze experiments, and in projects involving plant specific design and severe accident analyses. These analyses have included baseline and sensitivity calculations.

2.1 Containment Phenomena Identification

To establish a strong linkage between an experimental program, code validation, and containment accident analyses, it is important that we identify and assign importance to various phenomena occurring within the containment. Phenomena is defined to include all potentially dominant processes, events, and characteristics involving containment components (atmosphere, structures, and pools). Once the identification process has been accomplished, criteria are established based on a set of regulatory requirements (i.e., pressure, temperature, and concentration limits) and used to rank the importance of each phenomenon. The ranking helps researchers focus their experimental and code validation programs in what has been called an efficient and sufficient manner [Wil96]. The purpose of this section is to first identify and describe various containment phenomena taking place during a design basis and beyond design basis accident. In the following section, a ranking of the phenomena is provided for an accident scenario that poses a potentially high risk to containment integrity by exceeding containment load limits and/or hydrogen concentration. The ranking table is developed as an illustrative example, where it is also assumed that the accident will be initiated by a LOCA in a PWR containment. Other plant types, such as BWRs, will include phenomena that will vary only slightly from those listed.

Phenomena identified in this report do include phenomena associated with typical pressure suppression techniques such as sprays and fan coolers. Ice condenser phenomena are listed but these plants are not covered in this report. Combustion events (diffusion flames, deflagrations, and detonations) are not considered - although it is recognized that such events may affect the behavior of gas distributions within the containment and maximum containment loads. In the context of design basis and beyond design basis analyses, combustion events are neglected here.

The identification process proceeds without reference to the CONTAIN code or modeling capability; rather, the identification effort draws on a physical interpretation of processes that are judged to occur in current and advanced light water plants during postulated reactor accidents.

In order to provide some structure to the discussion of key phenomena and to eliminate redundant entries in the identification table, phenomena are grouped by containment component and process - these are the first two columns in the "generic" phenomena identification table presented as Table 2.1. The definition of these components and the description of the processes and phenomena are discussed in the following subsections.

2.1.1 Components

A component is a generalized type of geometry and composition that encompasses a broad grouping of phenomena. A component is distinguished by a volume with a general type of physical composition and its boundaries (surfaces) across which the exchange of mass and energy occurs between volumes. The general composition classes within the containment are gases, liquids, and solids. Energy and mass exchanges may take place within a volume (as a source or sink or as exchanges between the constituents within a volume), at the surfaces between volumes, or between the depth of a volume and a surface or the depth of another volume (emitting or absorbing thermal and gamma radiation).

There are three key components in a PWR dry containment: atmosphere, structure, and pool. All containment codes have models to represent these basic components, and most of the experimental and validation efforts described in this report investigate phenomena associated with these components. Usually, describing an atmosphere refers to a region inside the containment building; however, it can also refer to the normal earth atmosphere external to the containment. The constituents of an atmosphere are predominantly gases, although two-phase mixtures, liquid droplets, and solid particles may be present during a transient. The constituents of a pool are predominantly liquids, although two-phase mixtures, gas bubbles and solid particles may be present during a transient. In certain cases one component may transform into another component; for example, water runs onto a structure (dry floor) forming a pool, or a pool is drained away leaving a structure.

The three key components are defined as follows:

* Atmosphere. The open volume or free flow volume for gases. It excludes an existing pool of water or a pool of water that may form during an accident.

* Structure. A solid material which communicates with the containment atmosphere or pool through a surface. It may be an exterior wall or floor which forms the containment system boundary, an interior wall which divides the containment into subcompartments or otherwise forms a barrier to flow of gases, and another solid barrier which consumes interior space, such as a pipe or other fixture.

* Pool. A volume of water which lies on a floor.

Communication between components is through their surfaces. A surface is an interface between the containment atmosphere and a structure, between the containment atmosphere and a pool or between a pool and a structure. A surface includes the boundary layers of air and of water which condenses on a solid surface, through which heat and mass transfer occur.

Note that the reactor coolant system (RCS) is not a component in a containment but forms a

boundary condition for the containment. A break in the RCS during a LOCA is the major source of water and hydrogen flowing into the containment during an accident.

All containment codes have models to represent these basic components, and most of the experimental and validation efforts described in this report investigate phenomena associated with these components. When all the components are designed into an experimental program, the testing program is considered to be integral. Tests limited to one component (or phenomenon within a component) are generally referred to as separate effects tests. In the phenomena identification listing shown in Table 2.1, the components are listed in the first column.

2.1.2 Processes

Phenomena can be further classified by the main processes occurring within the containment. In the second column of Table 2.1, five categories of processes are defined:

1. pressurization/depressurization
2. mixing,
3. transport,
4. heat transfer, and
5. mass transfer.

Pressurization is the process where the atmosphere pressure changes by means other than as a result of energy or mass exchange with structures or pools. In this process the atmospheric boundaries are considered adiabatic. Rapid blowdowns into the containment are an example of a pressurization process. Depressurization can occur during the expansion of gases when the containment boundary is breached. Such a condition may be the result of a planned action, in the case of containment venting schemes, or the result of structural failure. Additionally, depressurization can also take place as a result of some exchange taking place within the atmosphere, as in the case of energy and mass exchange with containment sprays.

Mixing is a process where separate fluids with distinguishable characteristics tend to come together to form a fluid with a single characteristic. Mixing is an intra-compartment process, whereas transport is an inter-compartment process. Mixing includes all phenomena that affect the mixing process occurring within a single open compartment or room. The characteristics can be temperature or constituent concentration. For instance, when hydrogen is injected into a mixture of air and steam, the incoming gas stream mixes with the surrounding atmosphere. If the mixing process proceeds to completion, a uniform composition of hydrogen, air, and steam will be created. However, in many cases the mixing process is incomplete for a substantial time period and during this time period the atmosphere is considered to be in an unmixed state. If mixing does not proceed to completion, but flow stagnates, then a stratified condition will be created.

Transport is a process where fluids or aerosols move from one defined region to another. Transport usually refers to movement between compartments, such as convection loops that develop between a series of coupled compartments or the flow of liquids between various compartments. Transport may occur between components within a compartment, such as between pools or from structures to pools. And, transport may also occur on a single component, as in the case of the flow of liquids along walls.

The most commonly investigated processes within containments are heat and mass transfer. These exchange processes take place both within and at the boundaries of components. For a solid component the interior process is conduction. For a fluid component the interior processes

usually are convection, but can include conduction and diffusion under certain circumstances. Aerosols and sprays can exchange energy and mass with the atmosphere through evaporation or condensation or through sensible heat transfer; however, since aerosols and sprays are considered part of the atmosphere, these exchanges are grouped under the pressurization/depressurization process. Condensation and evaporation also are important processes at the interface between the atmosphere and the other components: structure and pool. Condensation and evaporation are classified as a combination of mass and latent energy transfer processes. The exchange of energy without an accompanying exchange of mass is classified as a sensible energy transfer process.

2.1.3 Phenomena

In many physical processes, a number of phenomena can be involved. Therefore, dissection of a process, like mixing, will indicate an overlapping of various phenomena where boundaries are difficult to distinguish; however, each process can usually be identified, and in most situations observations of the process can reveal one or two phenomenon that dominate. As previously noted, the phenomenon definition is a broad one that includes characteristics and events as well as phenomenological processes. Also, it should be realized that the chosen level of detail used in identifying phenomena associated with a process will often be a judgment based on our current ability to differentiate phenomenon with the instrumentation commonly found in both integral and separate effects testing, in fundamental experiments, and according to the details of the modeling. (Tests limited to specific, local phenomena are called fundamental experiments.)

Phenomena can be characterized by reference to safety equipment or a device if the phenomena are specific to that equipment and not otherwise described in a process group. For example, fan cooling/dynamics, spray mass and energy exchange, and spray dynamics are phenomena specifically associated with safety equipment and not considered in other basic phenomena descriptions.

In the last column of Table 2.1 are listed the phenomena that affect containment thermal hydraulics and hydrogen gas distributions, grouped according to containment component and process. In the following subsections these phenomena are described.

2.1.3.1 Phenomena Identification for the Atmosphere Component

Pressurization/Depressurization

Multi-component gas compression/expansion

This phenomenon describes the physical behavior of compressible gas mixtures. It can be quantified through application of the energy equation and equation of state for gas mixtures. The

phenomenon applies to a homogeneous mixture that is undergoing pressurization or depressurization primarily as a result of large additions or removal of single- or two-phase fluids. For example, in the case of a rapid blowdown of superheated steam into a single volume compartment, pressure and temperature are typically determined mainly through the accommodation of the injected gas mixture within the volume. Likewise, rapid depressurization of a containment due to catastrophic containment failure or venting will be determined by the phenomenon of gas depressurization as a result of an expansion processes. Since the atmospheric gas mixture can be two-phase, the phenomenon can also include the bulk processes associated with two-phase thermodynamic equilibrium that involve the partitioning of water between vapor and liquid during thermodynamic state changes.

Aerosol mass and energy exchange

Liquid aerosols provide internal energy storage primarily as a result of the latent energy that is represented by their presence in the atmosphere, and the aerosols serve as a mass repository for condensed water vapor. As water aerosols form (due to bulk condensation) they are either deposited or settle out of the atmosphere. Therefore, by aerosol behavior processes (deposition, agglomeration, condensation) condensed water is removed from the atmosphere. When water aerosols are suspended in the atmosphere, the gas mixture tends to remain in a saturated state (condensation or evaporation).

Spray mass and energy exchange

Sprays are an engineering safety feature used in many plants to suppressed containment pressurization, acting as a contact mass and thermal sink to 1) condense steam and 2) cool the atmosphere. The mass and energy exchange processes associated with spray droplets are different from aerosols since the sprays are larger in size than aerosols, and therefore are generally not in thermal equilibrium with the gas mixture and, compared to aerosols, have residence times in the atmosphere of relatively short duration. AC power is required for spray operation.

Volume displacement due to pool filling/draining

The volume of atmosphere of a compartment may change as a pool is formed or drained. As the reactor coolant system, ECCS, and spray system liquid water is transferred to the containment building, the containment free volume will be reduced slightly. However, individual room volumes in the lower regions of the containment may be significantly affected such that these regions may undergo extensive flooding. The free volume will increase again, if the pool drains by gravity or by pumping to other compartments.

Atmosphere cooling by fan-cooler

Fans force gas mixtures to pass over cooling coils that extract sensible and latent heat (with accompanying condensate mass) from the atmosphere. AC power is required for fan-cooler operation.

Mixing (Intra-compartment)

Jet-plume gas interaction/entrainment (localized)

Jet and plume behavior are involved processes driven by buoyancy, momentum, and shear forces. The interaction and entrainment that characterize the phenomenon is dependent on very localized momentum transport processes that occur in a free shear flow environment. For most injection scenarios, an unobstructed jet of hot or light gas will quickly develop into a buoyant plume. Since behavior of this jet-plume is dependent on the jet or buoyancy-driven momentum transport and entrainment processes, this component of the mixing process is classified separately.

Buoyancy/stratification (regional)

Buoyancy/stratification refers to circulation processes that take place outside of plume boundaries in the ambient gas region that usually represents most of the volume within a compartment. The phenomenon again involves buoyancy but in this instance the buoyancy of the fluid is distinguished not by local mixing patterns or large circulation loops; rather, the main feature of the mixing is described in terms of stability limits and stratification wherein a vertical density profile is established and maintained within an open compartment. A fully developed stable stratification for instance would have less dense gases overlying denser gases.

In situations where a light gas is injected into a heavy ambient gas, forming a buoyant plume, the ambient mixing will rapidly develop a stable stratification provided that the injection rate is not too large. In a fully developed state, circulation will have formed essentially a two layered distribution of lighter gases above the more heavier gases. The circulation processes that are responsible for this end state typically do not depend on the details of plume or the entrainment processes near the plume boundary but depend on a basic phenomenon characterized by buoyant-driven flow (excluding momentum transport) within the ambient gas mixture. This type of mixing process is distinguished from other localized processes (jet-plume) and larger scale mixing and transport processes that involve convective loops established by gas/wall interactions or buoyant flows between various containment compartments, respectively.

Buoyancy/wall interaction (regional)

This mixing processes involves large circulation patterns that develop within a compartment as a result of the heating and cooling of gases along walls. Whereas the above mixing processes can be described completely assuming an adiabatic wall boundary, this process is dependent on mixing via circulation patterns developed as a result of gas/wall heat and mass transfer. For example, in an enclosure with a hot vertical wall that is opposite from a cold wall, a circulation loop will be set up where gases near the hot wall rise and along the cold wall fall. Even without a calculational model, it is quite apparent that a convection loop affecting mixing (constituent concentrations) will develop; in this case, the dominating phenomenon is buoyancy with mixing behavior dependent on the convection loops that develop.

Turbulent diffusion

This phenomenon is defined as a gas mixing process whereby a gas constituent mixes across an interface between two relatively well mixed fluids purely as a result of turbulent diffusion across the relatively small transition layer. In general, within the bulk containment atmosphere, diffusion is of second order importance compared to other containment mixing phenomena because the dimensions of the free volumes are large and the concentration gradients are, in most cases, quite small. Molecular diffusion, which is a much slower process, is generally not included in this category.

Spray dynamics

The interaction of falling spray droplets with the atmosphere will induce gas mixing processes. Small air vortices can be formed as the result of the hydrodynamic drag created by drops falling through the atmosphere -- these vortices can in turn induce gas mixing. Large numbers of droplets together can form a virtual stream which creates a downdraft in the atmosphere gas by momentum transfer, thereby creating a regional convection loop.

Fan dynamics

Fan coolers are installed in some containments to provide air cooling by removing sensible and latent heat from the atmosphere as gas and vapor passes over cooling coils. The mechanical action of the fans on the gases will induce mixing in the containment.

Transport (inter-compartment)

Buoyancy

Buoyancy is defined as a process or characteristic of an atmosphere by which less dense gases rise and denser gases fall. In the compartment mixing processes, buoyancy is considered the driving process primarily responsible for regional mixing patterns, such as stratification. On yet a larger scale, involving the transport of gases between compartments, buoyancy can also be a significant driving term that determines large convective loop flows within a containment. These loop flows transport gases and suspended liquid throughout the containment, and can also affect compartment mixing processes through the various inflows and outflows that develop.

Form and Frictional losses

Given a pressure differential between compartments, the rate of gas flow through a pathway will depend on form and frictional drag that resists fluid motion. The characteristics of the flow path may include transient features as implied by rupture disks, or composite form and frictional losses required for ventilation ducts and shafts.

Aerosol coupling

Aerosols are transported between compartments as the gas in which they are suspended flows from one compartment to another. Although the suspended aerosols (water or solid) are considered to be an integral part of the atmospheric component typically referred to as "gas" in the context of flows, they actually represent a separate field -- particles are coupled to the gas field by drag and inertia forces. In addition to the coupling forces, the presence of aerosols increases the effective density of the transported gas/aerosol mixture between compartments. Coupling is therefore a general term to group all phenomena (drag, inertia, density effects, etc.) that affect both the transport of aerosols in flow paths and also the gas flow as a result of the presence of aerosols in the flow. (Note: aerosol coupling as a result of decay heating, for radioactive aerosols, has been considered previously for pressurization/depressurization processes under the phenomenon heading, aerosol mass and energy exchange.)

Liquid water carry over

During rapid blowdowns, a portion of the two phase water injection will be in a liquid water form (large mass size compared to water aerosols) suspended in the flow stream and transported out of the break compartment.

2.1.3.2 Phenomena Identification for the Structure Component

Interior heat transfer

1-D transient conduction

1-D transient conduction requires the solution of the generalized one-dimensional Fourier's energy transport equation for solids. The conduction solution should include all thermal resistances such as paints, composites (steel lined concrete), and small air gaps that create a contact thermal resistance.

2- or 3-D transient conduction

2- or 3-D transient conduction is similar to the 1-D transient conduction description with addition of two or three dimensions to the Fourier's energy transport equation.

Interior mass transfer

Outgassing (concrete)

At elevated temperatures, both H_2O and CO_2 gases will be released from concrete structures that are not lined. Both evaporable and bound water are the sources for a steam release.

Surface Sensible Heat Transfer

Spray/aerosol deposition or impingement

Spray droplets may contact wall surfaces as they fall through the containment building and therefore be a source of mass and enthalpy transfer to the surface films. Water aerosols may also be deposited on wall surfaces transferring mass and enthalpy. These deposition processes are a result of various effects, including settling, diffusion to surfaces, thermophoresis (a Brownian process causing migration of aerosols toward higher temperatures) and diffusiophoresis (deposition induced by condensation of water vapor on surfaces).

Free convection

Free convection for the process of sensible heat transfer at a structure surface refers to energy transfer as a result of buoyancy induced flow along the surface. In this transfer process the

induced flow is developed in a boundary layer adjacent to the heated or cooled structure. The induced boundary layer flow may be either laminar or turbulent.

Forced/mixed convection

Forced/mixed convection for the process of sensible heat transfer at a structured surface refers to energy transfer as a result of gas flow over the surface. When the gas flow is caused primarily by forces other than induced buoyancy in the boundary layer (fans, inter-compartment pressure differentials, free jets, etc.) the convection is referred to as forced. In cases where the induced buoyancy and forced flows each represent a significant transfer phenomenon required for describing the energy exchange, the processes are combined and this regime is referred to as mixed convection.

Radiation (structure to atmosphere)

This type of thermal radiation exchange involves sensible energy transfers between structures and an absorbing-emitting gas. The gas description may include the compartment atmosphere or more locally, a high temperature gas injection source.

Radiation (structure to structure)

Thermal radiation in this case refers to sensible energy exchanges between structures within an enclosure containing a participating gas.

Liquid film resistance

Film resistance refers to the thermal resistance that the film represents to the transfer of energy from the film surface to the wall structure. The resistance for a given film thickness will generally depend on the film flow regime, that is, whether the film flow is laminar or turbulent.

Liquid film advection

Liquid film advection refers primarily to mass and energy transfers in the film as a result of the film flowing along the structure surface.

Surface Latent Heat and Mass Transfer (condensation/evaporation)

Free convection

Latent heat and mass transfer is characterized by the transfer of vapor from/to the bulk to/from

the liquid water film surface through a concentration boundary layer (diffusion resistance layer) that is formed as a result of induced buoyancy flow. The driving force for the film surface transfer is the difference between the partial pressures of vapor at the surface and bulk. It is noted that mass transfers as a result of condensation can affect the containment volume concentrations by effectively enriching the noncondensible gas concentrations. This can be especially important for the hydrogen-air-steam mixtures since condensation will increase the hydrogen-air concentrations and can also deinert a mixture.

Forced/mixed convection

Latent heat and mass transfer for forced/mixed convection is similar to that indicated for free convection except that the concentration boundary layer across which the vapor is transported by forced gas flows along the surface. When this boundary layer thickness is affected by both the forced and induced buoyancy flows, the flows have a combined effect and the entire mass transfer process is characterized as being in a mixed convection regime.

Transport (film flow)

Liquid film advection

From the standpoint of containment water inventories, liquid film flow will affect the amount of water on structures and the partition of water between all three containment components.

Interfacial shear (film/gas interaction)

When film and gas flow velocities are significantly different (relative velocities), the frictional drag of the gas flow can transfer momentum to the film flow. This interaction can therefore affect the transport of liquid along the surface. This type of interaction, by changing the flow characteristics of the film, can also affect the film thermal resistance and advection.

2.1.3.3 Phenomena Identification for the Pool Component

Mixing

Buoyancy/stratification

Temperature variations in the pool may preclude uniform mixing due to the buoyancy effect that tends to stratify the pool layers. This phenomenon is similar to the buoyancy/stratification processes occurring in the atmosphere as a result of gas layer density variations.

Bubble dynamics

Steam or air injection into pools (suppression pools, quench tanks) can agitate the pool, breaking up stratified layers.

Transport

Filling and draining

This process includes the addition and removal of water from pools mainly by gravitational flows (drain-down of condensate, overflow, or pipe flow). Pumping of liquids may also be included in this category.

Displacement (pressure driven)

Liquid may be displaced, as gases, through the action of pressure forces. For instance, the dynamics of vent clearing and suppression pool swell would be included in this category.

Interior Heat Transfer

Convection (flooded structures)

Structures that are flooded during an accident will have their surfaces heated or cooled by pool water. This heat transfer process will typically be characterized as convection (generally assumed to be free convection).

Boiling

Water in pools overlying or in contact with vertical hot surfaces may undergo local boiling, producing a source of steam to the atmosphere. Steam injected into pools may also result in local

pool boiling; and, deposits of significant quantities of fission products may boil-off small pools. The boiling process will produce a source of steam to the atmosphere.

Steam condensation (bubbles)

Steam injected into pools (suppression pools) will form bubbles that will rise to the surface. Depending on the pool temperature and depth, a portion of the steam injected will condense, heating the pool water. The steam not condensed will exit from the pool and be considered a source of steam for the overlying atmosphere.

Surface Sensible Heat Transfer

Free convection

Sensible heat transfer at a pool surface may occur as a result of buoyancy induced flow above the surface. In this transfer process the induced flow is developed in a boundary layer adjacent to the heated or cooled pool surface. The induced boundary layer flow may be either laminar or turbulent.

Forced/mixed convection

Sensible heat transfer at a pool surface may occur as a result of gas flow over the surface. When the gas flow is caused primarily by forces other than induced buoyancy in the boundary, the convection is referred to as forced. In cases where the induced buoyancy and forced flows are both significant features required for describing the heat transfer, the processes are combined and this regime is referred to as mixed convection.

Spray/aerosol deposition

Spray droplets may deposit onto a pool surface as a result of gravitational settling and therefore transfer significant mass and enthalpy to the pool. Likewise, solid and water aerosols may also be deposited on pool surfaces. Water aerosols formed in the atmosphere can deposit on the pool surfaces thereby transferring mass and enthalpy to the pool.

Surface Latent Heat and Mass Transfer (condensation/evaporation)

Free convection

The term, used in relation to mass transfer, is characterized by the transfer of vapor from/to the bulk to/from the pool surface through a concentration boundary layer (diffusion resistance layer)

that is formed as a result of induced buoyancy flow. The driving force for the surface transfer is the difference between the partial pressures of vapor at the pool surface and bulk.

Forced/mixed convection

The term, used in relation to mass transfer, is as indicated for free convection except that the concentration boundary layer across which the vapor is transported by forced gas flows along the surface. When this boundary layer thickness is affected by both the forced and induced buoyancy flows, the flows have a combined effect and the entire mass transfer process is characterized as mixed convection.

2.2 Containment Phenomena Ranking

The phenomenon identification described in Section 2.1 has been completed for all phases of a potential accident, applying mainly to PWR large dry containments; and, through the inclusion of a generic pool component, the list of phenomena extends to include BWR containments. Through the ranking process, the complete list of phenomena is reduced depending on the specifics of the plant type, scenario, and phase of the accident. The experiments and code applications discussed in this report are directed primarily towards a PWR-like plant; therefore, the ranking process will assume that the containment type is a PWR. In order to develop a ranking that is not too specific to an accident scenario, a more general approach is used to establish and identify three critical accident phases: the rapid pressurization phase associated with the primary system blowdown into the containment; the slow depressurization phase during which critical equipment is expected to operate; and, the potential core damage phase which is often referred to as the beyond DBA phase where hydrogen can be released from the core into the containment. In the first subsection below, these accident phases are described in general. Then the criterion for ranking is stated in terms of design limits placed on maximum pressure and temperature, rates of pressure and temperature decline, and maximum hydrogen concentrations. Ranking tables are then presented for the three accident phases. Finally, the implications of the rankings are discussed. It should be noted that all DBAs will include both pressurization and depressurization phases associated with the determinations of maximum containment loads and long-term transients, respectively; therefore, by introducing "core damage" as a phase implies that there is some overlapping of phase definitions. However, not all accidents can be expected to progress to a core damage state and the release of hydrogen. The "design" in DBA assumes that the reactor and containment will function during an accident such that no sustained core damage will occur. Beyond DBA scenarios therefore include some sustained damage of the core, and while they might be considered accidents of low probability they still require rigorous analysis.

2.2.1 Accident Scenario and Phase Definition

DBA accident scenarios, from the standpoint of the containment, are characterized as LOCA type accidents where a release of a portion of the primary and ECCS coolant pressurizes the containment. And in the case of a beyond DBA, where break releases conditions the containment prior to the release of hydrogen. A "generic" DBA may be described using an accident matrix that identifies events, periods of interest for regulatory review, the regulatory limits, and the types of engineering safety features that can affect the containment response. An illustrative containment accident matrix is shown in Table 2.2.

2.2.2 Ranking Criteria

The PIRT process requires a primary evaluation criteria that will be used to judge the relative importance of phenomena/processes for the containment behavior of interest. In the accident phases considered here, the containment behavior of interest is based on regulatory guides, not on containment threat conditions. During DBAs, for instance, the maximum containment loads must remain below the design limits.

We note that typically pressure is a global parameter while temperature and gas species concentrations are regional or local indicators of containment conditions. In the case of hydrogen limits, the intent is to represent a potential combustion condition prior to ignition. The condition, although given only in terms of hydrogen concentration also includes limits on condensible and noncondensible species in the atmosphere since combustion conditions (i.e., hydrogen limits) are governed by hydrogen, oxygen, and steam concentrations. Implicit therefore in the evaluation of important phenomena/processes for hydrogen limits is our knowledge of the entire atmospheric composition. Although the prediction of local temperatures may be equated in many cases to predictions of local concentrations, for the purposes of regulation, the criterion for evaluation of phenomena/processes is generally developed separately for temperature and composition. This is because the times periods and location for critical temperature predictions can be quite different from that required for hydrogen analysis. For instance, in the former there are two review periods: the first occurs typically during the blowdown period or shortly afterward; and, the second occurs very late in the accident, 24 hours after the maximum pressure and temperature are reached. The location of interest for equipment qualification may be confined to the lower regions of the containment where most critical equipment is placed. In contrast, for hydrogen analyses during beyond DBA, the maximum concentrations typically occur shortly after the injection period which is itself somewhat uncertain, but we can anticipate from past studies that the time period will be somewhere in the range of 2 to 5 hours after the start of the accident. Furthermore, peak hydrogen concentration will generally occur either in the breakroom or above the operating deck. Since the time periods and locations for local assessment are different, separate columns for temperature and composition in the ranking table are required in order to provide a distinguishable phenomena/process ranking. In Section 4, which describes the code assessments, the three comparison quantities are pressure, temperature, and composition – in consort with the ranking tables. In addition, key phenomenological models are evaluated based on agreements between these predicted and measured quantities. Other primary quantities, such as flow rates and heat transfer coefficients are also assessed as specific indicators of model accuracy; however, these indicators must also be reviewed in the context of the three ranking parameters listed in the PIRT.

2.2.3 Ranking Components and Phenomena Importance

Ranking is based on subjective decisions regarding the importance of phenomena/processes in

relation to the criteria set. The ranking is dependent on expert opinion and engineering judgment. The process is aided by review of the experimental data base, and plant and experimental analyses that include reference and sensitivity calculations. In establishing a ranking scale, it is common practice to evaluate the criterion using a scale of low, medium or high. The low, medium, and high ranks have definitions that correspond to the intended uses [Wil96]. For the three PIRT objectives that are of concern here, these definitions are:

1) Experimental Guidance:

- Low = Phenomenon should be exhibited, but accurate measurement and prototypicality are of low importance,
- Medium = Phenomenon should be exhibited; measurements may be derived; prototypicality may be somewhat compromised,
- High = Phenomenon should be explicitly exhibited and well measured; phenomenon should be prototypical.

2) Code Development:

- Low = Phenomena has small effect on the primary parameter of interest. Phenomena should be represented in the code, but almost any model will be sufficient,
- Medium = Phenomena has moderate influence on the primary parameter of interest. Phenomena should be well modeled; accuracy maybe somewhat compromised,
- High = Phenomena has dominant impact on the primary parameter of interest. Phenomena should be explicitly and accurately modeled.

3) Code Uncertainty:

- Low = Combined uncertainty of phenomena may be determined in a bounding fashion, or may be eliminated when justified,
- Medium = Phenomena should be evaluated to determine if uncertainty should be treated individually as are high ranks, or in a combined manner as are low ranks,
- High = Phenomena uncertainty should be individually determined and then combined statistically with other uncertainty sources.

In this report, the last two objectives are of primary interest.

2.2.4 Phenomenon Identification and Ranking Table (PIRT)

Shown in Tables 2.3 and 2.4 are illustrative PIRTs for a PWR large dry containment during design basis and beyond design basis accidents. Since the key parameters selected for the ranking process depend to some extent on prior phases of the accident, some consideration of conditioning prior to the core damage phase is required and therefore implicitly included in the ranking shown in Table 2.4.

In the case of the rapid pressurization phase, the time to reach maximum pressure is typically measured in seconds. That rapid rise due to the magnitude of the injection mass and energy rate from the blowdown means that the containment pressurization is essentially an adiabatic pressurization process. As a result, the importance of mass and heat transfer processes are reduced; for example, the forced and free convective condensation heat transfer is rated medium for the rapid pressurization phase whereas free convection condensation is rated high for the slow pressurization and core damage phase.

Note that in Table 2.4 the localized mixing phenomena occurring in or near a jet or plume resulting from an injection is ranked low. This choice is a reflection of the lack of either experimental or analytical confirmation that within the jet/plume boundaries combustion ignition conditions occur. The high concentration of steam present in the injection source, along with the large uncertainties associated with injection type (orientation and break size) and surrounding geometry, makes any ranking judgment difficult to rationalize. More research in the area of local mixing processes however may provide the information that will alter this ranking; this is indicated by the conditional (H) ranking given this phenomenon.

There are some additional points to be made with regard to the outcome and rationale behind the ranking for regional mixing processes. The low ranking of the mixing phenomena influencing containment pressure reflects past experiences (analytical studies) showing that local and regional mixing processes are of minimal importance for global energy balancing during either the slow depressurization or the core damage phase. These phases typically are characterized as periods of low steam injection rates. Mixing processes, resulting from buoyancy/stratification (regional) phenomena, however, may give rise to regional stratifications that can be highly important in determining temperature and concentration gradients that affect conditions important for equipment qualification or hydrogen combustion.

The variations in phenomena ranking for global (pressure), regional, and local parameters are dependent partly on the relative importance that parameter represents based on the criterion, as explained above. Generally, local and regional gas mixing patterns do not significantly affect pressures because the areas of nonuniform mixing that influence atmospheric energy transfers, and therefore pressure, are confined to small portions of the containment. During the slow depressurization or during the core damage phase of the accident, where the containment

injection sources are relatively small and prolonged, pressure variations within the containment are insignificant. Mixing processes however can cause temperature and gas compositions to vary considerably within regions of the containment and especially between regions above and below source injections. For these reasons buoyancy/stratification phenomena affecting regional temperatures, and even more so compositions, are considered to have a medium and high importance, respectively.

In a somewhat similar outcome, transport processes are considered to have only a medium impact on containment pressure during this accident phase but a higher impact on temperature and gas concentrations. The upgrading to medium for pressure, for transport processes, is the result of a realization that inter-compartment mixing extends over a larger volume of the containment than regional mixing processes. As the entire containment volume begins to mix, pressure varies as atmospheric energy is transferred to cold structures now being continually exposed to high steam concentrations. As discussed in Section 3, there are numerous experimental and, as documented here, analytical studies of mixing phenomena associated with multiple compartment containments having near prototypical configurations (relative compartment volumes, connections, and heat sink mock-ups). These studies have been undertaken to increase our understanding of convection patterns that may occur during postulated DBA and severe accident conditions, and to improve our predictive capabilities for transport processes. In Section 3, there are also discussions of procedural and geometric scale distortions associated with gas mixing experiments and, as a result, cautionary comments regarding direct transfers of conclusions, based on an interpretation of experimental modeling accuracies, to full plant accident analysis.

For the active engineering processes like sprays and fan coolers, there can be a significant influence on both global, regional, and local conditions within the containment. These processes, if present during the slow depressurization or core damage phase of the accident, may dominate as the most important phenomena/processes affecting pressure, temperature, or composition. The inclusion of engineering safety features in the PIRT highlights their importance for consideration in these accidents.

Under the category of surface heat transfer processes, those phenomena responsible for sensible heat transfer are considered to have a low ranking since the amount of energy transfer associated with this exchange is generally insignificant compared to the latent energy transfers from condensation/evaporation. There are a number of features associated with the latent heat and mass transfer process: gas phase resistance; condensate film resistance; and, film advection. The PIRT shows that the energy transfers associated with presence of the film is insignificant, and that the governing phenomenon for condensation (or evaporation) is gas phase resistance, which is dependent on the convection regime. Further, during the slow pressurization and core damage phases, forced circulation patterns within the containment are minor with respect to free convection flows that determine gas species boundary layers near most heat conducting structures. Free convection flow processes are therefore most important for latent heat transfers

during these phases. The large energy exchanges associated with these transfers obviously has a major affect on energy balances (pressure) and other key parameters such as temperature and concentrations. Gas compositions are affect by these potentially large transfers since the steam concentration in the containment atmosphere is directly affected by such processes. Especially near cold walls, condensation on surfaces can produce local regions of high hydrogen concentrations and drive local convection. These potentially critical conditions are reflected in a high ranking given to the mass transfer processes and a medium ranking for two-phase thermodynamics associated with the pressurization process that determines the state of multi-component gas mixtures for the long-term phases.

2.2.5 Implications of Rankings

The main implication for these rankings are that experiments require explicit instrumentation to measure regional temperatures and compositions, and that attention to prototypical conditions for each containment phase should be maintained in order to investigate the highly ranked phenomena. Beyond the obvious prototypical geometrical requirements are the requirements to precondition the containment (pressure, water vapor concentration, structure temperature) prior to the hydrogen/steam injection and provide injection rates that are properly scaled. Because inter-compartment mixing by buoyancy can be of high importance, compartment temperature and velocity measurements at major flow path junctions should be measured. Since mass transfer by condensation is the most important mass and energy transfer process, wall surface instrumentation should be used to determine heat flux, condensate amount, and atmospheric temperature near the surface. Velocity measurements near the surface should be included, if possible, to confirm that the convection regime is free convection.

Code development programs need to focus on models that can predict gas compression for rapid injections and regional stratification, mixing, and inter-compartment transport due to buoyancy-driven forces during the long-term scenarios. Models for free convection mass transfer should be developed using methods that assure a high degree of accuracy. Since the condensation models require an accurate determination of the bulk atmospheric conditions along a surface, an integral assessment of these models together with the mixing and transport models are required to complement separate effects testing. Models developed through all these efforts must be able to be scaled-up to full scale containments. Scaled-up models may be verified through assessment at various scales.

The most likely areas for critical uncertainty analysis are the modeling methods for predicting free convective condensation, regional stratification, mixing, and inter-compartment gas transport. Lumped parameter codes like CONTAIN have been criticized for their approximate modeling methods in the mixing and transport areas. These criticisms have led to the emergence of an improved computing technique, the hybrid flow solver.

Table 2.1 Phenomena for Containment Thermal Hydraulics and Hydrogen Distributions during Design Basis and Beyond Design Basis Accidents.

Component	Process	Phenomena
Atmosphere:		
	pressurization/ depressurization	multi-component gas compression/expansion
		aerosol mass and energy exchange
		spray mass and energy exchange
		volume displacement/pool filling or draining
		atmosphere cooling by fan-cooler
	mixing (intra-compartment)	jet-plume gas interaction/entrainment (localized)
		buoyancy/stratification (regional)
		buoyancy/wall interaction (regional)
		diffusion (turbulent)
		spray dynamics
		fan dynamics
	transport (inter-compartment)	buoyancy
		form and friction losses
		aerosol coupling
		liquid water carry over
Structure:		
interior	heat transfer	1-D transient conduction
		2- or 3-D transient conduction
	mass transfer	outgassing (concrete)
surface (solid and film)	sensible heat transfer	spray/aerosol deposition or impingement
		free convection
		forced/mixed convection
		radiation (structure to atmosphere)
		radiation (structure to structure)

		Phenomena
		liquid film resistance
		liquid film advection
surface (solid and film)	latent heat and mass transfer (condensation/evaporation)	free convection
		forced/mixed convection
	transport (film flow)	liquid film advection
		interfacial shear (film/gas interaction)
Pool:		
	mixing	buoyancy/stratification
		bubble dynamics
	transport	filling and draining
		displacement (pressure driven)
interior	heat transfer	convection (flooded structures)
		boiling
		steam condensation (bubbles)
surface	sensible heat transfer	free convection
		forced/mixed convection
		spray/aerosol deposition
	latent heat and mass transfer (condensation/evaporation)	free convection
		forced/mixed convection

Table 2.2 Containment Accident Matrix

Accident Phase		Time Period by phase (approx.)		Containment Event	Source	Regulatory Limits by Phase		Engineered Safety Features	
DBA	Beyond DBA	DBA	Beyond DBA			DBA	Beyond DBA	Active	Passive
I. RCS depressuri-zation	Conditioning	sec. to min.	sec. to min.	Rapid pressurization	High pressure two-phase RCS water	$(P,T)_{des}$		Pressure suppression sprays and fan coolers	Containment volume, pressure suppression with pools or ice
II. Adequate core cooling	Conditioning and inadequate core cooling	hours (24 hrs)	min to hours	Slow pressuriation or depressuriztion	ECCS/RCS water heating	$(P,T)_{des}$ or (P,T) at 24 hrs. less than 50% design			Passive containment cooling system
	III. Core damage		(2-5 hrs)	hydrogen release	Core uncovery with clad/steam reaction		H_2 vol. conc.		Containment volume, inerting

Table 2.3 Illustrative Phenomena Identifcation and Ranking Table for Containment Thermal Hydraulics during the Rapid Pressurization Phase of a Design Basis Accident in a Large Dry PWR Containment.

Component	Process	Phenomena	Rank	
			Pressure	Temperature
Atmosphere:				
	pressurization/ depressurization	multi-component gas compression/expansion	H	H
		aerosol mass and energy exchange	L	L
		spray mass and energy exchange	M	M
		volume displacement/pool filling or draining	L	L
		atmosphere cooling by fan-cooler	L-M	L-M
	mixing	jet-plume gas interaction/entrainment (localized)	L-M	M-H[a]
		buoyancy/stratification (regional)	L-M	L-M
		buoyancy/wall interaction (regional)	L-M	L-M
		diffusion (turbulent)	L	L
		spray dynamics	L-M	M
		fan dynamics	L	L-M
	transport (inter-compartment)	buoyancy	M	M-H
		form and friction losses	L	M-H
		aerosol coupling	L	L
		liquid water carry over	L-M	M

			Pressure	Temperature
Structure:				
interior	**heat transfer**	**1-D transient conduction**	**M**	**M**
		2- or 3-D transient conduction	**L**	**L**
	mass transfer	**outgassing (concrete)**	**L**	**L**
surface **(solid and film)**	**sensible heat transfer**	**spray/aerosol deposition or impingement**	**L**	**L-M**
		free convection	**L**	**L**
		forced/mixed convection	**L**	**L-M**
		radiation (structure to atmosphere)	**L**	**L-M**
		radiation (structure to structure)	**L**	**L-M**
		liquid film resistance	**L**	**L**
		liquid film advection	**L**	**L**
	latent heat and mass transfer (condensation/evaporation)	**free convection**	**M**	**M**
		forced/mixed convection	**M**	**M**
	transport (film flow)	**liquid film advection**	**L-M**	**L-M**
		interfacial shear (film/gas interaction)	**L**	**L**

			Pressure	Temperature
Pool:				
	mixing	**buoyancy/stratification**	**L**	**L**
		bubble dynamics	**L**	**L**
	transport	**filling and draining**	**L**	**L**
		displacement (pressure driven)	**L**	**L**
interior	**heat transfer**	**convection (flooded structures)**	**L**	**L**
		boiling	**L**	**L**
		steam condensation (bubbles)	[b]	[b]
surface	**sensible heat transfer**	**free convection**	**L**	**L**
		forced/mixed convection	**L**	**L**
		aerosol/spray deposition	**L**	**L**
	latent heat and mass transfer	**free convection**	**L**	**L-M**
		forced/mixed convection	**L**	**L**

[a] **The high ranking of this phenomenon is conditional, depending on the characterization of the injection (break size, location, orientation).**

[b] **Not applicable for this accident phase or reactor type (may apply for BWR type)**

Table 2.4 Illustrative Phenomena Identifcation and Ranking Table for Containment Thermal Hydraulics and Hydrogen Distributions during the Slow Pressurization/Depressurization and Core Damage Phase of a Design Basis or Beyond Design Basis Accident in a Large Dry PWR Containment.

Component	Process	Phenomena	Rank		
			Pressure	Temperature	Composition
Atmosphere:					
	pressurization/ depressurization	multi-component gas compression/expansion	M	M-H	M
		aerosol mass and energy exchange	L	L	L-M
		spray mass and energy exchange	M-H	M-H	M-H
		volume displacement/pool filling or draining	L	L	L
		atmosphere cooling by fan-cooler	M-H	M-H	H
	mixing	jet-plume gas interaction/entrainment (localized)	L	L (H)*	L (H)*
		buoyancy/stratification (regional)	L-M	M	H
		buoyancy/wall interaction (regional)	L	M	M
		diffusion (turbulent)	L	L	L
		spray dynamics	L-M	M	H
		fan dynamics	L-M	M	H
	transport (inter-compartment)	buoyancy	M	M-H	H
		form and friction losses	L	L-M	L-M
		aerosol coupling	L	L	L
		liquid water carry over	L	L	L

Structure:			Pressure	Temperature	Composition
interior	heat transfer	1-D transient conduction	M-H	M-H	M-H
		2- or 3-D transient conduction	L	L	L
	mass transfer	outgassing (concrete)	L	L	L
surface (solid and film)	sensible heat transfer	spray/aerosol deposition or impingement	L	L-M	L-M
		free convection	L	L	L
		forced/mixed convection	L	L-M	L
		radiation (structure to atmosphere)	L	L-M	L
		radiation (structure to structure)	L	L-M	L
		liquid film resistance	L	L	L
		liquid film advection	L	L	L
	latent heat and mass transfer (condensation/evaporation)	free convection	H	H	H
		forced/mixed convection	L-M	L-M	L-M
	transport (film flow)	liquid film advection	L-M	L-M	L-M
		interfacial shear (film/gas interaction)	L	L	L

Pool:			Pressure	Temperature	Composition
	mixing	buoyancy/stratification	L	L-M	L
		bubble dynamics	L	L	L
	transport	filling and draining	L	L-M	L-M
		displacement (pressure driven)	L	L	L
interior	heat transfer	convection (flooded structures)	L	L-M	L
		boiling	L	L	L
		steam condensation (bubbles)	[b]	[b]	[b]
surface	sensible heat transfer	free convection	L	L	L
		forced/mixed convection	L	L	L
		aerosol/spray deposition	L	L	L
	latent heat and mass transfer	free convection	L	L-M	L-M
		forced/mixed convection	L	L	L

[a] The high ranking of this phenomenon is conditional, depending on the characterization of the injection (break size, location, orientation).

[b] Not applicable for this accident phase or reactor type (may apply for BWR type)

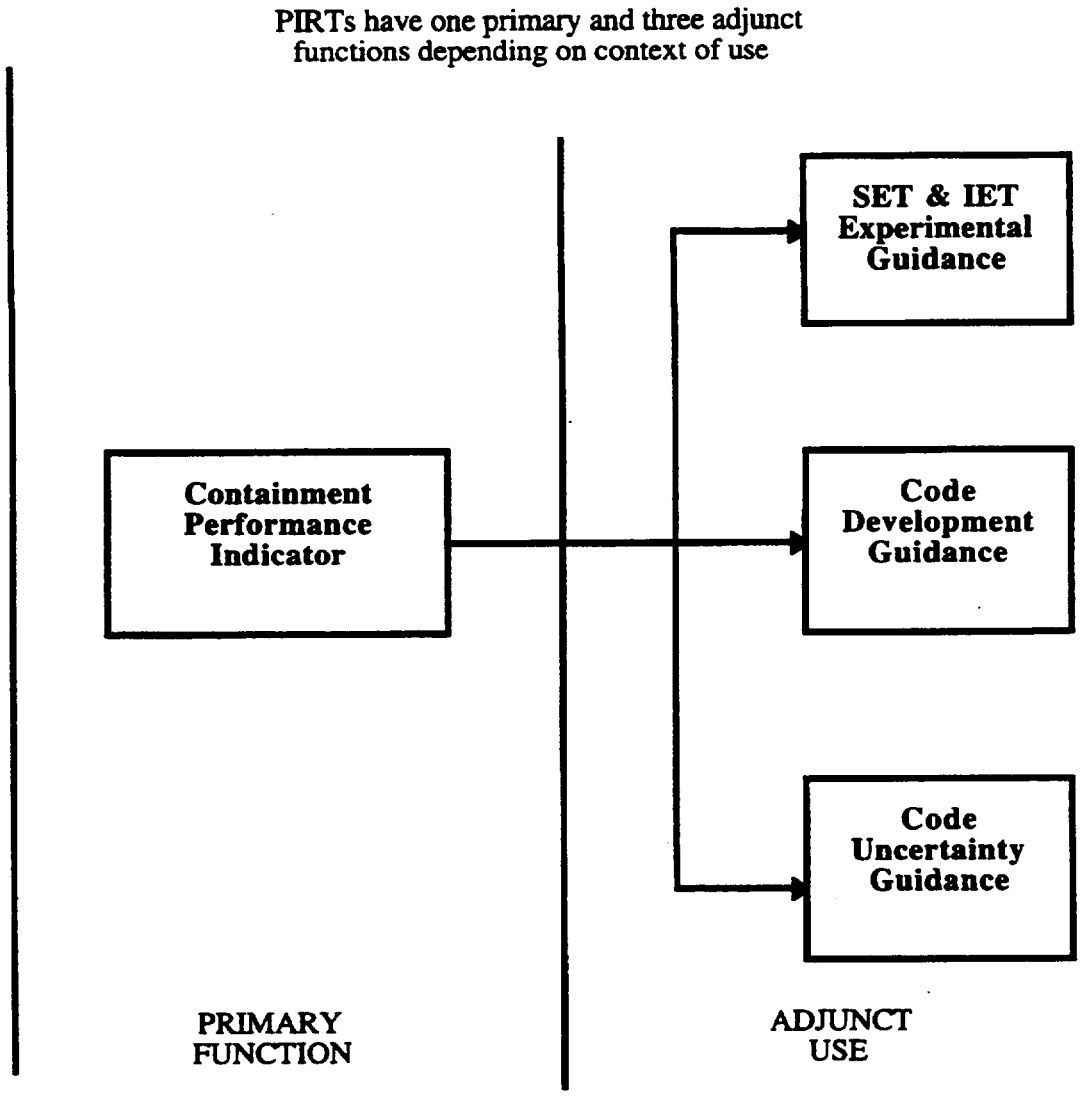

Figure 2.1 Conceptual use of PIRT[Wil96]

3 Code Assessment Activities [Reference Studies]

This section describes efforts to assess the CONTAIN code for applications involving design and beyond design basis accident analysis. The assessments are based on a series of experiments, twenty in all, that include both integral and separate effects testing. In the case of the integral tests, the experiments cover volumetric scales ranging from 2 to 17% of full scale containments, with and without prototypical heat sinks, and with steam injections representative of rapid and slow pressurization/depressurization accident scenarios. The time periods investigated for accidents in the integral assessments range from seconds to many hours, with one test exceeding a day. Two integral tests and two separate effects test are included to study pressure suppression modeling during periods when containment sprays are functioning. Seven integral light gas distribution experiments are analyzed to provide an assessment of the code's capability for beyond design basis accident analysis where hydrogen gas is released into the containment. In addition to the separate effects tests for sprays, seven separate effects tests are included to verify heat and mass transfer modeling. A listing of these assessment tests is presented in Table 3.1.

As noted in Table 3.1, four of the integral experiments were also selected as international standard problems (ISPs) and therefore have received considerable attention within the community of containment code developers and analysts. These experiments are listed in Table 3.2 according to the experiment and ISP designation along with references that provide detail on the exercises. Each of the ISP tests has been previously analyzed with earlier versions of the CONTAIN code[1]; except for ISP-29, all of these exercises where performed as blind test exercises. In the case of the CVTR tests, JAERI spray tests, Phebus test FPT0, and the Wisconsin flat plate condensation tests, this report is the only documentation of the comparison of CONTAIN code results to published data.

In the following subsections, some general remarks are provided concerning code assessment and the type of phenomena measured and analyzed in the list of tests; the geometric and boundary condition scaling in the tests are discussed; and, each test and code assessment is explained for a reference calculation. A listing of CONTAIN input decks for each reference calculation is provided in Appendix A. Later, in Section 4, sensitivity calculations are included for most of the test series in order to address code modeling, experimental, and user based uncertainties.

3.1 Background

Since it is not feasible to conduct full scale, prototypical experiments of design or beyond design basis accidents, accident simulations using containment codes are vital to the NRC's program of licensing review and confirmatory analyses. Reliance on codes necessitates that a carefully

[1] The participation in ISP-16 was as a participant in the blind post-test analysis of HDR test V44. Results of this effort are described in Reference Wol83.

designed plan of verification and validation be formulated. In the case of the CONTAIN code, this plan must demonstrate simulation accuracy, quantify uncertainties, and provide guidance for a conservative application of code for licensing reviews.

Within the scope of the various simulations there are requirements of applicability and reliability. Code applicability is judged by whether the code has the ability to reproduce physical phenomena present during a postulated accident, or whether employed empirical data are relevant for the range of conditions anticipated in the containment. As an example, if water evaporation from a hot wall during spray activation is a process that is believed to be important for accurate representation of thermal hydraulic conditions yet the heat and mass transfer modeling in a code does not allow for evaporation (an example would be a Uchida type formulation,[2]), such a code would be considered not applicable for predicting either the scenario or experiment were this process occurring. Installed physical models are at issue for this requirement. Code reliability, on the other hand, is generally judged by assessing the accuracy of a code's result. Qualitative and quantitative comparisons with data are indications of the code's reliability in predicting thermal hydraulic phenomena in a containment. In this regard, code assessment based on experiment data comparisons requires us to focus attention on the *analytical simulation modeling* effort. The analytical simulation model (ASM) includes three components; the code, user, and scenario. A schematic of the model is shown in Figure 3.1. As indicated, the model is dependent on user knowledge, analytical model limits, and the representation of the scenario. Results can vary accordingly by these dependencies and as a consequence of the intended use of the output (i.e., whether the results are to be used for licensing regulation, design, or analysis). The solid lines in the figure show these relationships; the dashed line connecting user and scenario blocks indicate the implied relationship between user knowledge and an ability to represent a scenario initial and boundary conditions. It is often difficult to judge whether a variation between results and data is caused by any one of the three main ASM components. To help in this judgement, for example, sensitivity calculations are performed to help eliminate or minimize both the user and conditional modeling from the mix so as to highlight code modeling influences on end results. This is the rationale behind the sensitivity calculations that involve uncertainties in user (nodalizations) and experimental conditions (heat sink properties, initial and boundary conditions) discussed later in Section 4.

Obviously, there can be no experimental assessment without measured data. Therefore, one would prefer that all phenomena or processes believed to occur inside containments be represented and measured in a series of assessment experiments. However, that preference is not possible either due to cost or instrumentation limits. For this reason, we revert to the information

---

[2] The Uchida formulation (total heat transfer coefficient versus steam/air mass fraction) is an empirical fit of condensation data under saturated air/steam conditions. The coefficient and the method of implementation (CONTEMPT-LT/028, etc.) is not applicable to evaporation processes.

provided in the PIRT discussed in the previous section to determine if at least highly ranked phenomena are specifically present, and the primary indicators of the phenomena are measured. We noted in that discussion on ranking that modeling accuracy is especially important for phenomena and processes that are estimated to be ranked as highly important to containment accident simulations, according to the criteria established from regulatory limits and guidelines. Using the PIRT defined in Section 2 for three accident phases (rapid pressurization, slow depressurization, and core damage) in a typical containment, key phenomena known to occur in PWR plants are cross-referenced to phenomena either present or not present in various experiments. Phenomena ranked medium to high (M-H) or high (H) in the PIRT are grouped as ranking high in Table 3.3a. Table 3.3b lists only the medium (M) ranked phenomena, excluding those phenomena ranked as low (L), or low to medium (L-M). The tables show whether the phenomena were present, present and significant in the experiment, and finally, whether the phenomena were measured. The only highly ranked phenomenon or process that is not addressed and measured in the experimental series presented in this report is fan cooling of the atmosphere that involves pressure suppression and fan dynamics for gas mixing. This report primarily emphasizes assessments related to highly ranked phenomena. The PIRT and cross-reference tables are used here as vehicles to 1) demonstrate that the experimental database is sufficient to address most highly important phenomena occurring in plants, and 2) to focus the assessment in a way that emphasizes the ASM evaluations for those key phenomena.

In assessing code reliability, phenomena or process modeling, assessments are based on comparison to measured quantities. A question arises: what quantities reflect the phenomena being investigated? Clearly, one set of quantities are the criteria set – pressure, temperature, and composition. However, there is also a set of primary quantities (quantities that directly represent model performance) that are helpful also in establishing confidence that the code is accurately representing the phenomena or process. Some of these quantities are structure temperature, heat transfer coefficients (including condensation/evaporation), heat fluxes, and local gas velocity (free field or within pathways). In many of the experiments discussed below, these quantities have also been measured and therefore provide an expanded database for model and experiment comparisons.

Table 3.1 Experiments on Containment Thermal Hydraulics and Hydrogen Distribution

Facility/Experiment	Type	Test Conditions	General Observations
Wisc. Flat Plate 6 tests	SE**	Steady state condensation - downward steam/gas mixture flows of 1-3 m/s along a constant and uniform temperature flat plate. Saturated conditions in the test chamber.	local and averaged force/mix and free convection condensation measured for plate.
Phebus FPT0	SE	Transient test with steam/gas mixture injection - vessel walls maintained above steam saturation temperature. Condensation on temperature controlled vertical cylinders. Superheated conditions in the vessel.	Uniform steam/gas mixture with condensation on vertical cylinders. Pressure fluctuations dependent on variable steam/gas mixture injection. Condensation heat transfer estimated using timed collections of condensate during the test.
JAERI spray tests PHS-1 PHS-6	SE	Sprays from a range of nozzle numbers (1-12) and at varying elevations. Water injected into a stagnant steam/air mixture at 3.5 bar. Vessel has steel insulated walls pre-heated by steam injection.	Clean test of pressure suppression due to spray cooling. Single spray nozzle test has minimum spray/wall interaction and provides good separate effect test. Multiple nozzle test require an estimate of spray/wall interaction.
HDR V44 (ISP-16)	INT* DBA	55 sec 2-phase steam blowdown in a small (280 m^3) mid-elevation room.	Test provides an indication of the affect of force convective condensation during a blowdown event. Pressure differentials between blowdown and adjacent compartments are recorded.
HDR T31.5 (ISP-23, Project HDR benchmark)	INT DBA	55 sec 2-phase steam blowdown in a large (793 m^3) mid-elevation room. ISP-23 exercise extends to 20 minutes. Hydrogen/He injection began at 20 minutes after blowdown and lasted for 15 minutes.	Pressure response similar to V44. Hydrogen tracing in the containment 20 minutes to 1hour provide a database for gas distribution modeling.
HDR E11.2 (ISP-29)	INT SBLOCA	12h steam injection for pre-heating prior to 20 min hydrogen/He injection (injections at mid-elevation). Followed by 3h steam injection in lower containment and 3h45 outer spray cooling.	Stable temperature and steam stratification developed near the injection location. Hydrogen stratification observed with enhancement in the upper containment due to low steam injection and later spray cooling.

Table 3.1 Experiments on Containment Thermal Hydraulics and Hydrogen Distribution (cont.)

Facility/Experiment	Type	Test Conditions	General Observations
HDR E11.4 (Project HDR benchmark)	INT SBLOCA	similar to E11.2 but with 34h pre-heat. Steam and hydrogen/He release into lower containment. Simulation of core degradation effects on containment response using dry heat addition to low containment atmos. and steam injection into sump.	uniform mixing (no stratification) due to low injections. Alpha block heat transfer data provides assessment of long-term natural convection condensation.
CVTR test #3	INT MSLB	superheated steam blowdown (166 sec) in upper containment.	stable temperature and steam stratification observed.
CVTR test #4, #5	INT MSLB	similar to CVTR test #3 except pressure reduction is aided by sprays.	Pressure reduction with the addition of sprays - data indicates ~ 100% spray efficiency. Enhanced mixing observed with the addition of sprays.
NUPEC M-7-1 (ISP-35)	INT	steam pre-heating 30min helium/steam release at the low-elevation and internal water spray followed by mixing period.	good mixing due to strong spray source. Early pressure reduction reversed by hydrogen/steam injection.
NUPEC M-8-2	INT	similar to M-7-1 except with mid-elevation injection.	internal sprays enhances mixing.
NUPEC M-8-1	INT	similar to M-8-2 except no internal water spray.	stable temperature and gas stratification.
NUPEC M-4-3	INT	similar to M-8-1 except with low-elevation injection.	reduced temperature and gas stratification effect.

** SE - Separate Effects
* INT - Integral Effects

Table 3.2 Summary of the International Standard Problems used for CONTAIN Code Assessment

Facility	Test	ISP #	Accident Simulation Type	References
HDR	V44	ISP-16	LOCA*	Fir85, Val83, Wol83
HDR	T31.5	ISP-23	LOCA Beyond DBA**	Kar89, Wen87
HDR	E11.2	ISP-29	SBLOCA*** SA****	Kar92, Til92, Mur96
NUPEC	M-7-1	ISP-35	SBLOCA SA	OECD94, Sta95, Sta98, Mur96

* Loss-of-Coolant Accident

** Beyond Design Basis Accident (includes hydrogen release)

*** Small Break Loss-of-Coolant Accident

**** Severe Accident (includes hydrogen release in addition to other core debris effects)

Table 3.3a Highly ranked containment phenomena addressed in experiments based on the design and beyond design basis ranking criteria.

		Experiment												
		separate			integral									
Component/Process	Phenomena	Visc. flat plate	Phebus FPTO	JAERI spray	HDR V44	HDR T31.5	HDR E11.2	HDR E11.4	CVTR test #3	CVTR test #4,5	NUPEC M-7-1	NUPEC M-8-2	NUPEC M-8-1	NUPEC M-4-3
Atmosphere:														
pressurization	multi-component gas compr./exp.		3	3	3	3	3	3	3	3	3	3	3	3
	spray mass and energy exchange			3						3	2	2		
	atmospheric cooling by fan cooler													
mixing	jet-plume gas interaction/entrainment				1	1	2	1	1	1	1	1	1	1
	buoyancy/stratification (regional)			3	3	3	3		3	3	3	3	3	3
	spray dynamics			2						2	2	2		
	fan dynamics													
transport	buoyancy				1	3	3	3	3	3	3	3	3	3
	form and friction losses				3	3	1	1	1	1	1	1	1	1
Structure Interior:														
heat transfer	1-D transient conduction				3	3	3	3	3	3	3	3	3	3
Structure Surface:														
mass transfer(cond/evap)	free convection	3	3	1	3	3	3	3	3	3	1	1	1	1

[ ] not present, 1 - present, 2 - present and significant, 3 - measured

Table 3.3b Medium(only) ranked containment phenomena addressed in experiments based on the design and beyond design basis ranking criteria.

		Experiment												
		separate			integral									
		Wisc. flat plate	Phebus FPTO	JAERI spray	HDR V44	HDR T31.5	HDR E11.2	HDR E11.4	CVTR test #3	CVTR test #4,5	NUPEC M-7-1	NUPEC M-8-2	NUPEC M-8-1	NUPEC M-4-3
Atmosphere:														
mixing	buoyancy/wall interaction (regional)				1	1	1	1						
transport	liquid water carry over				2	2	1	1						

[ ] not present, 1 - present, 2 - present and significant, 3 - measured

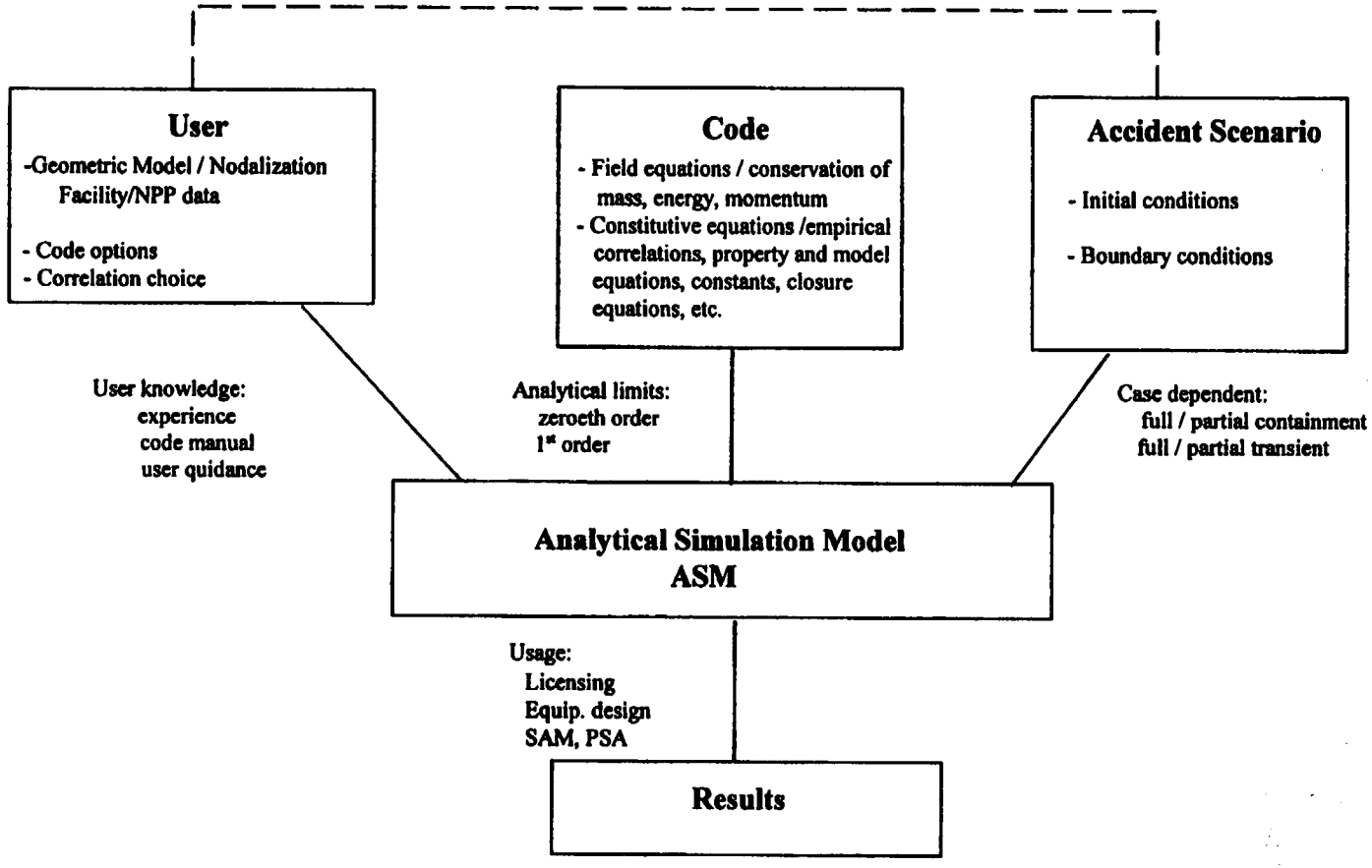

Figure 3.1 Components of a Analytical Simulation Model

3.2 Facility and Test Scaling

A listing and brief description of each facility modeled for the experiments is given in Table 3.4. An issue that is especially important for the integral facilities is scale distortion. Distortions can occur mainly from geometric and boundary condition scaling. In most cases attempts are made to minimize distortions so that the interaction of phenomena in the test is similar to the prototype. In separate effects testing the scaling issues that involve interacting phenomena are minimized. Scaling of separate effects tests is typically addressed through the experimental procedure such that the appropriate test limits are set to ranges expected in the prototype. For instance, in condensation tests the air/steam mass ratios will be chosen as representative of typical containment atmospheric composition during a postulated accident event, and the flow velocities of the mixture along a condensing surface will be selected to be similar to observed or estimated flows. In the case of separate effects for spray phenomena, representative volumetric spray rates are used to investigate spray pressure suppression phenomenon. In the case of integral testing, the complicated nature of the test scenario or procedure will tend to obscure some of the effects of scale distortions on interacting phenomena. For this reason it is important to exercise codes for a variety of scales together with well planned separate effects testing. In this way scale effects on phenomenon and phenomena interactions can be evaluated. Once the phenomena modeling and the effects of scale are demonstrated by application and assessment of the code to various tests, the code can be used to perform scaled-up analysis of prototypical plants and accident scenario. It is therefore important that the assessment matrix for the code be comprised of a variety of integrated test facilities and complemented by separate effects. Some topics relating to geometric and boundary condition scaling are discussed in the following subsections.

3.2.1 Geometric Scaling

Shown in Figures 3.2 to 3.4 are drawings of each integral test facility considered in this report: HDR, CVTR, and NUPEC. Figure 3.5 is a sketch of the approximate size for each facility compared to a representative large dry PWR containment. Listed in Table 3.5 are key geometric dimensions and other parameters for these facilities compared to a typical PWR containment. The entries in this table are combined in Table 3.6 to give geometric scaling parameters. From these tables a number of observations can be made: first, the volumetric scales range from 2% to 17% of a full size containment; second, the amount of long-term heat sinks in each facility is significantly greater than a comparable containment; third, the amount of short-term heat sinks is greater for these facilities than in a prototypical containment; and finally, except for the NUPEC facility the linear scales of both HDR and the CVTR are distorted somewhat with respect to U.S. containments; the facilities have a larger aspect ratio than the containments that they model.

The range in volume and linear scales provides a limited basis on which to address scale distortion effects in assessed phenomenological models, specifically with regards to heat and mass transfer modeling. Presence of both short and long-term heat sinks in the HDR and CVTR mean that these facilities are useful for investigating transients of both short and long duration.

However, since all the facilities have more heat sink material than a properly scaled containment would have, it can be anticipated that heat and mass transfer effects will tend to be over-emphasized in these types of facilities compared to full containments. Discrepancies in mass and heat transfer models will therefore tend to be amplified for these facilities. Furthermore, the large aspect ratios of the facilities will tend to accentuate buoyancy and stratification effects, the exception being the linearly scaled NUPEC facility. It is also recognized that the facilities will typically have flow path characteristics (flow resistance and end path elevations) that are quite different from most containments, and these differences as well should be considered when discussing issues related to geometric scaling. For instance, some facilities may have tortuous flow path connections coupling source regions with lower regions that have significant heat sink area, as is the case with the HDR facility compared to typical containments. Since flow path characteristics may also influence the behavior and modeling of flows driven by small pressure differentials, geometric scaling may in some extreme cases extend beyond the key dimensional factors given in Table 3.5. These concerns however are typically covered on a case by case basis when making comparisons of code and experimental results.

3.2.2 Blowdown Rate Scaling

The type (single or two phase), duration and magnitude (mass rate) of the steam injection for each test can be compared to typical plant LOCA and MSLB blowdown. The steam blowdowns for the HDR tests are two phase during the first 10-20 seconds of the blowdown. This initial two phase period is followed by a short period of superheated steam injection, with a decreasing injection rate. Overall, the injection profile for the HDR blowdown tests are similar to a plant LOCA, as shown in Figures 3.6 and 3.7. The rate of energy addition per unit free volume and total energy addition per unit volume are, however, smaller in the tests than in the plant LOCA, as illustrated in Figures 3.8 and 3.9, respectively. In the case of CVTR, test #3 simulates a rupture in the secondary loop of the reactor system, as would occur in a MSLB scenario. As seen in Figure 3.10, the injected steam is superheated for both the test and plant; therefore both injection types are similar. The injection mass rate comparison for test and plant in Figures 3.11 and 3.12 shows that the test blowdown mass injection rate and energy addition per unit facility volume are significantly below that for the plant. In addition, the test blowdown lasts about twice as long as that for the plant MSLB (this observation assumes successful closure of pipe valves for the plant -- there is some uncertainty with regard to this assumption). As a result, the blowdown period is skewed to longer times for the MSLB simulation even though the total energy addition per unit volume at the end of both plant event scenario and test is comparable, as shown in Figure 3.13. The protracted steam injection in the CVTR test will tend to allow more energy transfer to heat sinks during the blowdown than one would expect in a MSLB plant scenario.

Both the HDR and CVTR facilities used either an impingement plate or diffuser to minimize steam jet interactions with the surrounding containment walls or equipment, since direct interactions could damage the facility. As a result of the use of an impingement plate or diffuser,

Froude numbers can not be calculated for these blowdowns.

With relatively high heat sink (area or mass) to volume ratios and lower energy injection rates per unit volume, the tests will presumably have pressure responses that are significantly more sensitive to containment heat transfer than that of the plant. Therefore, uncertainties in the modeling of heat transfer processes, such as condensation, might appear more important than they are in the plant. The scale variations of the heat sinks and injection rates should be recognized when using the test comparisons to validate codes for DBA analysis. For example, pressure errors in the CVTR blowdown tests due to inaccurate heat and mass transfer modeling (i.e., forced/mixed convective condensation) would be reduced if the injection period was scaled to a typical plant blowdown release interval. In the case of variations in gas temperature and concentrations, those variations will be greater in a facility like HDR where large stratification gradients may develop as a result of the extended vertical dimension of the facility. And the very high metal to volume ratio of the NUPEC facility will tend to exaggerate short-term pressure response caused by the interaction of sprays with the metal walls. These anticipated distortions must be recognized during the assessments, since they are part of the known facility and test boundary conditions that affect our efforts to provide a similar ranking of the phenomena and processes in both experiment and plant during a design or beyond design basis accident.

3.2.3 Spray Injection Scaling

Shown in Table 3.7 are the scaled spray injections for the various pressure suppression tests calculated in this report. The spray flows are given according to the specific volumetric spray rates F/V ($m^3/hr/m^3 \rightarrow hr^{-1}$), where F is the spray rate in m^3/hr and V is the containment volume, and specific mass spray flux $\dot{M} / A$ ($kg/s\text{-}m^2$), where $\dot{M}$ is the mass spray rate in kg/s and A is the containment cross-sectional area. Spray temperatures are also listed in the table; the nominal values (comparable to plants) range from approximately 310 to 313 K. Scaled injection rates $(F/V)_{facility}/(F/V)_{plant}$ and $(\dot{M}/A)_{facility}/(\dot{M}/A)_{plant}$ range from 0.82 to 8.7 and 1 to 2.6, respectively, based on a single spray train operating during a postulated DBA in the San Onofre plant.[3] The JAERI test PHS-6 is perhaps the best scaled test for this type of scenario where at least some spray trains are expected to fail. Other integral tests in the CVTR and NUPEC facilities are more representative of multiple spray trains in operation.

[3] San Onofre 2/3 plant data are used to represent a typical PWR large dry containment.

Table 3.4 Experimental facilities			
Facility	**Type (status)**	**Configuration/Size/ Typical Problems**	**Instrumentation**
Integral:			
HDR	German decommissioned steel PWR containment with internal and external spray systems (decommissioned test facility, 1995)	MC* (~70), 11300 m^3 full, about 1/3 of volume in open volume above operating deck very complex containment with large surface/volume ratio	pressure gas and steam concentrations gas temperature structure temperature and heat transfer blocks (conc. and lead) velocity
CVTR	decommissioned research reactor containment - steel lined concrete, with internal spray (decommissioned test facility)	Volume divided vertically into three relatively open regions, ~6400 m^3 with ~2500 m^3 below the operation deck, flow paths not prototypical	pressure gas temperature structure temperature and two heat transfer plugs in above deck concrete shell
NUPEC	insulated steel containment model of Japanese PWR with steel internal partitions, with internal sprays (to be decommissioned)	MC (25-26) 1300 m^3 short-term tests only, no concrete structures	pressure gas concentration (29-30) gas/steam temperature(34) structure temperature(146)

Table 3.4 Experimental facilities (continued)			
Facility	**Type (status)**	**Configuration/Size/ Typical Problems**	**Instrumentation**
Separate Effects:			
Phebus	generic steel vessel, part of integrated fission product transport test rig (currently in use)	SC** 10 m^3, 5.7 m height	pressure gas concentration (1) gas temperature(25) structure temperatures condensate mass sump temperature (4)
JAERI spray vessel	generic steel vessel, no partitions. Spray nozzles located at various elevations	SC 700 m^3, ~ 20m height simulated dome spray	pressure (3) gas temperature (59) sump temperature (1)
Wisc. Flat Plate	channel configuration - test chamber can be rotated from vertical - concurrent flow	~1.9 m in length with 1m cooled plate.	Plate temperature gas temperature in channel flow rate heat flux to plate (local and integral) gas/steam composition

* MC - multiple compartment
** SC - single compartment

Table 3.5 Dimensions and Scaling Parameters of Typical PWRs (approximate) and Integral Experimental Facilities					
	Containment Type		Experimental Facility		
	Large Dry	Ice Condenser	HDR	NUPEC	CVTR
Shape[1]	C	C	C	C	C
Type[2], Pressure[3] (kPa(a))	L, 520	S, 185	S, 300	S, 150	L, 300
Volume (m^3)	65000	36000	11300	1310	6426
Height (m)	64	60	60	17.4	35
Diameter (m)	43	40	20.7	10.8	17.4
Dome shape[4]	H	H	H	H	H
Dome vol. (m^3)[5]	50000	23000	4800	930	3964
# Compartments	20	12	70	25	6
LT heat sink S/V ratio[6]	0.25	0.32	0.88	0.0	0.56
ST heat sink M/V ratio[7]	38.6	86	48.3	70	65.6

Notes: [1] cylindrical (C); [2] type of pressure boundary: steel (S), steel-lined concrete (L); [3] design pressure for reactors, typical max. test pressure for exper.; [4] hemi-spherical (H), elliptical (E); [5] open region above opertion deck; [6] long-term heat sink surface-to-volume ratio (concrete and steel clad concrete); [7] short-term heat sinks mass-to-volume ratio (misc. steel, steel partitions, shell, etc.)

Table 3.6 Geometric Scaling Ratios for Test Facilities [Based on the San Onofre Plant]				
Facility	$V_{facility}/V_{plant}$	$\frac{(A_{conc} / V)_{facility}}{(A_{conc} / V)_{plant}}$	$\frac{(m_{fe} / V)_{facility}}{(m_{fe} / V)_{plant}}$	$\frac{(H / D)_{facility}}{(H / D)_{plant}}$
HDR	0.17	4.1	1.25	2.65
CVTR	0.1	2.24	1.7	1.75
NUPEC	0.02	0	1.8	1.08

Table 3.7 Containment spray tests for pressure suppression						
facility/plant	test/scenario	F/V* (hr^{-1})	$\frac{(F/V)_{facility}}{(F/V)_{plant}}$	$\dot{M}/A$** ($kg/s\text{-}m^2$)	$\frac{(\dot{M}/A)_{facility}}{(\dot{M}/A)_{plant}}$	spray temperature (K)
San Onofre	LOCA***	0.0061	1	0.076	1	310
JAERI	PHS-6	0.005	0.82	0.025	0.33	313
	PHS-1	0.03	4.9	0.15	2	313
NUPEC	M-7-1	0.053	8.7	0.2	2.6	313
CVTR	test #4	0.010	1.64	0.077	1	288
	test #5	0.018	2.95	0.13	1.7	288

* total volume
** total cross-sectional area
*** one spray train assumed to be operational

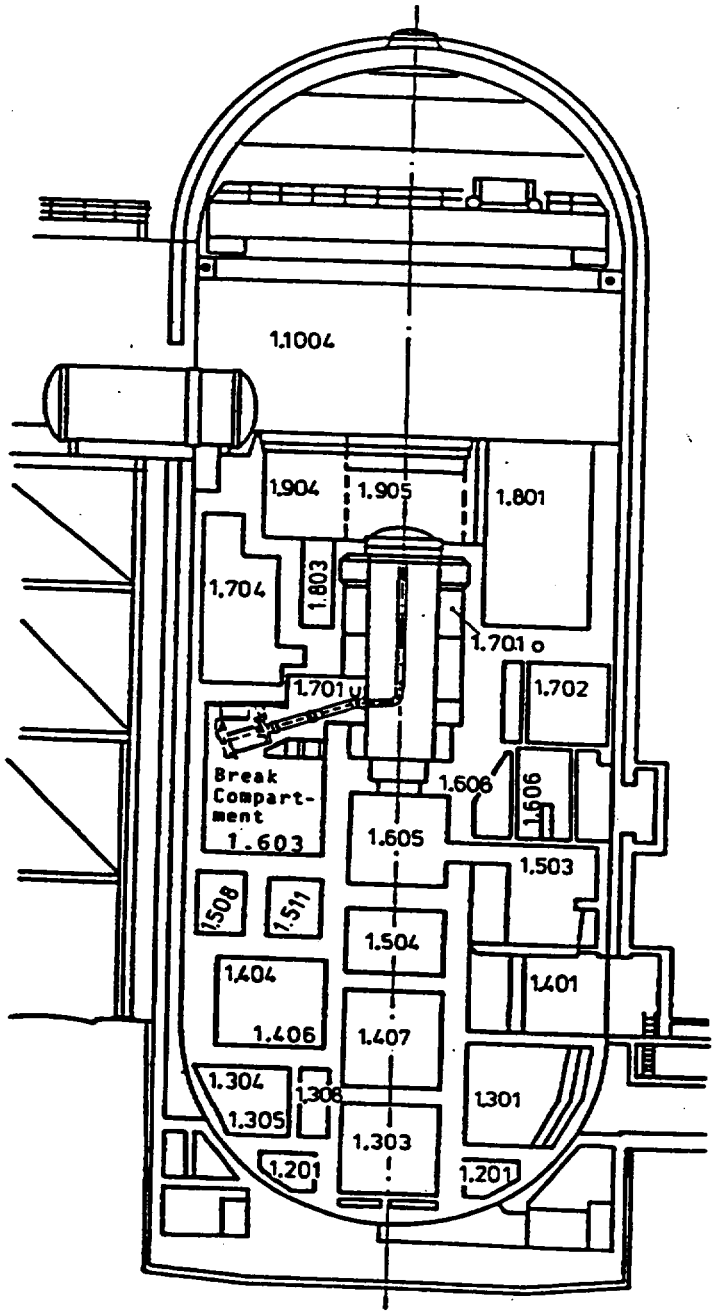

Figure 3.2 HDR test facility showing the breakroom 1603 for test V44; 1704 was used for test T31.5; 1805 and 1405 were the injection rooms for E11.2; and, 1405 was the injection room for E11.4

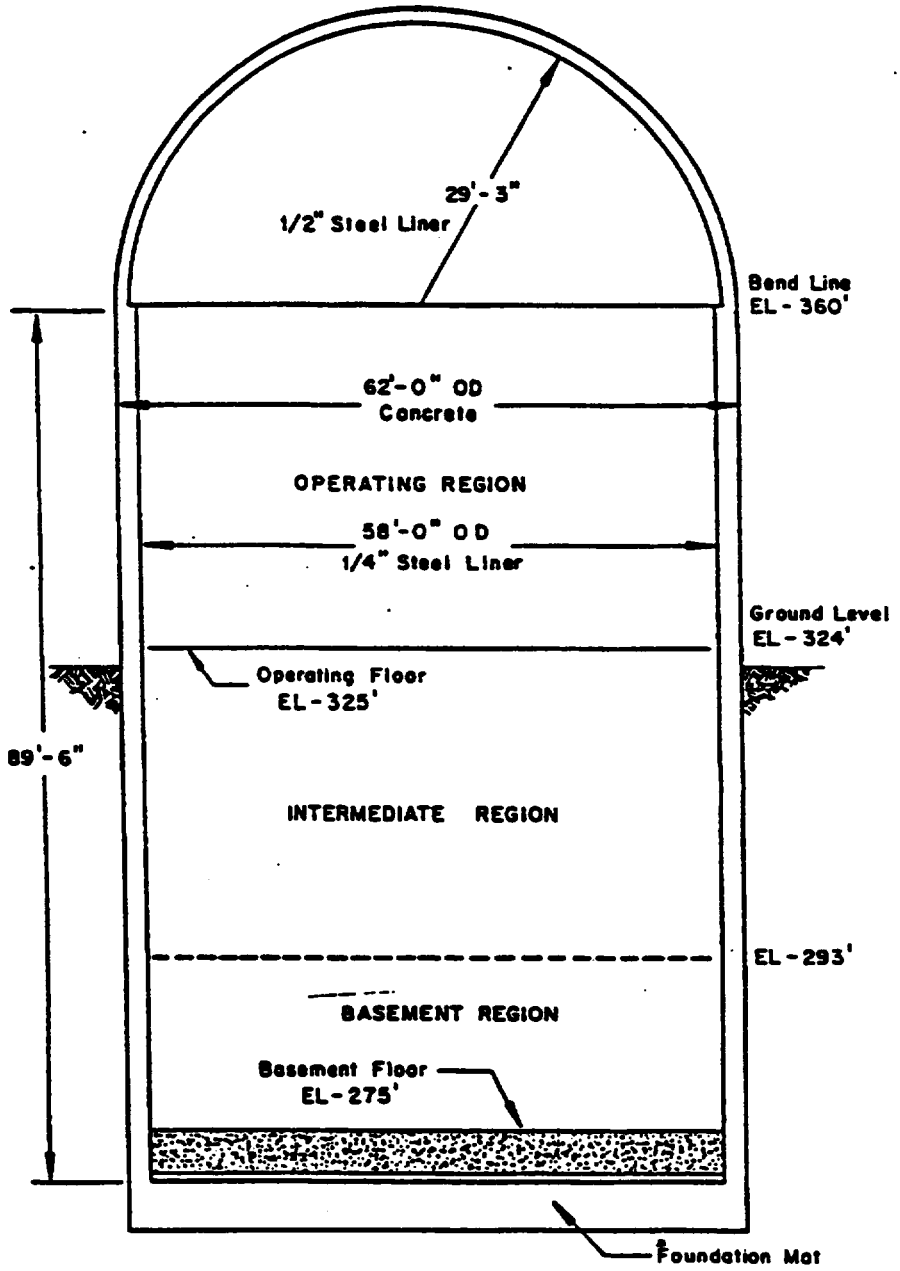

Figure 3.3 CVTR test facility.

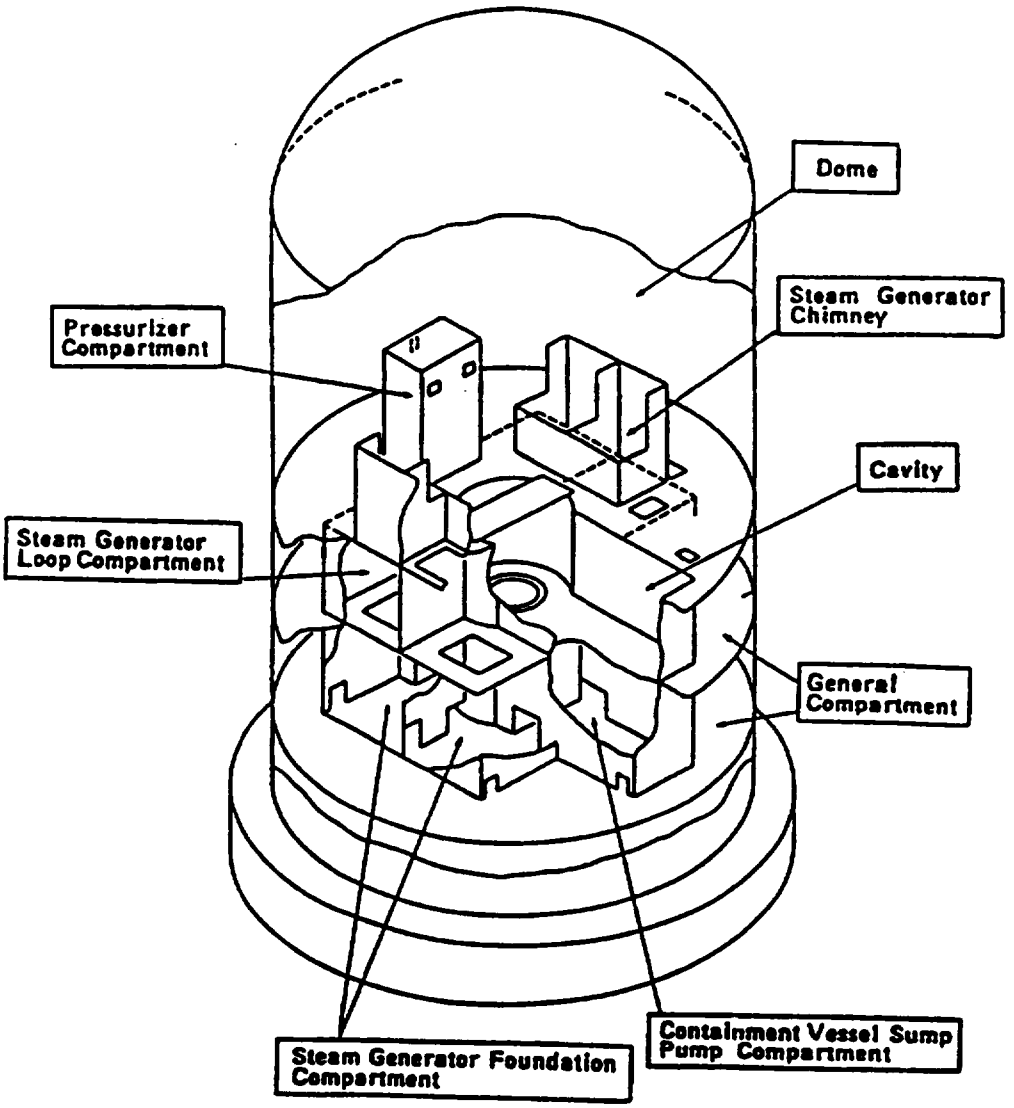

Figure 3.4 NUPEC test facility

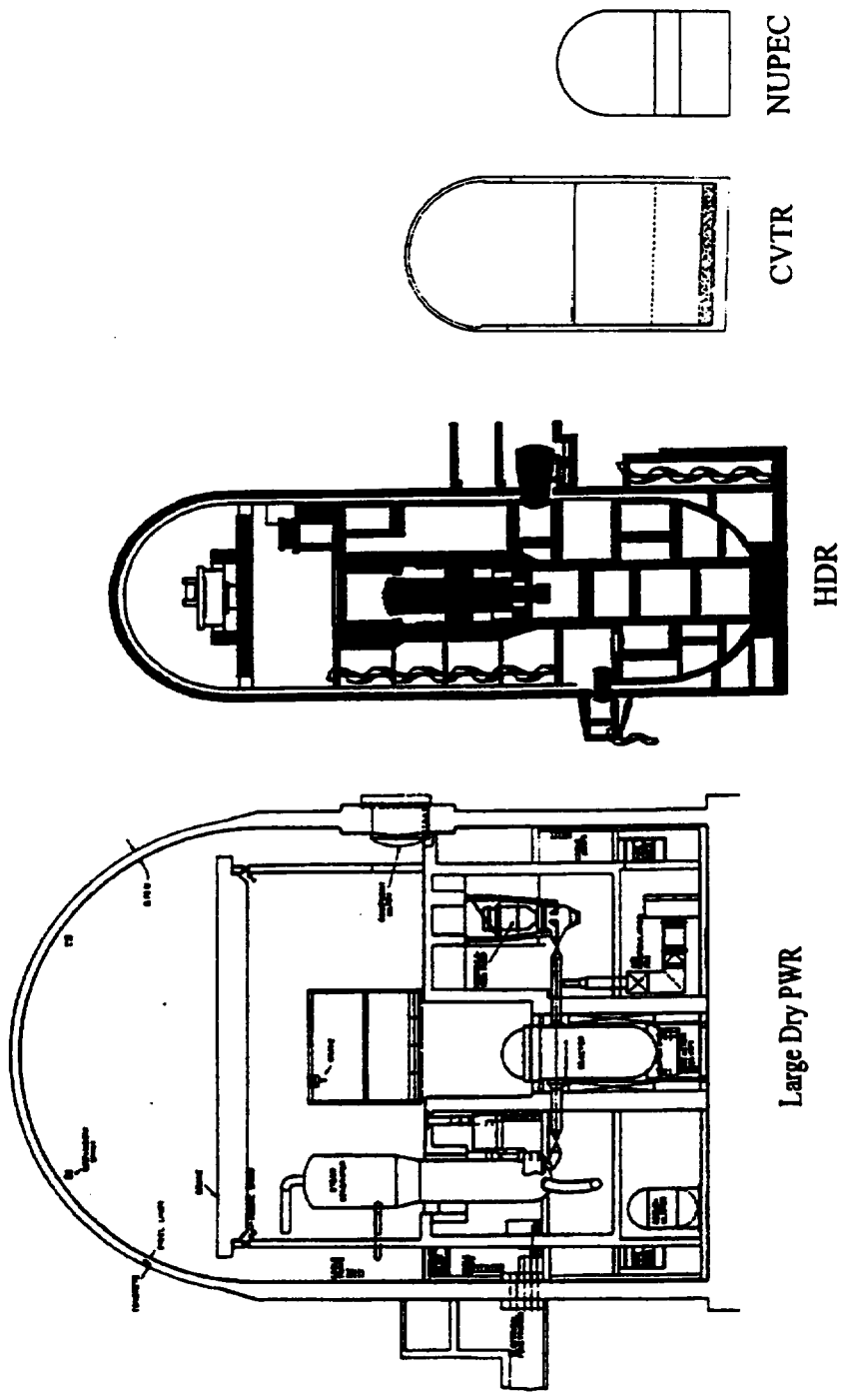

Figure 3.5 Approximate scales of integral test facilities compared to a large dry PWR containment.

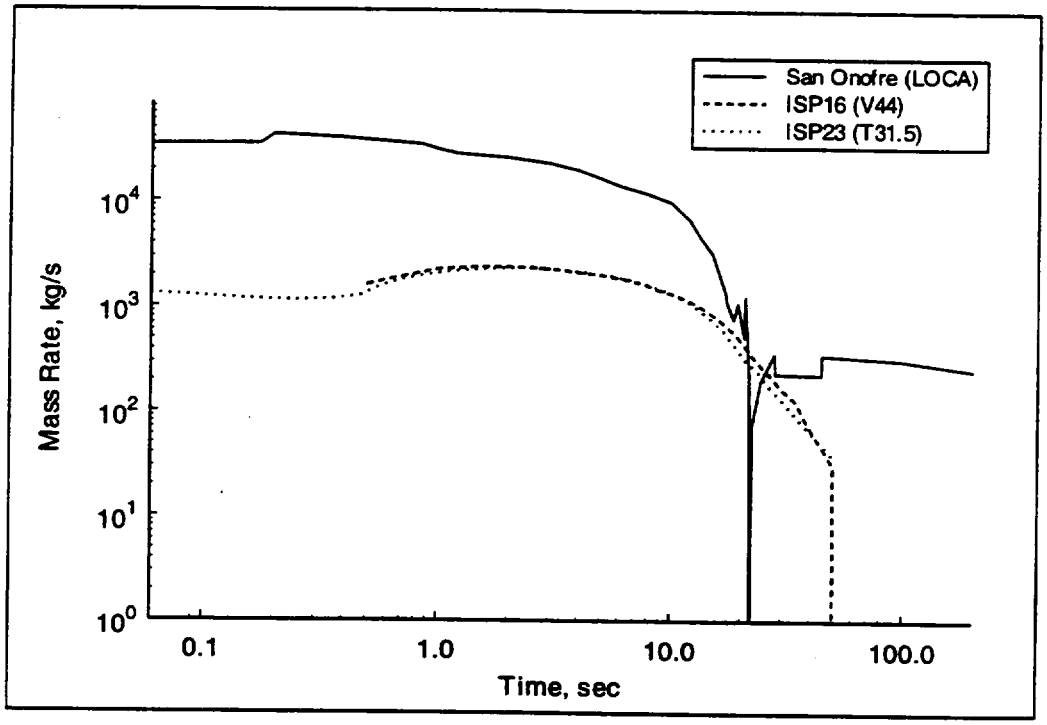

Figure 3.6 Steam injection rates for large pipe ruptures in the HDR facility and San Onofre plant

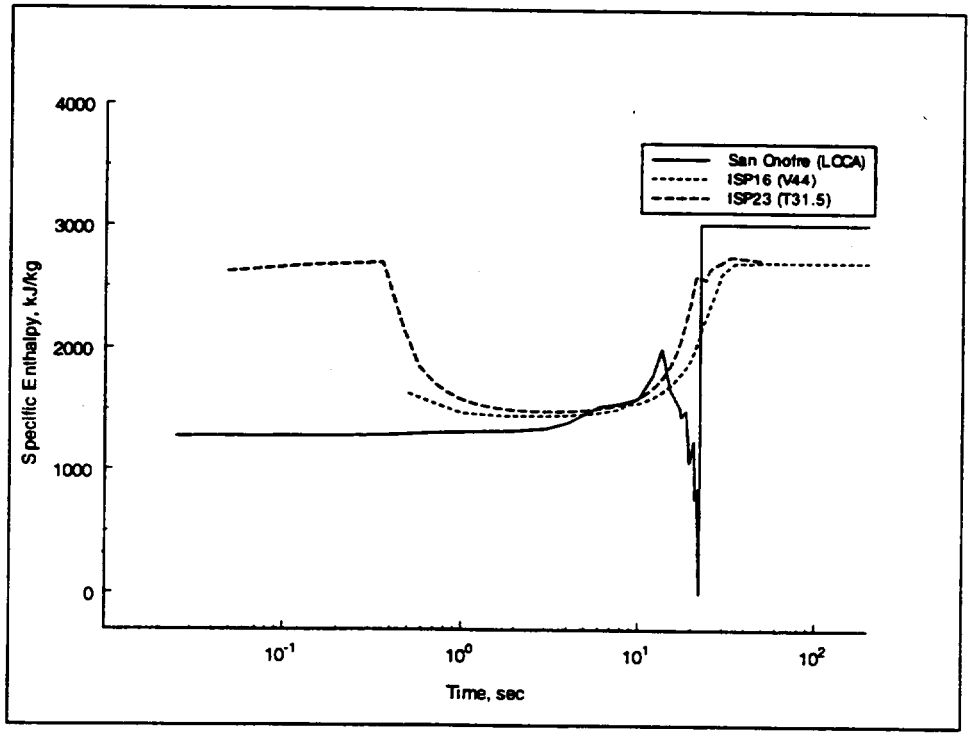

Figure 3.7 Steam enthalpy for large pipe ruptures in the HDR facility and the San Onofre plant.

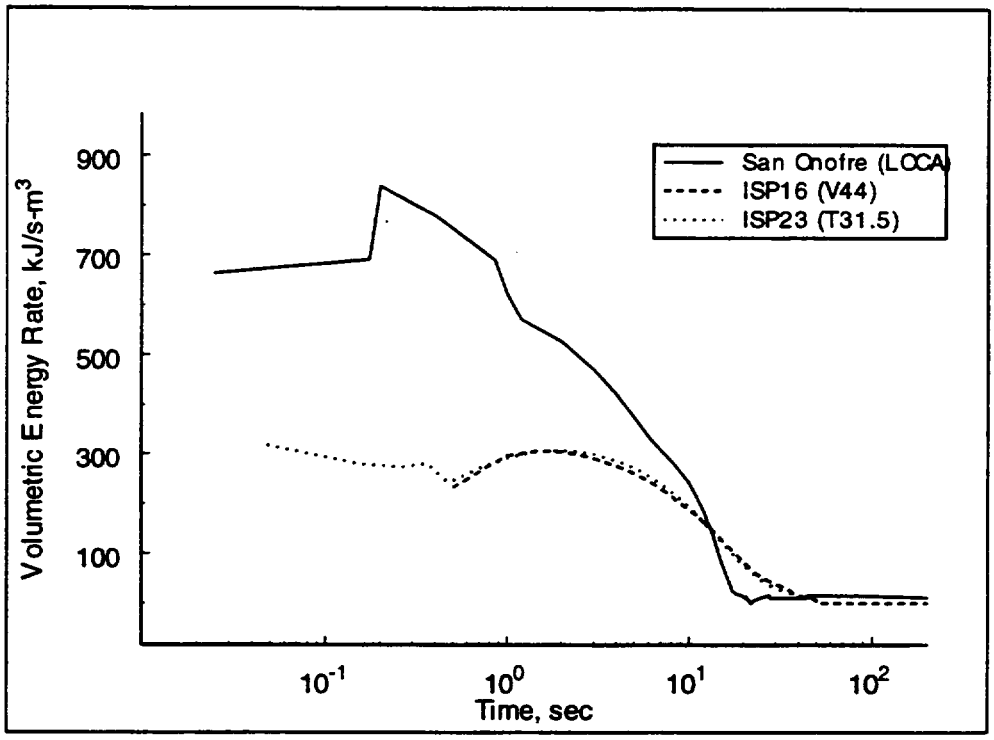

Figure 3.8 Specific energy rates for steam injection to the HDR facility and San Onofre plant.

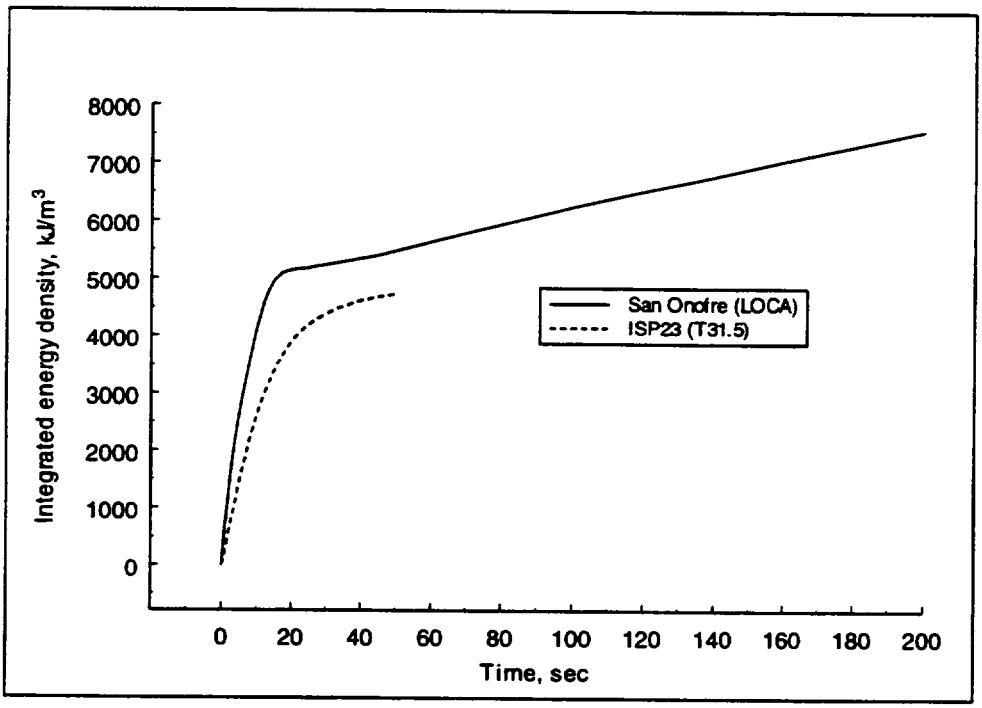

Figure 3.9 Cumulative energy addition for the HDR facility and San Onofre plant.

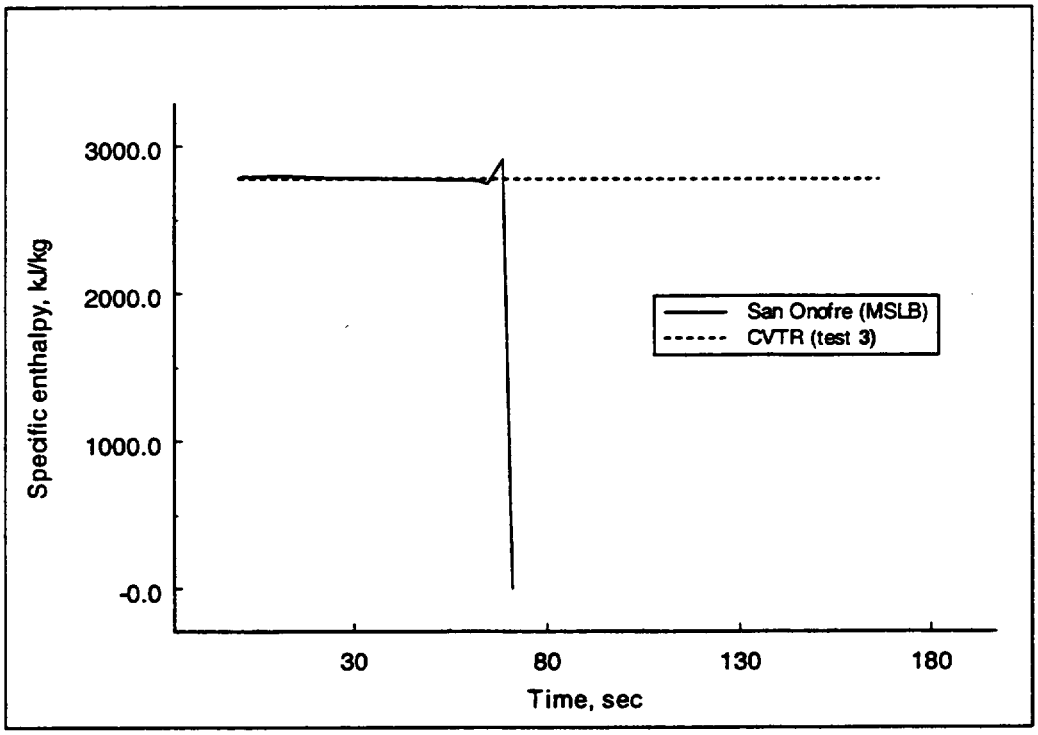

Figure 3.10 Steam enthalpy for the CVTR test#3 and San Onofre MSLB.

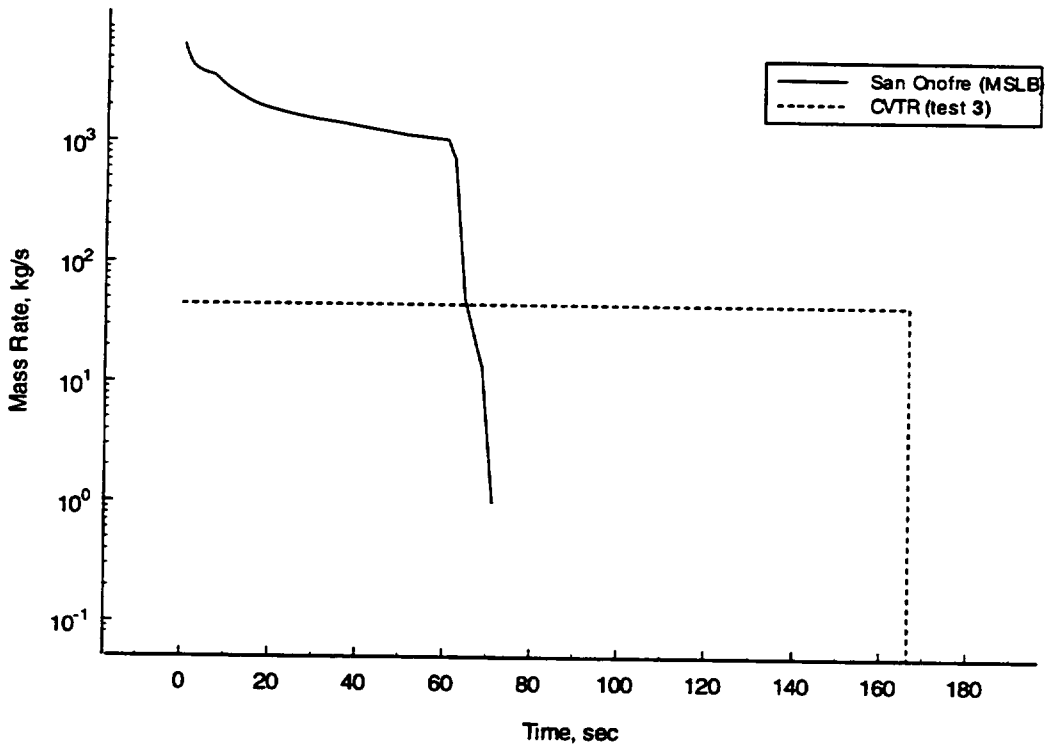

Figure 3.11 Steam mass rate injection for CVTR test #3 and the San Onofre MSLB.

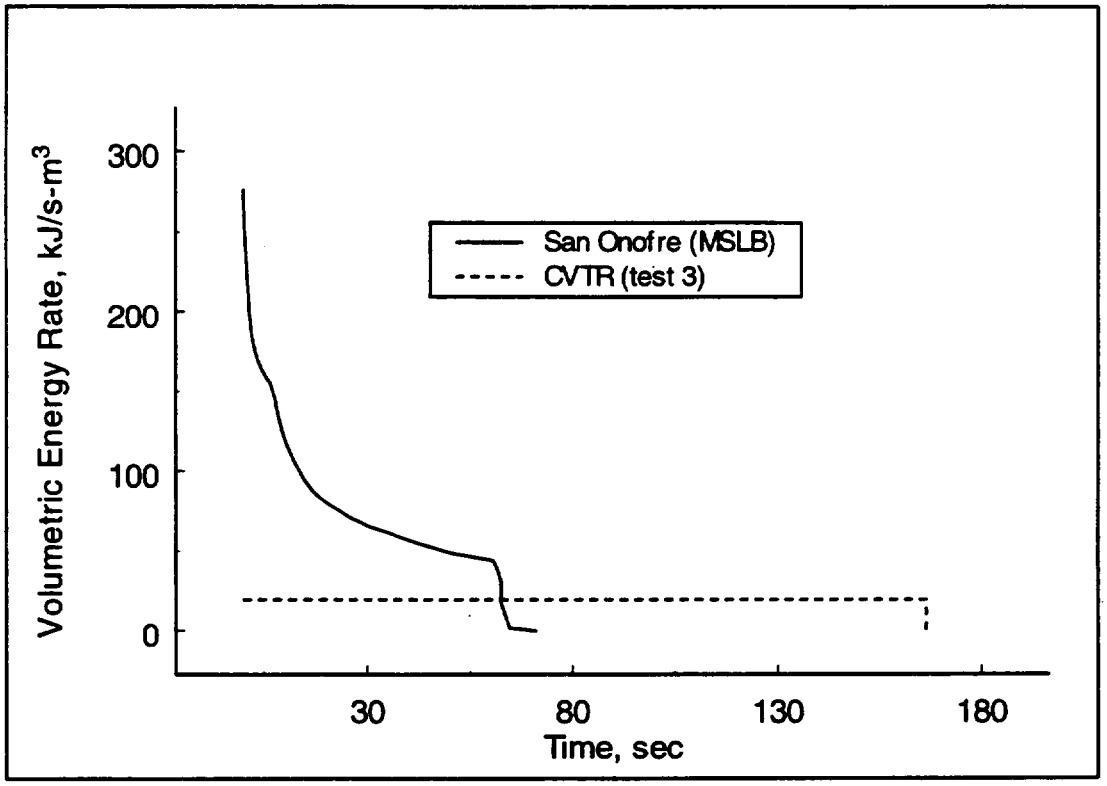

Figure 3.12 Specific energy rate for the CVTR test #3 and the San Onofre MSLB.

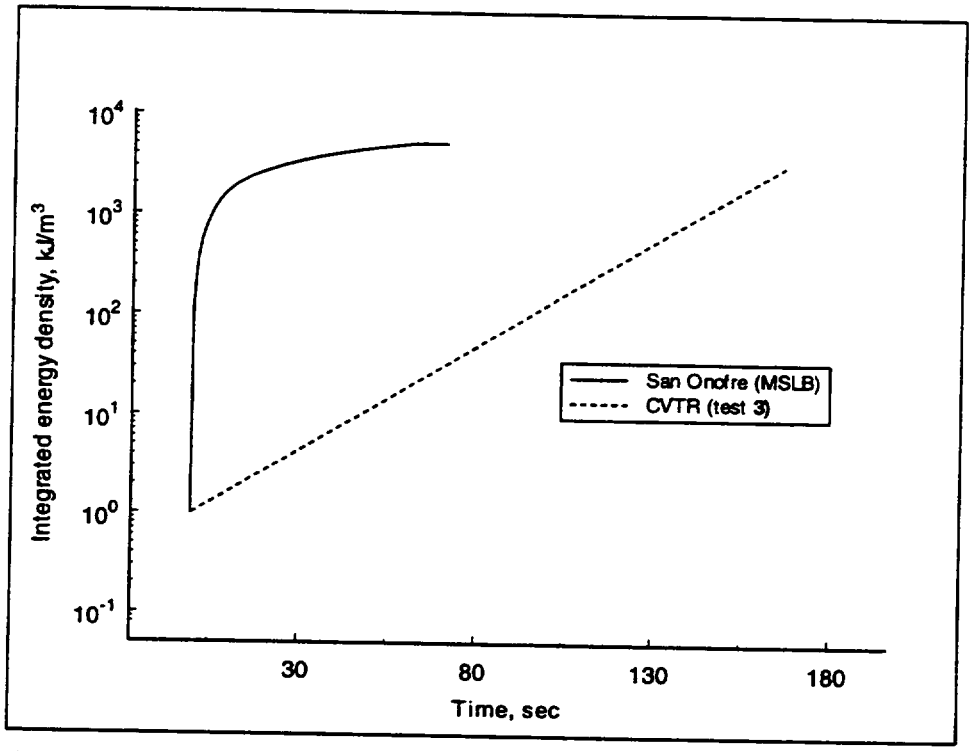

Figure 3.13 Cumulative specific energy addition for the CVTR test #3 and the San Onofre MSLB.

3.3 Reference Calculations

CONTAIN input decks are provided for all reference calculations in Appendix A. These decks archive assessment calculations for twenty tests, nine separate effects and eleven integral tests. The inclusion of these decks, in addition to providing a paper trail for the assessments, serve to clarify any questions that the reader has on the details of the input (model options, etc.); the listings are also useful in reviews for user guidance in preparing other CONTAIN code input for test analyses, design basis, or beyond design basis accident simulations.

3.3.1 Separate Effects

3.3.1.1 Wisconsin Flat Plate Condensation Tests

The Wisconsin flat plate condensation tests are described in Huh93. These tests examine the effects of surface orientation on the condensation of steam in the presence of air. An air-steam mixture is directed into a rectangular flow-channel over a condensing surface that has a painted surface finish of high thermal conductivity and good wetting characteristics. The mixture flow is concurrent with the condensate flow. A series of tests were run for various surface orientations that varied from 0 to 90 degrees (vertical wall), air-steam mass fractions of 0 to 0.87, and mixture velocities of 1-3 m/s. Surface condensation was found to be a weak function of orientation; therefore, only the vertical test orientation is reported here, i.e., the flow direction is downward.

Local heat transfer coefficients are determined from measured bulk atmosphere, surface temperature data and heat flux measurements taken along the length of the condensing plate. Average heat transfer coefficients are calculated using the measured total energy transfer to the entire plate via an energy balance on the plate coolant fluid. The coolant fluid is used to maintain a constant plate temperature throughout a test sequence. All the measurements are taken at steady state.

Shown in Figures 3.14 and 3.15 are sketches of the experimental apparatus. The test section is made of 1905 mm long polycarbonate-plates that are sandwiched to form a 152 mm square duct. The first 838 mm of the test section functions as an entrance length for the condensing mixture. This length is calculated to be sufficiently long so that the free stream turbulence level of the gas stream is dampened. The total length of the apparatus is such that the boundary layers of the opposite walls do not interact significantly; therefore, the test duct is a simulation of a flat plate condensing experiment. Condensation takes place on the cooled plate which is 1066 mm in length. The tests are conducted at 1 bar total pressure.

The CONTAIN code was used to calculate the heat transfer coefficient for six tests that included air to steam ratios of 0.29 to 3.5, bulk to surface temperature differentials of 30 to 60 degrees,

and flow velocities of 1 to 3 m/s. The results of these comparisons are shown in Table 3.8.

At issue for this assessment were: 1) the accuracy of the heat and mass transfer analogy method under controlled condensing conditions (natural to forced convective regimes); 2) usage of the default CONTAIN mixed convective algorithm; and 3) adequacy of the film theory correction factor included in the CONTAIN model for adjustments during high mass transfer rates.

The results from this assessment show that the CONTAIN calculated condensation coefficients (i.e., total heat transfer coefficients) for five of the six case runs are within ~ 10% of the measured coefficients, only one case is calculated with a coefficient error greater than 10% (14% error). The measurement accuracy for these tests is reported to be +/- 10%; therefore, by including the experimental error bounds, all CONTAIN results are within 10% of the experimental measurement band for measured total heat transfer coefficients.

The reference cases shown in Table 3.8 for each test run were calculated using the default mixed convection heat transfer algorithm which uses the maximum of the forced or natural Nusselt number and the film flow calculated by the code which assumes laminar flow along the plate. The use of the maximum Nusselt number for this flow condition is consider appropriate since the buoyancy and force convective contributions are opposed and therefore, for turbulent flow, are aiding in the mixed convective regime.

Condensation (or evaporation) is calculated in the CONTAIN code using a film-theory algorithm that corrects for high mass transfer effects on the mass transfer coefficient. This correction can be extracted from the implemented condensation equation in the code and written as a ratio of an corrected to uncorrected Sherwood number, F = Sh / Sh*, where Sh is the corrected Sherwood number and Sh* is the uncorrected Sherwood number. Shown in Table 3.9 are the ratios for each test in the flat plate condensation tests. The subscript "nc", "f", and "mix" refer to the Sherwood number for natural, forced, and mixed convection, respectively. According to the default mixed convection algorithm, and the film theory correction factor, the Sherwood number used to determine condensation rates in the tests is $Sh_{mix} = F \bullet \max(Sh_{nc}, Sh_f)$. Tests #3 through #6, specifically, are conducted with substantial temperature differentials such that the condensation rate is high; and therefore, the correction factor F for adjusting the mass transfer coefficient is significant, ranging from 1.33 to 2.1, respectively. These correction factors were applied, in an essentially direct fashion, also to the derived condensation coefficients listed in Table 3.8. The fact that the derived coefficients are within the 10% uncertainty band at these high mass transfer rates is an indicator that the film theory algorithm used in the code for correcting for mass rate effects is sufficiently accurate. More detail on this subject is included in Section 4.0, dealing in

part with sensitivities to various modeling assumptions such as the treatment of high mass rates effects.[1]

Table 3.10 shows the relative magnitude of the various component heat transfer phenomena for film condensation on the plate. The components are q_{conv} (sensible heat transfer by convection), q_{cond} (latent heat transfer by condensation), and q_{film} (sensible heat transfer by film advection). The total heat transfer to the plate q_w is given by

$$q_w = q_{cond} + q_{conv} - q_{film}$$

From this table, the importance of latent heat transfer for air/steam mixtures is shown to be high. Other components are shown to be less than 10% of the total energy transferred from the atmosphere to the plate surface.

The mass rate correction is substantial for test cases #4, #5, and #6. In case #6, the correction is determined to be greater than a factor of two. The consistent agreement of calculated and measured coefficients over such a range in mass transfer rates validates the use of the film correction theory for air/steam mixture condensation under the conditions of this test series, which is similar to atmospheric to metal condensation conditions in a containment during DBA like conditions.

3.3.1.2 Phebus Test FPT0

The Phebus Fission Product program includes a series of in-vessel and ex-vessel experimental efforts performed by the Institut de Protection et de Surete Nucleaire (IPSN) with contributions from the European Community Commission, Japan, Korea and the USA, at the Research Center of Cadarache (France) [Phe93]. In this report, only the thermal hydraulic behavior of the steam/gas mixture in the containment vessel during Phebus test FPT0 is considered. Initial conditions and transient results for this test are recorded in Reference [Phe94]. The test has a variable steam and hydrogen injection into a steel vessel (10 m^3) with temperature controlled surfaces, Figure 3.16. Condensation is allowed to occur only on three vertical condenser cylinders that extended from the top of the vessel. A detailed drawing of one of the condensers is shown in Figure 3.17. The upper portion of the condenser is held at a low temperature to enable

---

[1] It should be noted that some analysts have mistakenly reported that the CONTAIN code does not include model corrections for high mass transfer effects. This is a false impression. The code does include these model corrections; however, the reported Sherwood number listed in the long edit output listing is the uncorrected Sherwood number. In the implementation of the HMTA in the code, the uncorrected Sherwood number is effectively corrected for mass rate effects according to a film theory method [Bir65].

atmospheric condensation while other surfaces (vessel walls, dry condenser, etc.) are kept at an elevated temperature in order to inhibit condensation. Condensate drains from the upper cylinder walls into an inner region of the lower, dry condenser region (held at a temperature above the saturation temperature). The condensate mass is measured at frequent intervals during the experiment. From these measurements, the rate of condensation on the condensing cylinders is determined.

Steam is injected in the core mockup vessel upstream from the containment vessel at injection rates that vary from 0.0005 to 0.003 kg/s, Figure 3.18. During the steam/clad interaction period, hydrogen is generated in the core mockup region and the steam rate to the containment drops as a result of the steam/clad reaction. The injection location in the containment vessel is at low elevation which favors a well mixing volume. Independent field code calculations have been performed for the program [Phe94a]. These calculations, along with measured gas temperatures in the vessel, have verified that the vessel atmosphere is uniformly mixed during the test, and that the flow velocity along the condenser surfaces is small, well below 1 m/s. As an example, when the injection rate is 0.0015 kg/s, the calculated flow along the condensers is calculated to be 0.4 m/s. As a result of these investigations, it is apparent that this test is a useful separate effects test for natural convection condensation.

This test is simulated with the CONTAIN code using a single cell to represent the vessel atmosphere. Measured condenser (as a function of time) and vessel wall temperatures are specified in the simulation, Figure 3.19. Film flow modeling is used to predict the condensate film thickness along the condenser tubes, and the natural convective heat transfer equation for vertical walls is used to predict the Nusselt number at the condenser surface. Condensation in the code is modeled using the heat and mass transfer analogy method. Sensible heat transfer by convection and radiation is calculated in the code. The atmosphere is conditioned prior to the transient portion of the test; these conditions (pressure, relative humidity, and temperature) are used as initial conditions for the test [Phe94].

Since the vessel walls are heated above the saturation temperature corresponding to the partial pressure of steam in the vessel, heat transfer to the walls is only by sensible heat transfer (convection and radiation) which is significantly less than the atmospheric energy transfer to the condensers that occurs as a result of latent heat transfer during condensation. As a consequence of the relatively high wall temperatures and steam injection temperature, the bulk atmosphere is superheated throughout the test, as indicated by humidity measurement taken within the vessel.

Shown in Figure 3.20 is the comparison between measured and calculated pressure for the transient period of FPT0. The time period for the complete transient, as simulated, is approximately 24000 seconds (400 min.). Variations in the pressure are a result of changes in the steam injection rate and the variations in the condenser surface temperature. The very good pressure agreement is an indirect confirmation that condensation heat transfer is being simulated within the code with very good accuracy. It is an indirect indicator since the pressure response is

dependent both on the total energy of the atmosphere, which is dependent on the condensation rate on the condensers, but is also subject to the equation of state representing the atmosphere steam/air/hydrogen mixture. A direct indicator of the accuracy of the condensation modeling is the rate of condensation. Figure 3.21 shows the comparison between measured and calculated condensation rates. The driving potential for condensation is the difference between the steam partial pressures in the bulk and at the condensate surface. Those partial pressures, as determined in the code, are shown in Figure 3.22. The influence of the condenser wall temperature is reflected in the steam partial pressures which are a function of the condensate temperature. The agreement shown in Figure 3.21 is very good, and confirms the high accuracy of the natural convective condensation modeling in the code under conditions simulated by the test. With the condensation modeling confirmed through independent measurements, we can observe that the agreement previously noted for pressure now can be interpreted as meaning that the modeling for multi-component gas compression/decompression is also validated.

Shown in Figure 3.23 is the comparison between measured and calculated humidity in the vessel. The general trends are clearly predicted but the absolute values during the reduced steam injection period (~3000-10000 sec.) are in slight disagreement. This discrepancy is not serious since the experimental uncertainty associated with humidity measurements is relatively large for this test program; therefore, the humidity agreement is also considered very good given the acknowledged uncertainties in the measurement method.

Figure 3.24 shows a comparison of calculated and measured saturation and superheated temperatures in the vessel. The "measured" saturation temperature for the vessel was determined from total pressure data and the knowledge (based on temperature measurements) that the vessel atmosphere was uniformly mixed during the test. The good agreement between measured and predicted degrees of superheat validates the heat and mass transfer modeling method in CONTAIN under condition of superheating.

3.3.1.3 JAERI Pressure Suppression Spray Tests

A series of pressure suppression spray tests were conducted in Japan during the late 70's in a 700 m^3 steel vessel (20 m high, 7 m in diameter) [Kit78]. Two tests from that series are calculated in this report, PHS-1 and PHS-6. Spray water at a temperature of 313 K is injected into the vessel containing a saturated air/steam mixture at 3.5 bar. The initial condition for the spray testing is obtained by first injecting steam into the vessel atmosphere that is initially at 1 bar pressure. Vessel pressure is increased to slightly greater than 3.5 bars and then the steam is turned off and the pressure is allowed to relax to 3.5 bars before the spray is injected. The vessel steel walls are insulated on the outside and pre-heated by the steam to an approximate saturation temperature of the air/steam mixture prior to the spray injection. During the tests no condensation occurs on the walls.

Shown in Figure 3.25 is configuration for the single nozzle test, PHS-6. The injection height is 18 meters. A single nozzle has a spray distribution as indicated in Figure 3.26. With this distribution, it is expected that essentially no spray water will contact the vertical walls of the vessel; therefore, pressure suppression is assumed to involve the interaction of 100% of the spray water with the atmosphere. Since the temperature measurements in the vessel show that the vessel atmosphere is well mixed during the test, a single cell is used to model the vessel. A default spray droplet diameter of 0.001 m is used in the CONTAIN calculation: the diameter is based on an approximate mean droplet diameter for the average spray drop at the outlet of a typical spray nozzle. A sump is modeled to collect the spray water.

Shown in Figure 3.27 is the comparison of the measured and calculated pressure decline due to the spray from the single nozzle. The agreement is very good, and therefore represents confirmation of the spray energy exchange calculated in the code. Shown in Figure 3.28 is the comparison between the measured and calculated uniform temperature in the vessel during the spray period.[2] The slight increase in calculated temperature at about 2000 seconds reflects a transition in the calculated temperature from saturation to a slightly superheated condition. This condition is caused by the high rate of vapor removal from the atmosphere with the default droplet diameter of 0.001 meter. In Section 4, the choice of droplet size is investigated in a series of sensitivity calculations to show how size can affect atmospheric superheating.

Test PHS-1 differs from the previous test in that six nozzles are used, and the height of the injection is lowered to 15 meters above the floor. A single cell is also used to model this test, and a sump with overflow is also modeled according to the description of the test procedure to drain excess water during the high spray volume tests. Temperature measurements indicate uniform mixing below the sprays and up to approximately 2-3 meters above of the injection. With the additional spray nozzles, it could not be assumed that spray water does not contact the vessel walls. As spray water contacts the hot vessel walls some of the water will be evaporated into the vessel atmosphere. The evaporation will increase the vapor content of the atmosphere and slow the rate of pressure and temperature reduction for the atmosphere. Shown in Figure 3.29 are comparisons of measured and calculated pressure for a spray water distribution where 90% of the injected spray water interacts with the atmosphere and 10% of the injection is assumed to form a water film on the vessel wall. To model the water film flow and evaporation, the film tracking model in the code is used. In Section 4, the sensitivity of pressure suppression to the amount of water distributed to the vessel wall is investigated. The temperature of the atmosphere, measured and calculated for this test, is shown in Figure 3.30. Mixing below and above the injection is shown in this figure with the single cell calculation giving good results, except for the region near the top of the vessel where the assumption of uniform mixing begins to breakdown.

---

[2] Atmosphere-structure thermal radiation is not modeled for the JAERI spray tests.

Table 3.8 Comparison of CONTAIN and Experimental average heat transfer coefficients for the Wisconsin flat plate condensation experiments.

Case #	T_{mix}, C	T_w, C	m_{air}/m_{steam}	V, m/s	h_{calc}(ref)	h_{exp}	$h_{exp(max.\ min)}$
1	70	30	3.5	1	**103.8**	111.1	122.2 99.99
2	70	30	3.5	3	**210.7**	213.9	235.3 192.5
3	80	30	1.78	1	**165.4**	163.9	180.3 147.5
4	80	30	1.78	3	**296.9**	305.6	336.2 275.0
5	90	30	0.68	1	**292.1**	255.5	281.1 229.95
6	95	45	0.29	1	**501.5**	546.	600.6 491.4

Table 3.9 Sherwood numbers calculated in the CONTAIN code for the Wisconsin flat plate condensation tests.

Case #	T_{mix}, C	T_w, C	T_{if}, C	V, m/s	Sh_{nc}*	Sh_f*	F	Sh_{mix}
1	70	30	30.7	1	235.8	201.15	1.173	276.6
2	70	30	31.68	3	234.01	483.4	1.172	566.5
3	80	30	31.65	1	259.9	196.46	1.327	344.9
4	80	30	33.35	3	257.12	471.34	1.324	624
5	90	30	34.05	1	283.75	191.46	1.686	478.4
6	95	45	51.22	1	274.05	183.17	2.103	576.3

* Uncorrected for mass transfer effects

Table 3.10 Component heat fluxes calculated in the CONTAIN code for the Wisconsin flat plate condensation tests.

Case #	T_{mix}, C	T_w, C	V, m/s	q_{conv}	q_{cond}	q_{film}	q_w
1	70	30	1	264	4089	200	4153
2	70	30	3	528	8321	419	8430
3	80	30	1	362	8321	416	8267
4	80	30	3	635	15001	790	14847
5	90	30	1	464	18026	964	17527
6	95	45	1	361	26884	2149	25096

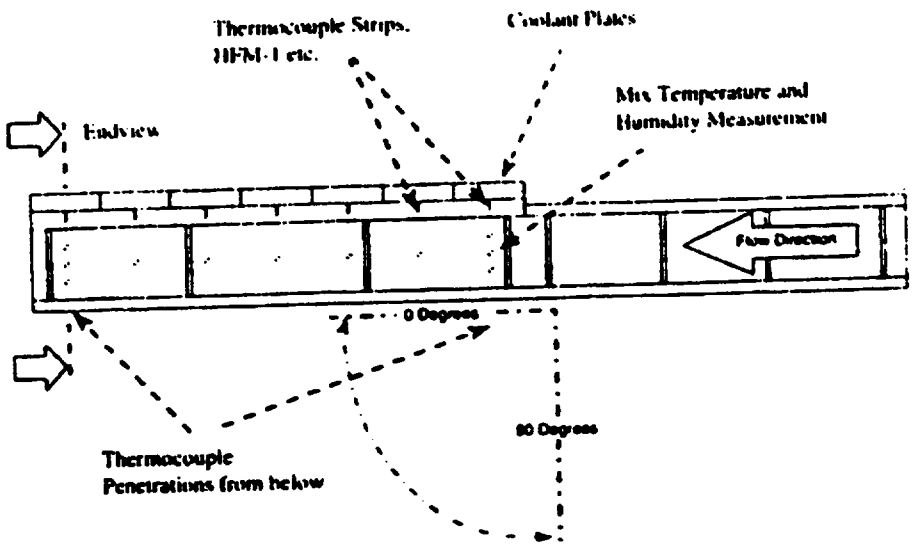

Figure 3.14 Condensing apparatus for the Wisconsin flat plate condensation tests.

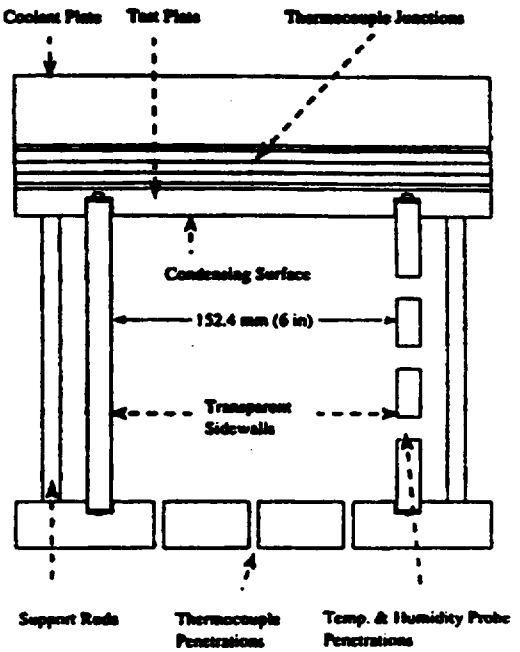

Figure 3.15 End view of the condensation duct used in the Wisconsin flat plate condensation tests.

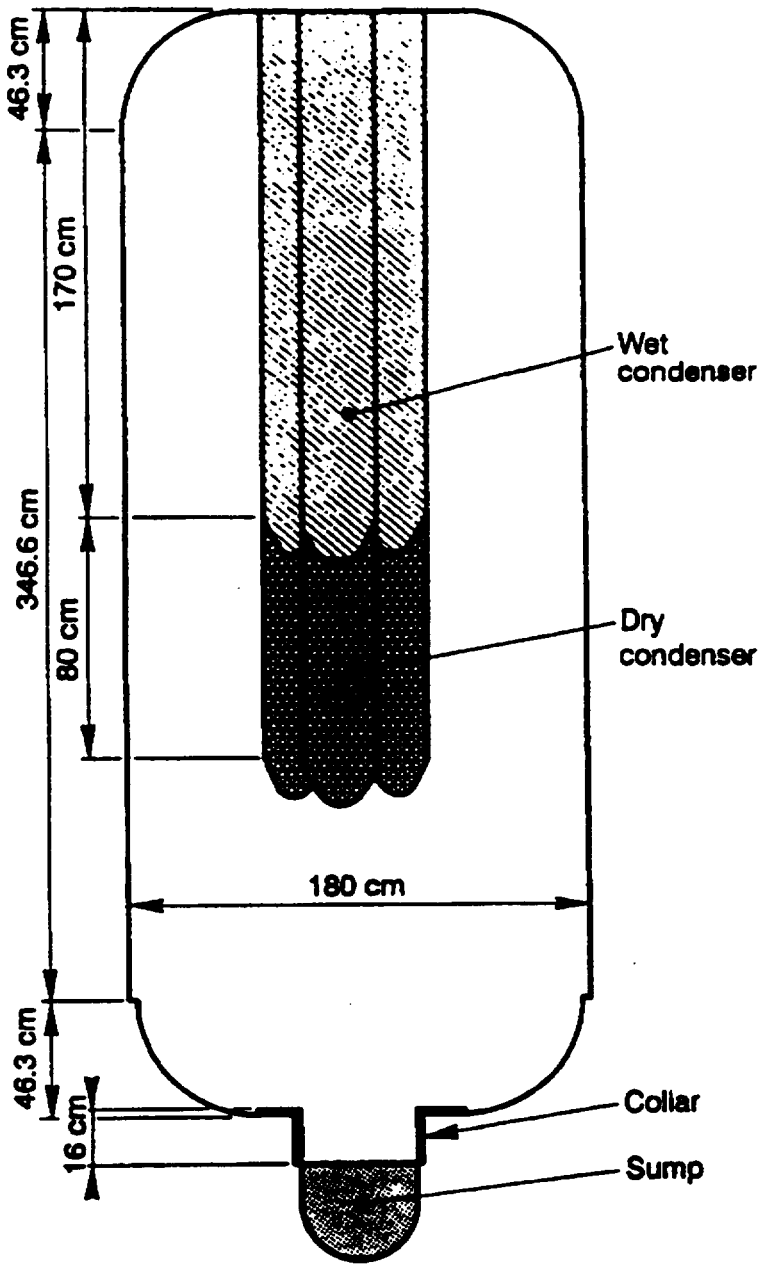

Figure 3.16 Phebus containment vessel

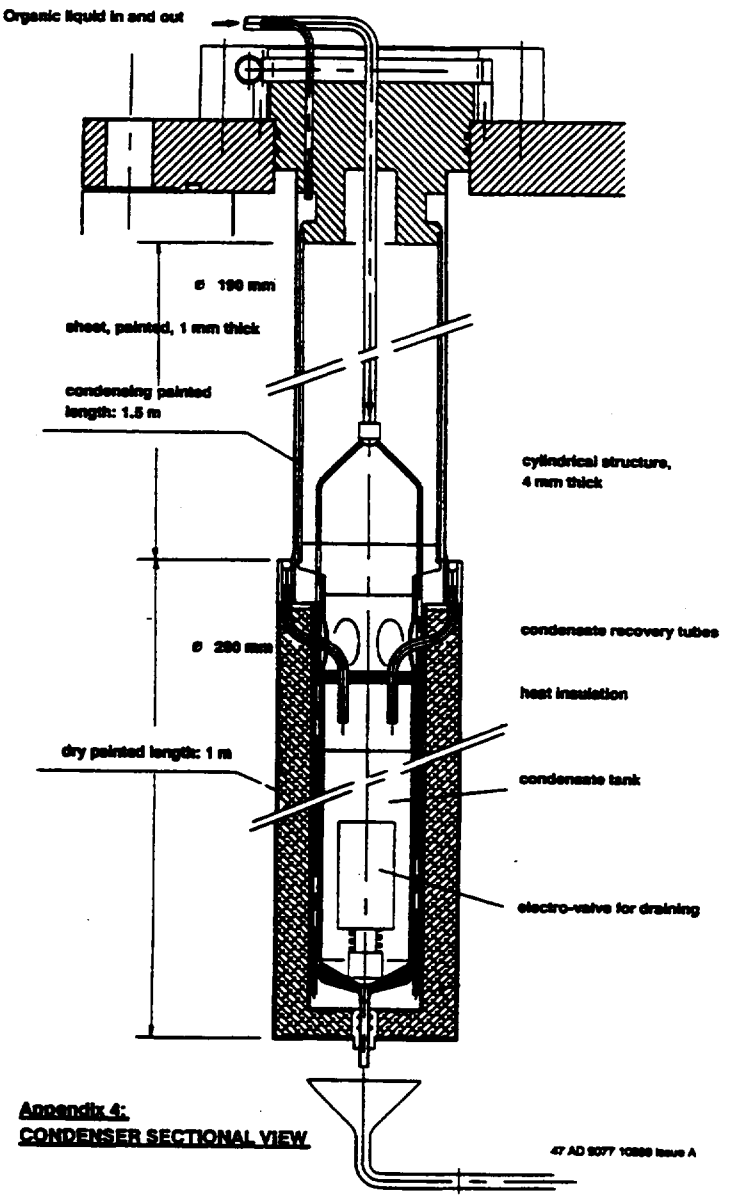

Figure 3.17 Condenser tube for Phebus testing

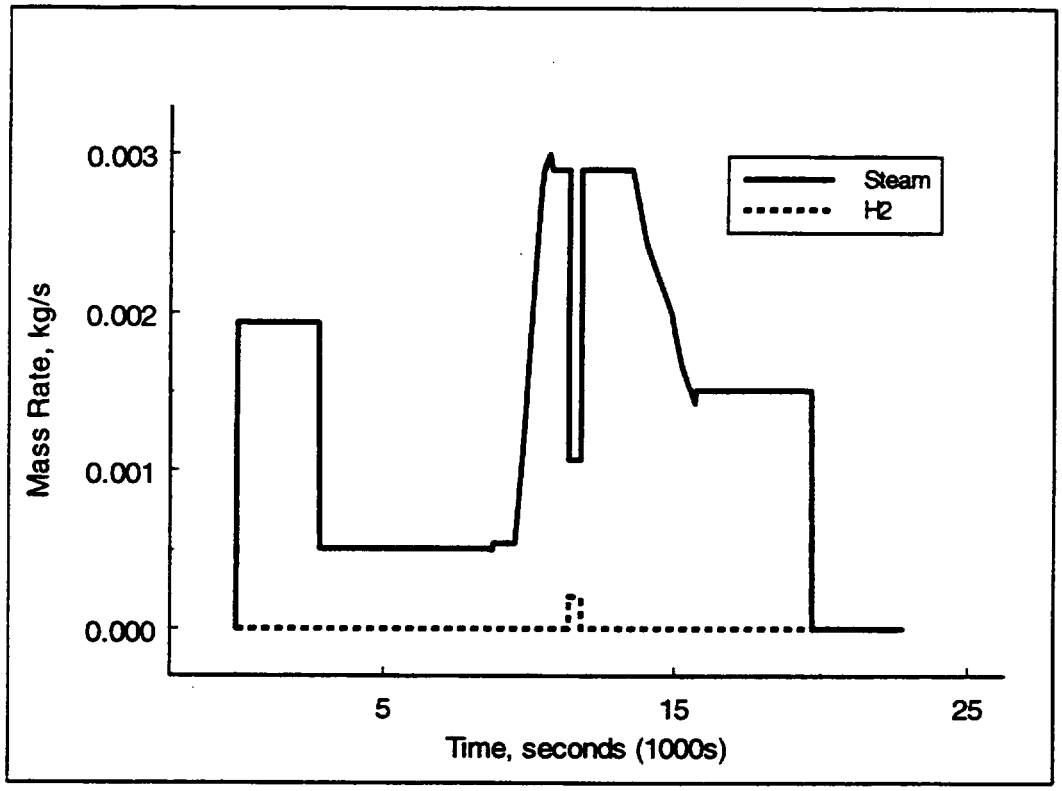

Figure 3.18 Steam and hydrogen injection rates for Phebus test FPT0.

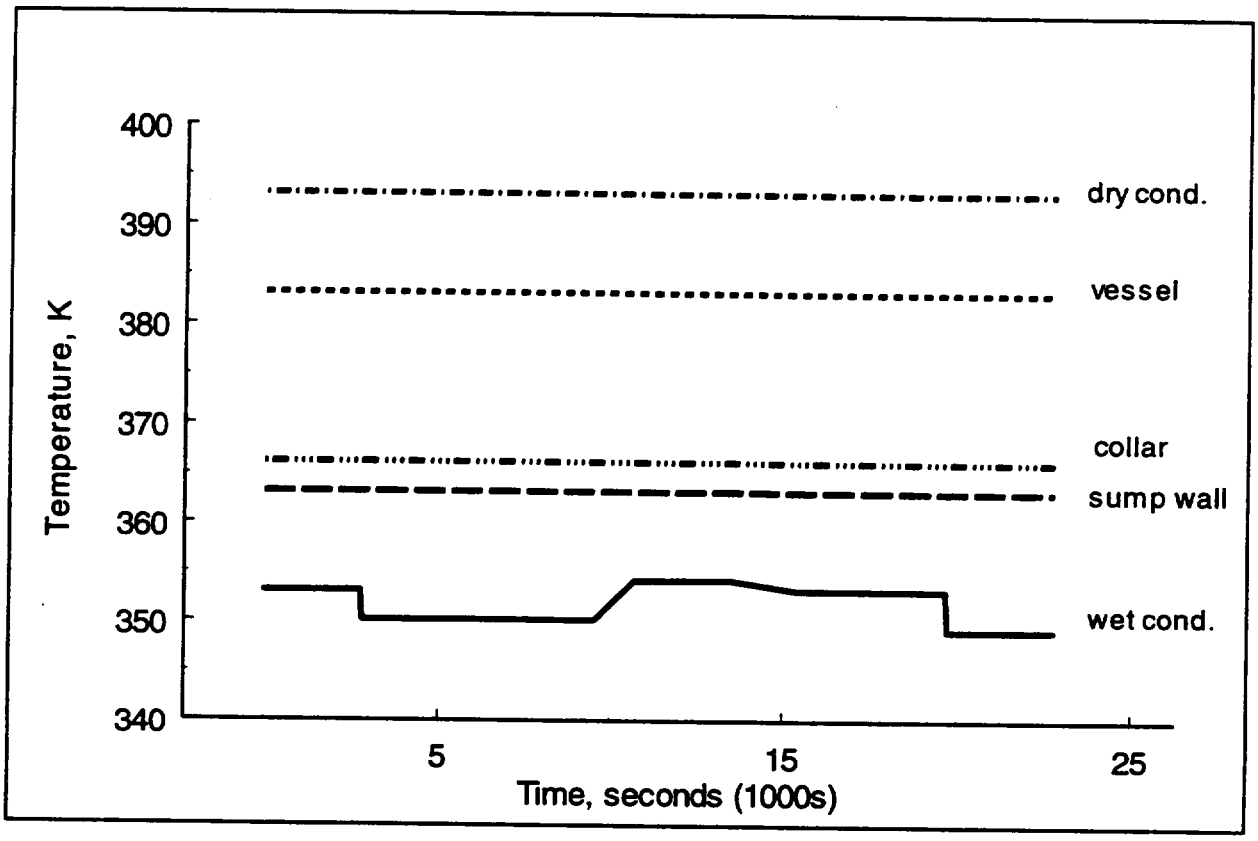

Figure 3.19 Containment surface temperatures measured in the Phebus test FPT0

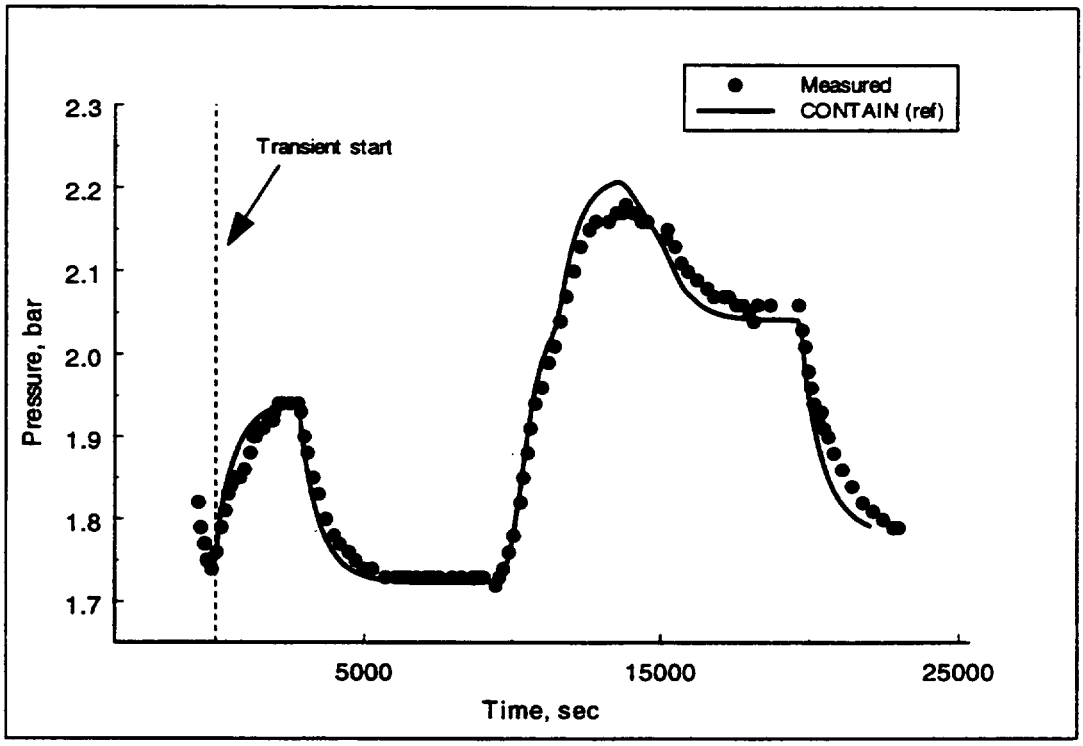

Figure 3.20 Comparison of calculated and measured vessel pressure for FPT0.

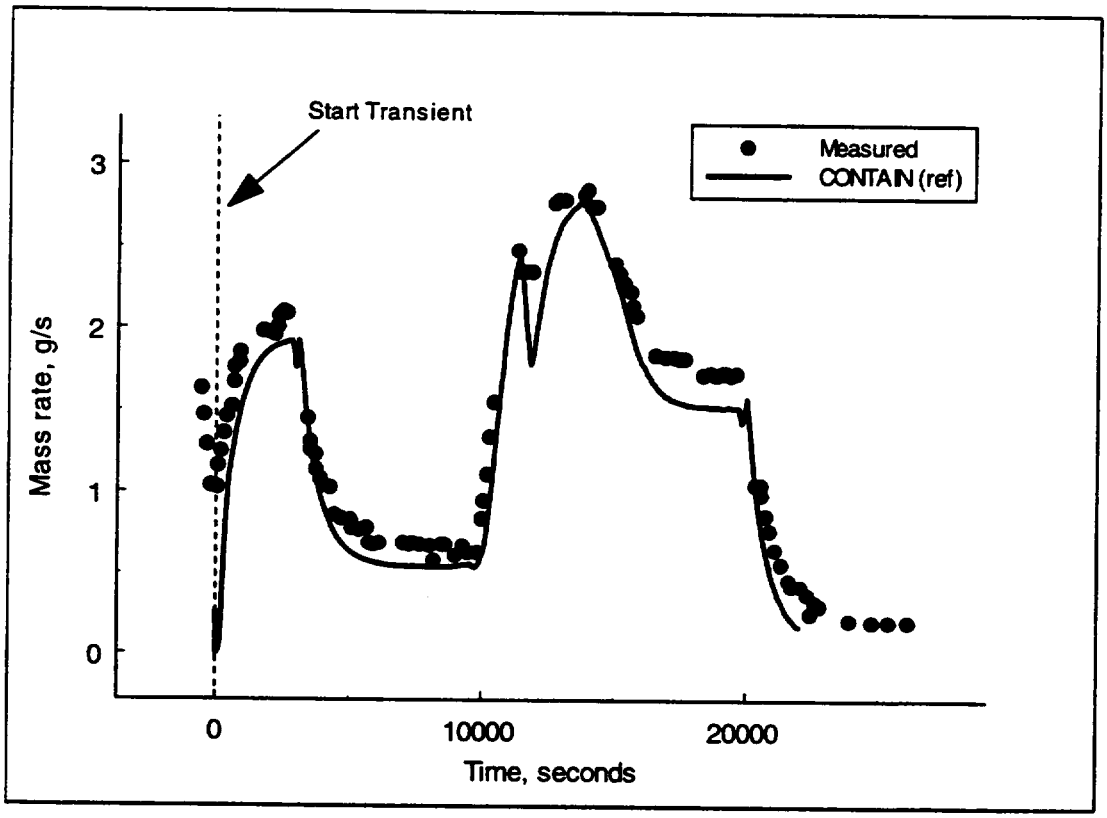

Figure 3.21 Comparison between measured and calculated condensation rates for Phebus test FPT0.

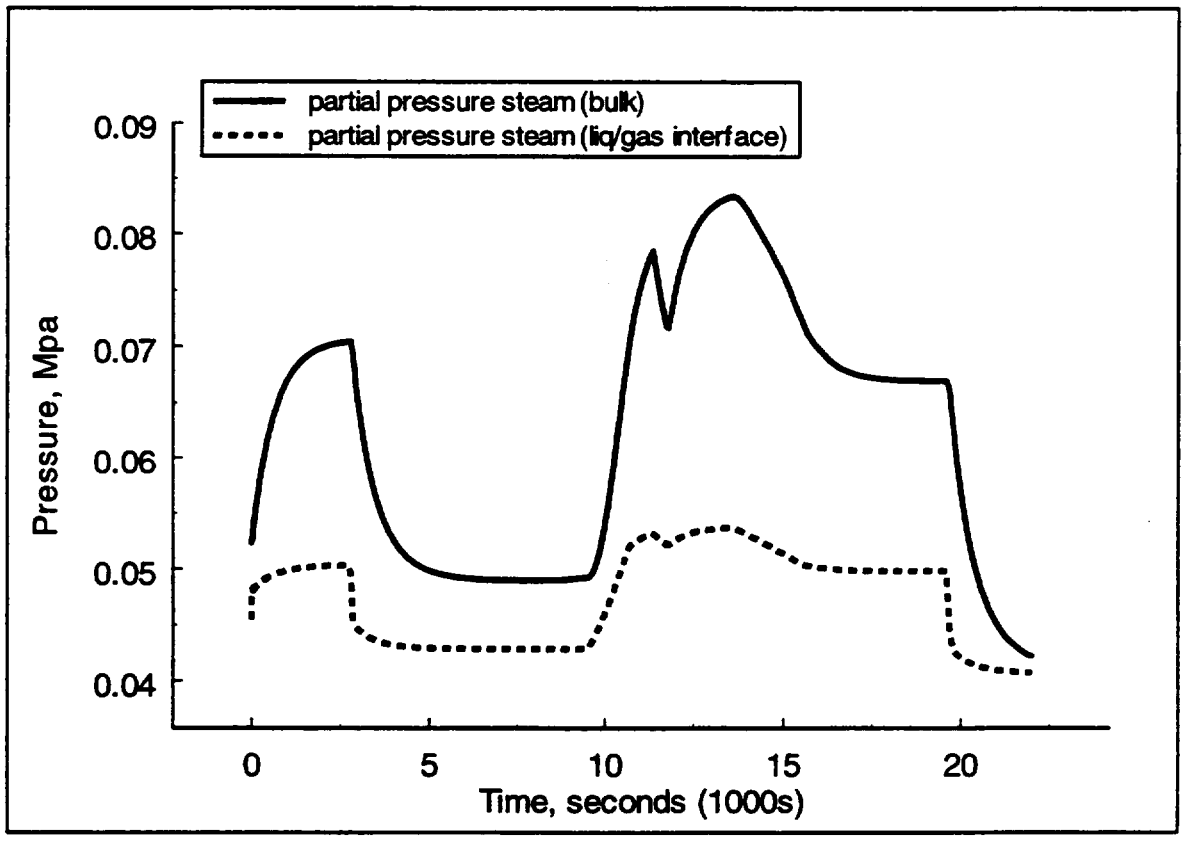

Figure 3.22 Calculated steam partial pressures for Phebus test FPT0 in the bulk steam/air/hydrogen mixture and at the condensate film gas/liquid interface.

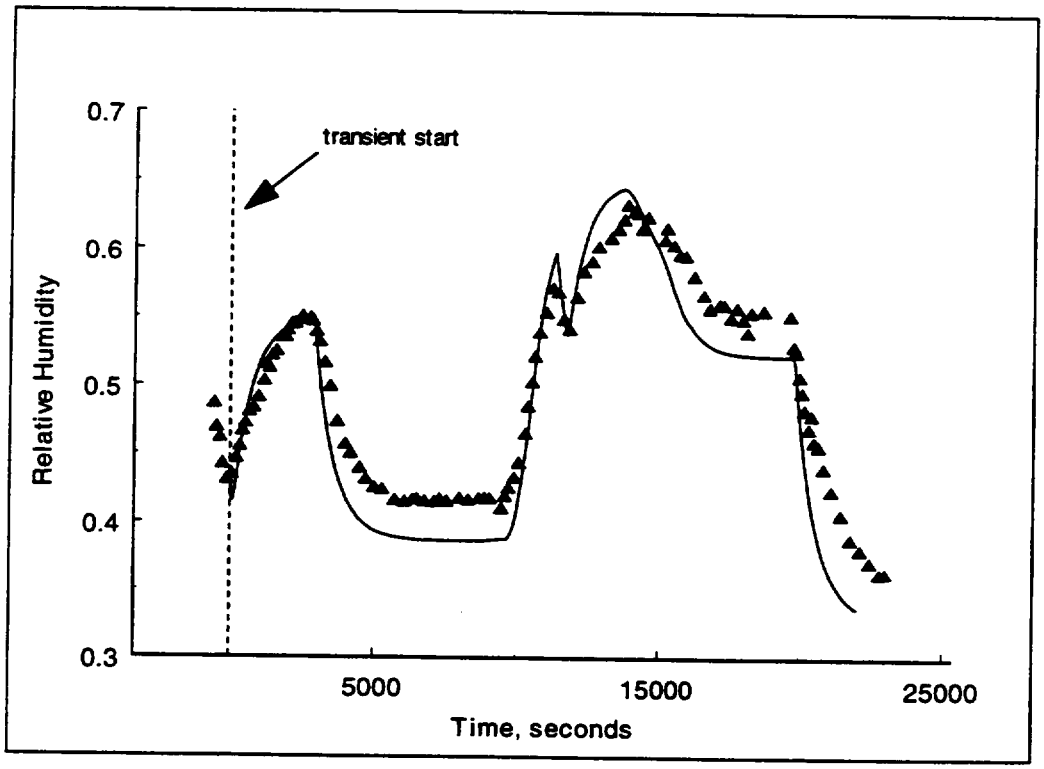

Figure 3.23 Comparison of calculated (CONTAIN - line) and measured relative humidity for FPT0

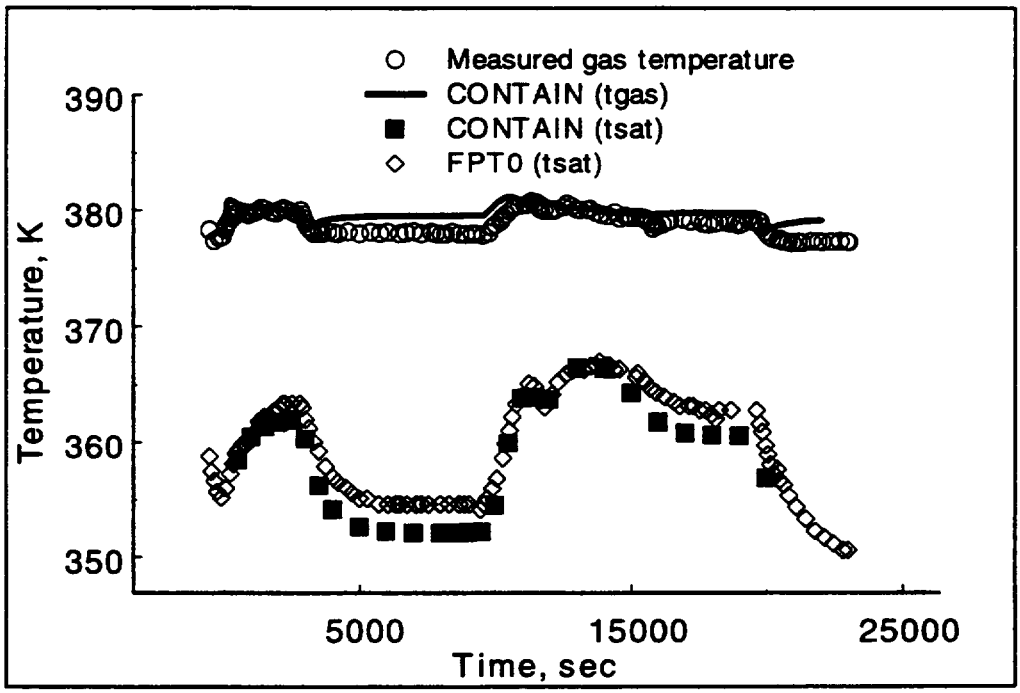

Figure 3.24 Comparison of calculated and measured saturation and superheated gas temperatures for Phebus test FPT0.

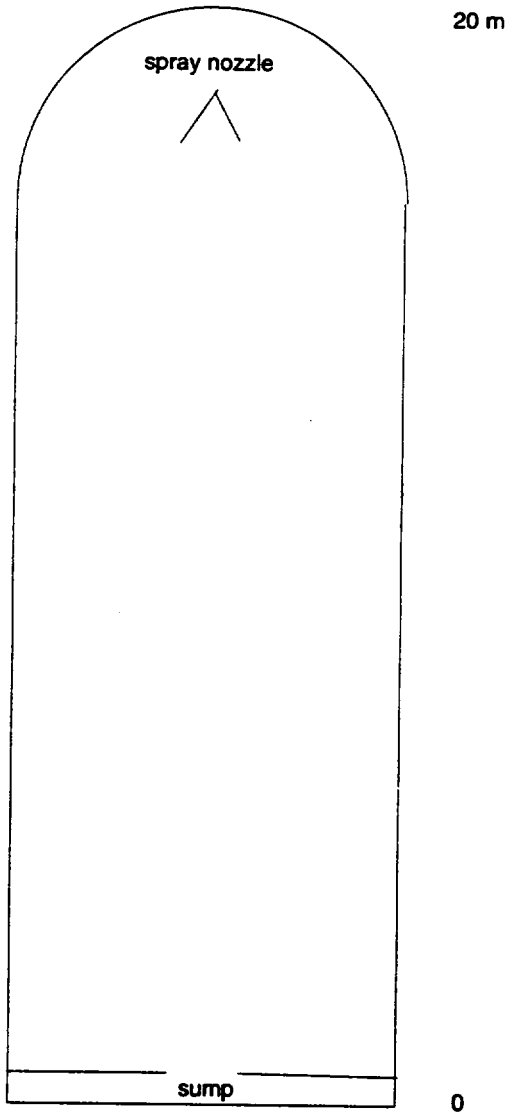

Figure 3.25 Containment vessel for the JAERI single spray test PHS-6.

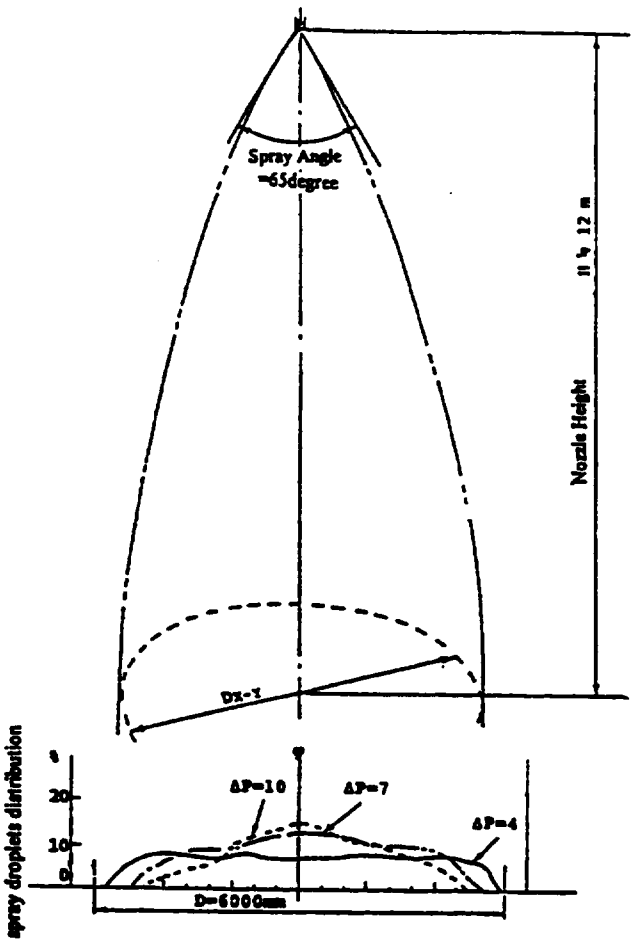

ΔP (kg/cm²·G)	2.8	4.0	7.0	10.0
Spray angle (degree)	66	64	62	61
$D_{v,v}$(m) at the ground	5.8~6.0	5.8~6.0	5.6~5.8	5.2~5.4

Figure 3.26 Typical spray distribution for a single spray nozzle [OECD94]

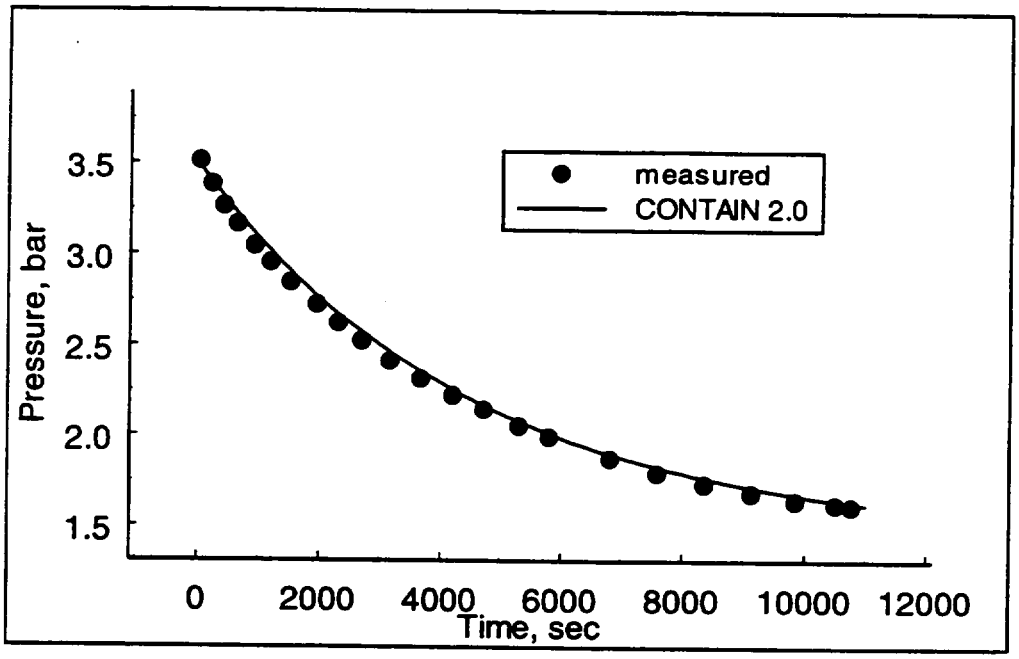

Figure 3.27 Comparison of measured and calculated pressure suppression for JAERI test PHS-6 (single nozzle spray).

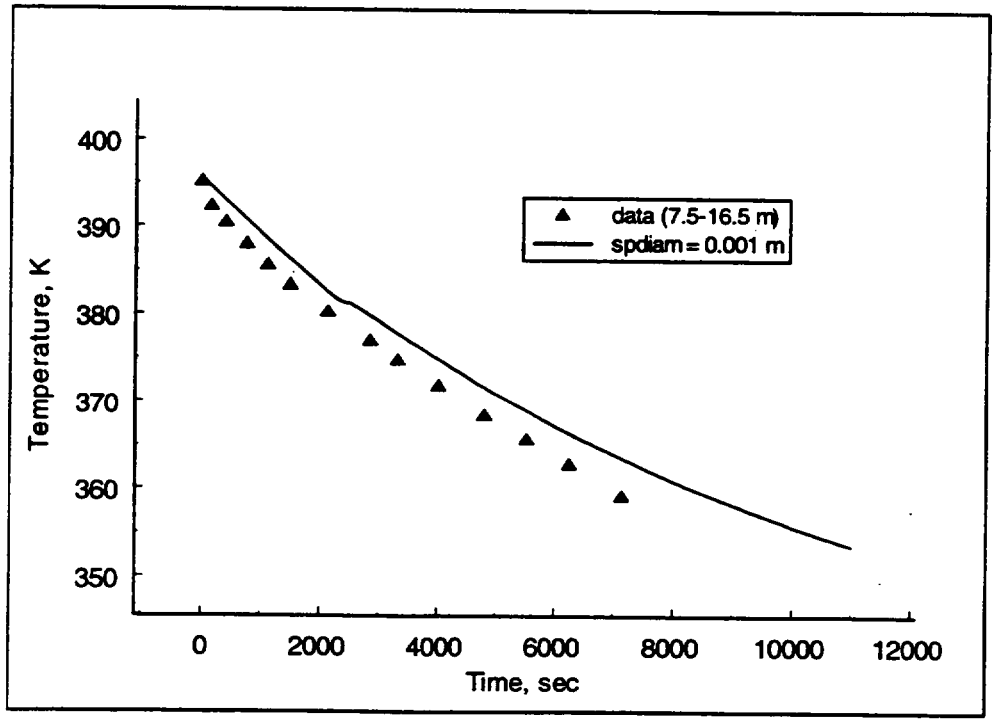

Figure 3.28 Comparison of measured and calculated atmospheric temperature for JAERI test PHS-6 (single nozzle spray).

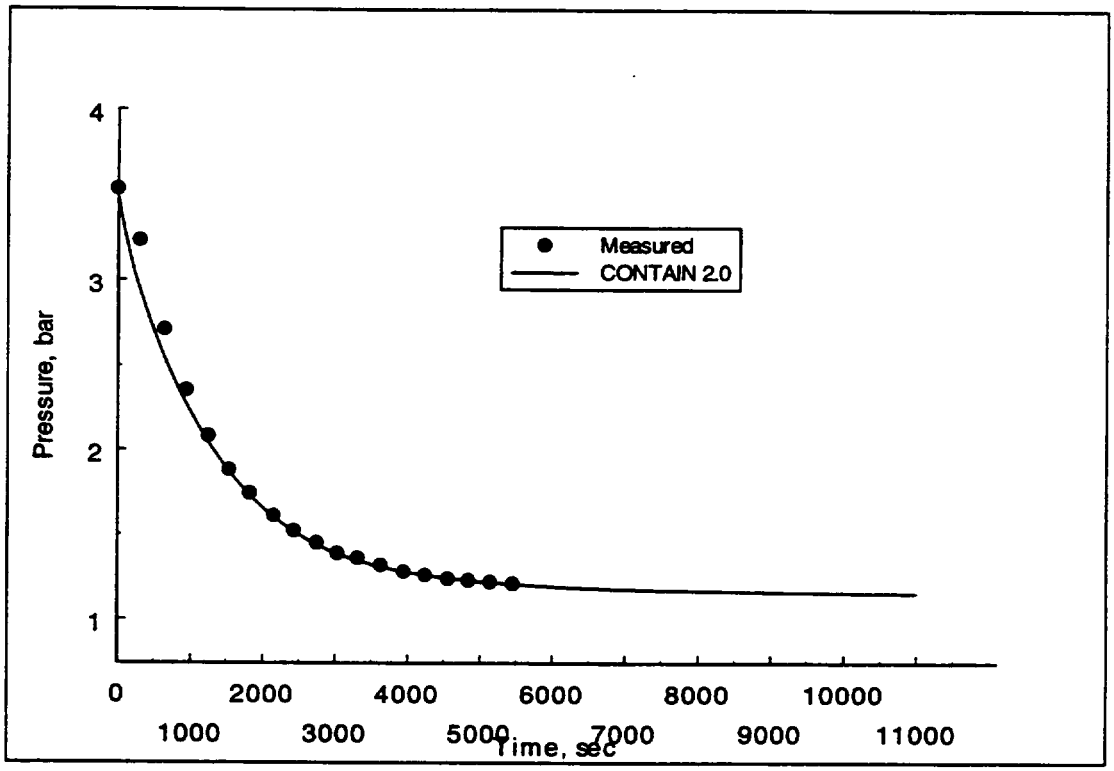

Figure 3.29 Comparison of measured and calculated pressure reduction for JAERI test PHS-1. The CONTAIN results are for a single cell calculation with a 90% spray/atmosphere interaction and 10% spray water injection to the vessel wall.

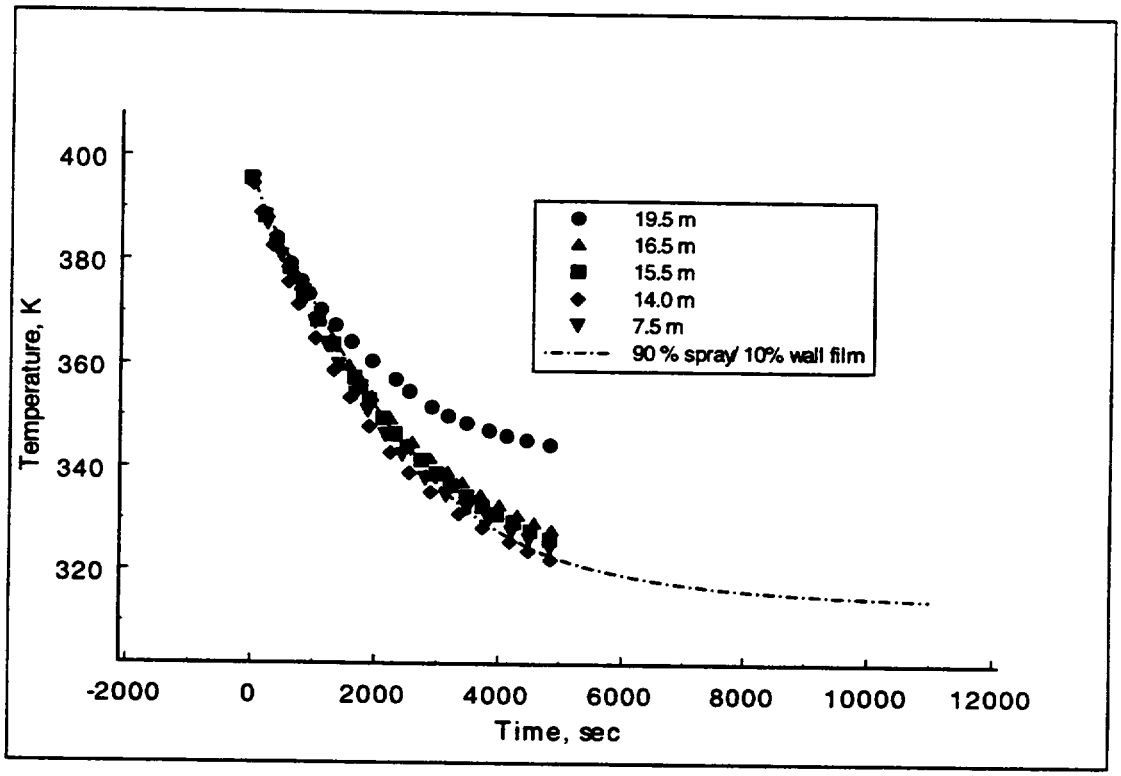

Figure 3.30 Comparison of measured and calculated temperature reduction for JAERI test PHS-1. The CONTAIN results are for a single cell calculation with a 90% spray/atmosphere interaction and 10% spray water injection to the vessel wall.

3.3.2 Integral Tests (Thermal Hydraulics and Hydrogen Distributions)

3.3.2.1 HDR Tests

Table 3.11 summarizes the key model/input options used in reference calculation for the HDR tests. The sensitivity of results to some of these options are discussed in Section 4.

3.3.2.1.1 V44 [ISP-16]

In 1982, an early version of the CONTAIN code was used to calculate the thermal hydraulic containment response for test V44. The result of that calculational effort was reported by Project HDR in a quick look report for blind predictions [Val83], and in a Project HDR conference paper [Wol83]. In this report, CONTAIN 2.0 used to calculated the test, with appropriate modifications to the original CONTAIN input to reflect new and improved models added to the code since the early 1980's.

The reference calculation uses the original CONTAIN five-cell model of the HDR facility, shown in Figure 3.31. In the reference calculation, liquid water condensed in the atmosphere is assumed to form water aerosols with settling, wall deposition, and transport through flow paths. Aerosols are transported from cell-to-cell in the code with 100% water carryover; that is, aerosols flowing through a pathway are transported using the aerosol inventories (mass fraction) of the upstream cell. No convective velocities are specified in the input. Figure 3.32 shows the predicted pressure for the reference calculation compared to the measured pressure. Comparisons of the predicted and measured temperatures in the upper containment, breakroom, and basement, respectively, are shown in Figures 3.33 to 3.35. The coarse nodalization used for this calculation limits the agreement possible with respect to the local temperatures. Better local comparisons are evident in the ISP-23 predictions, for which a more detailed nodalization was adopted.

Modeling issues related to differential pressure predictions (sub-compartment analysis) are also addressed in test V44. Of the HDR blowdown series of tests, V44 represents one of the most severe two phase blowdown injections, both in terms of the source injection rate and because the breakroom is the smallest of any HDR configurations tested. For example, shown in Figure 3.36 is a comparison of differential pressures between the breakroom and adjacent room for test V44 and T31.5. Both tests had a similar blowdown injections; however, the pressure differential is significantly higher for V44 with a breakroom free volume of 280 m3 compared to the T31.5 test with a volume of 780 m3. In V44, the prediction of the severe pressure differentials is especially subject to calculational problems. As shown in Figure 3.37, the differential pressure predicted with the reference is lower than measured. In the reference case, the loss coefficients for paths leading out of the breakroom are calculated based on highly turbulent flow through sharp orifices; the inertia parameter, A/L, for all paths are determined based on an inertia length equal to the V**1/3, where V is the smallest volume connect to the path. In Section 4, the variations of

pressure differentials calculated for reasonable modifications of loss coefficients, contraction coefficients, inertia lengths, suspended liquid water, and heat transfer are discussed.

Forced-convective velocities are not specified in the reference calculation; rather, the default treatment of forced convective velocities for heat and mass transfer along structure surfaces is used. The default convection option uses flow path velocities and a cell hydraulic area to represent surface velocities. In the default mode, the hydraulic area associated with a cell is the cell volume divided by the cube of the volume. The large hydraulic areas calculated for a default case and the HDR configuration result in small convective velocities. The velocities are small enough that natural convective process dominate heat and mass transfer. Forced convection velocities for heat sinks during a blowdown are very difficult, if not impossible, to estimate (even for fluid dynamic codes); therefore, there is considerable uncertainty associated with making such estimates. Sensitivity calculations used to explore the impact of modeling forced convection in the location of the blowdown are discussed in Section 4.

3.3.2.1.2 T31.5 [ISP-23]

For the ISP-23 calculation, a 33 cell nodalization of the containment is used as shown in Figure 3.38; this nodalization is identical to the nodalization used in the SNL blind calculation submittal for ISP23, and documented in Reference Kar89. ISP-23 differed from ISP-16 in the location of the steam injection location, which was moved from room 1603 to 1704, a larger room one level higher, at an elevation of approximately 22 meters. As noted above, the injection rate was similar to ISP-16 (V44), as shown in Figure 3.6. A comparison of pressures calculated in the reference case with the measured values is shown in Figure 3.39. The reference calculation, as with the V44 reference calculation, uses the default method for treating forced convection. Because the ISP-23 test was nodalized to better represent the compartmentalization of the facility, this calculation is a better reflection of the code's capability to predict local temperatures during a blowdown. Figure 3.40 shows local temperature comparisons at four vertical locations, ranging from -5 to 40 meters. As indicated in the figure, the early (0-50 seconds) temperature stratification predicted by the code agrees quite well with the local temperature maximums measured above the injection elevation, but temperatures below the injection point are over predicted. This is especially apparent for the 5 meter location. Overall, the prediction of late time behavior (50-200 seconds) is in better agreement. The over prediction of the 5 meter measurement may indicate that the modeling of rain-out liquid from the blowdown region into the lower containment is important. This rain-out may arise from liquid entrained during the blowdown or from entrainment of condensate films that have formed on heat sinks. Hence, the rain-out effect, may need to be modeled in the facility for better temperature comparisons.

Again, as with ISP16, another interesting feature of the ISP-23 calculation is the sub-compartment pressure differential comparison shown in Figure 3.41. Here the peak pressure differential between the breakroom and adjacent or upper containment is slightly over predicted

by the code; however, at a later time, the calculated pressure differential decreases too rapidly such that the prediction slightly under-estimates the pressure differential beginning at about 2.5 seconds. As shown in a sensitivity calculation discussed in Section 4, part of the reason for the dropoff is the use of the aerosol model in the reference calculation. The aerosol model neglects the inertial mass of the aerosolized water, and this causes the flow rate out of the blowdown cell to be too high. In general it is difficult to determine accurately the parameters, such as loss coefficients, that determine the pressure differential.

3.3.2.1.3 T31.5 (Project HDR Benchmark)

In a separate initiative from the T31.5 [ISP-23] effort, Project HDR sponsored a benchmark exercise for test T31.5 [Val89, Wolf89]. This exercise extended the time period for comparisons from 20 minutes to an hour after the initiation of the blowdown; included in this benchmark was the light gas (hydrogen/helium) injection period that began at about 36 minutes and lasted approximately 15 minutes. SNL participated in this exercise and the results of those comparisons were reported by Project HDR in Reference [Wolf89b]. This benchmark, including the thermal hydraulics and hydrogen is repeated here using the HDR nodalization scheme shown in Figure 3.38. The exercise represented an important benchmark since it was the first hydrogen distribution test conducted in a large-scale integral test facility.

Results are presented here for the pressure and the local temperature and hydrogen concentration at three locations in the facility. These locations are in the upper containment (40.5 m and 50 m) and the lower containment (6.5 m), cells 33 and 2, respectively. The injection location for both steam and hydrogen was in room 1704 of the facility, at an elevation of approximately 22 meters. Shown in Figure 3.42 is the comparison between measured and predicted pressure, extended out to one hour. As noted above, there is an over prediction in pressure during the blowdown period, mainly due to an underestimation in the heat transfer for the forced convection condensation occurring in the vicinity of the blowdown region. The pressure relaxation however is predicted with very good accuracy. Shown in Figures 3.43 are local temperature comparisons for the upper and lower containment. From these figures it is apparent that the temperature relaxation and difference of about 25 degrees at about 20-30 minutes is correctly predicted by the code. At about an hour after the blowdown the upper containment measured and predicted local temperatures are 333 and 336 K, respectively. In the lower containment the temperatures are about 26 degrees lower; the measured temperature in the lower containment is 306.5 K and the predicted temperature is 307 K.

At the time that hydrogen injection begins, pressure and local temperature in the facility are very close to the measured values, as noted above. Shown in Figure 3.44 are the measured and calculated hydrogen concentration in the upper and lower containment. There is a slight delay in the initial increase in the predicted hydrogen concentration. This delay is indicative of a lack of plume modeling in the code (see Section 4), which also is evident by slightly more light gas

being transported below the injection location than actually occurs. Nevertheless, after a few minutes the rate of increase is correctly calculated, and the final upper containment hydrogen concentration, is predicted with very good accuracy. As noted in the figure, in the lower containment, 15.5 meters below the injection, there is only a small amount of hydrogen gas measured and predicted by the code.

3.3.2.1.4 E11.2 [ISP-29]

The SNL submittal for test E11.2 (ISP-29) was sent in January 1992, and is documented in the ISP-29 report [Kar92] and in a SNL letter report to the USNRC [Til92]. More recently, the E11.2 test has been used to assess the hybrid flow solver model in the CONTAIN 2.0 code [Mur96]. Reference Mur96 may be consulted for details pertaining to the development of the 15-cell input deck, which is used here for the reference calculation. This 15-cell nodalization is shown in Figure 3.45. Some additional details concerning cell volumes, elevation, and compartment makeup of the cells are given in Table 3.12. The test setup is sketched in Figure 3.46, and the test procedure is shown in Figure 3.47. The pre-heat portion of the test, lasting approximately 11.5 hours, is used here to demonstrate long term thermal hydraulic modeling capability of the code. The pre-heat portion includes a vessel blowdown similar to ISP-16 and 23) but the source period is extended with a reduced flow of externally supplied steam (external steam supplied from a nearby heating plant). The injection location for both the steam and light gas mixture is in Room 1805 at an elevation of approximately 23 meters.

The hydrogen distribution portion of the test begins at 12 hours and 20 minutes into the test, just before the external steam source into room 1805 is turned off. A light gas mixture, 85/15% He/H_2, is injected into room 1805 over a 32 minute period. After this injection, a second source of external steam is injected into the lower containment, Room 1405, at an elevation of 0.84 meters. The lower steam injection lasts for about 3 hours and is followed by ~ 15 minutes of a natural cooldown. At the end of the cooldown, water is sprayed onto the external steel shell in the dome region of the upper containment - the dome is that region above the spring line of the upper containment. Figure 3.48 shows the relative location of the external sprays and the location of the mid- and lower elevation break locations.

With respect to modeling, one unfortunate incident with the E11 series of tests occurred (E11.1-E11.5) that complicated and also diminished somewhat our ability to model containment thermal hydraulics. The incident involved the presence of a significant amount of energy extracted from the atmosphere as a result of hydrogen sensor cooling lines left uninsulated [Wen91]. Although the total energy extraction from all the cooling lines was measured, Figure 3.49, the spatial distribution of the energy extraction within the containment was not. To model this feature a coding modification is required. The modification is based on the assumption that local energy extraction is mainly the result of condensation on the cooling lines; condensation is proportionally dependent on the relative location of sensors (i.e., exposed cooling lines) and the

steam partial pressure. As a result, a local energy extraction function is determined by

$$f_n = \frac{P_{v,n} w_n}{\sum_i P_{v,n} w_i}$$

where $P_{v,n}$ is the partial pressure of steam in cell n, and w_i is the cooling weighting factors which are dependent on the sensor placements [Val92]. The factors are shown in Table 3.13. Because the energy extraction function is dependent on the time dependent variation of the steam partial pressures, the function can not be included directly through code input; rather, the function must be evaluated during the updating of the cell atmospheric energy as the test is being calculated. To do this, a modification is made to the code, hardwiring in the energy extraction function.

A comparison of the calculated and measured containment pressures is shown in Figure 3.50. The over prediction of the pressure at late time is evident. It should be mentioned that analysts using other lumped parameter and field codes have also observed an over prediction in pressure of a similar amount and this has led to a number of suggested reasons for this disagreement (uncertainty in heat sinks, steam injection rates, coolant line energy extraction, and thermal properties). The issue concerning the over predictions of pressure in the E11.2 test has not been resolved yet, but a number of the suggested reasons are investigated with sensitivity calculations in Section 4.

Figures 3.51 and 3.52 show the comparisons between the calculated and measured local temperatures. The above-deck temperatures are predicted within approximately 5 degrees. Below deck, the trends are predicted well but the absolute comparisons show variations that have not been captured well by the present nodalization. The nearly equal temperatures predicted at the 17 m elevation, on different sides of the containment (partitioned by the reactor vessel), suggests that good lateral mixing is occurring below the operating deck. In contrast the differences in the measured temperatures at nearly the same elevation show that the mixing from side to side may not be that complete. The measured behavior shown in Figure 3.52 shows that the mixing process below the operating deck is complicated and varies with time; for instance, note the convergence of the temperatures at the 16.5 meter level for late times.

The temperature rise in the lower regions (e.g., cell 3) is due primarily to compressive effects from the blowdown. Very little steam is actually predicted to be present in the lower regions. Although the predicted temperature rise in cell 3, at 12.7 m, for example, is 48% of the temperature rise in the dome at 40000 seconds, the predicted steam concentration in cell 3 is only 13% of the dome steam concentration at that time.

As was mentioned for ISP-23, and illustrated in the sensitivity cases for CVTR in Section 4, the disagreement in the predicted and measured temperatures in the lower regions may be due in part to neglect of rainout of liquid from the upper regions of the containment where most of the steam condensation is occurring. Because the lower regions are highly superheated, evaporation of relatively small amounts of liquid may be sufficient to reduce the temperature substantially.

One of the more important aspects of the E11.2 test, concerns the stability conditions predicted by the code and how these conditions affect gas transport and mixing. Shown in Figure 3.53 are comparisons of measured and calculated light gas (hydrogen and helium) concentrations in the upper and lower containment. The significant stratification of the light gas mixture during the injection is predicted, as well as the important trends observed for the light gas concentration during the lower containment steam injection and external spray period. The initial injection of light gas is under estimated mainly due to the over prediction of steam in the upper containment, which is consistent with an over prediction of pressure as discussed above.

It had been theorized before the test that the lower containment steam injection, which begins shortly before the light gas injection is terminated, might serve to breakup the highly stratified light gas distribution in the upper containment. However, as was observed in the test, the lower containment steam injection creates a piston-like effect in the containment, forcing the steam/gas mixture above the injection location to move upwards with very little mixing of the injected steam and the overlying steam/gas mixture. As a result, the light gas mixture in the dome of the upper containment (region above 40 meters) shows a slow increase in gas concentration as light gas is forced into the upper regions; this process where overlying gases are transported vertically as a result of interaction with an expanding gas "bubble", as shown in Figure 3.53, is also predicted by the code.[1] Further evidence of this piston-like effect is shown in Figure 3.54. For this figure the air concentrations and temperature measurements in the region above the operation deck are used, together with the ideal gas equation, to calculate the total increased air mass above the operation deck. The comparison between the observed and predicted gas transport into the above deck region due to the lower containment steam injection is seen to be quite good. Because the concentration of light gas in the gas mixture below the operation deck is significantly lower than in the above deck region prior to the lower containment steam injection, the light gas mixture in the cylinder portion of the upper containment (between the operating

[1] In this instance, the influence on gas mixing and transport resulting from the use of the hybrid flow solver is demonstrated. In Section 4, the E11.2 test is recalculated using the "old" flow solver that does not maintain the observed stability conditions during the test. The "old" solver is representative of the gas mixing and transport modeling in most lumped parameter codes that tend to over-mix containment gases. In the CONTAIN 2.0 code, the "old" method of calculating gas flows can be activated by the keyword "mstable" in the FLOWS input block. For a more complete discussion of the hybrid flow solver and its usage, the reader is referred to references Mur96 and Mur97.

deck and spring line) begins to decrease as the lower concentration light gas mixture begins to displace the high concentration mixture that has moved into the dome region. This behavior is shown in Figure 3.55, along with the calculated results. The comparison of the measured and calculated light gas distributions during the lower containment steam injection verify that this portion of the E11.2 gas mixing and transport phenomena is being correctly modeled: further, the accuracy is considered good given the known over estimate of upper containment steam content, which is believed to be a feature of the calculation unrelated to stratification but caused by an unknown error associated with the boundary conditions used in the calculation.

At the end of the lower containment steam injection, the external sprays are activated. The cooling of the containment shell in the region above the spring line (> 40 meters) causes a rapid, local condensation of steam on the cooled shell surfaces. The reduction of atmospheric mass due to the condensation produces a local pressure drop that in turn (by pressure forces) continues the earlier upward movement of steam/gas mixture into the dome region of the upper containment. As a result of this condensation effect on gas transport, there is a rapid increase of light gas in the dome region as the bulk flow of gas into the region is greater than the outflow of gas due to secondary currents generated by cold, denser gases flowing downward along the cold wall surfaces. The rapid cooling effect of the sprays also creates circulation currents in the dome region that uniformly mix this region. As a result, the dome region light gas measurements shows a relatively well mixed volume of light gas. The gas concentration in the single dome cell, cell number 9, show this gas transport effect. Continuous flow of air into the above deck region is shown again during the external spray period in Figure 3.54, where good comparisons between measurements and calculations are evident. In Figures 3.53 and 3.55, the trends in the light gas concentration in the entire above deck region are also correctly predicted.

As the cooling effect from the external sprays continues, a point is reached when the density of the gases in the dome region exceed the regions below, the entire mixture above the operation deck becomes unstable. At this time the dome and cylinder portions of the gas volumes begin to mix. Since the lower gas volume has a smaller concentration of light gas, the overall effect is to rapidly reduce the concentration in the dome region while the light gas concentration in the cylinder region above the deck increases. Again, this effect is also predicted by the code; however, the rate of the mixing is not well predicted, nor is the longer term mixing behavior captured. Evidently, there is transport and mixing between the above and below deck regions after the initial inversion of gas volumes that is not well predicted by the code. The onset of the inversion process, as well as the longer term mixing of gases above deck is a complicated and difficult process to capture even with a 3D finite volume code, having thousands of nodes to represent the containment gas volume [Roy95]. The detailed modeling of the onset of the dome gas inversion and subsequent mixing during the E11.2 test remains somewhat of an open issue in this test; resolution of that modeling issue still requires further analysis. The severe conditions caused by the external sprays are, however, not prototypical of any current US containment or accident scenario (nor is the HDR facility geometry prototypical of any US PWR); therefore, additional effort to investigate modeling aspects of the specific gas mixing and transport

processes involved in this portion of the test has not been pursued.

3.3.2.1.5 E11.4 (Project HDR Benchmark)

The E11.4 test was used as a benchmark exercise for codes, sponsored by Project HDR [Val92, Gre92]. Layout of the E11.4 test is shown in Figure 3.56 and the experimental procedure is described in Figure 3.57. The main difference between the E11.2 and the E11.4 test was the different injection locations for the steam and light gas mixture. In the E11.4 test, the injection location was moved to the lower containment (room 1405) at an elevation of approximately 3 meters. The low injection position meant that the containment would not exhibit the severe stratification observed in the mid-elevation injection of E11.2. The E11.4 test also include an extended pre-heating period of about 34 hours, 3 times the length of the pre-heating period for E11.2.

The CONTAIN geometric model of the E11.4 consists of 48 cells, as detailed in Table 3.14; this nodalization scheme is similar to a nodalization used for the pre-test calculations for E11.2 [Val92]. Instrument cooling was modeled as describe for E11.2, using the E11.4 measured cooling rates which were slightly different from E11.2. An additional cell was added to the lower containment region to better represent the region near the injection.

Shown in Figure 3.58 is the comparison between the measured and predicted containment pressure during the pre-heat portion of the test. The break in the pressure increase at about 800 minutes is the result of a failure in a steam supply valve. The valve was repaired and the pre-heat portion of the test continued. Clearly, the agreement between measured and calculated pressure over the pre-heat portion of the test is impressive. After 34 hours the absolute error in pressure is 6.2%, while error in the over-pressure prediction is 12.7%. These errors are essentially within the measurement accuracy of the pressure transducers (3-10 kPa). We can compare the two pressure measurements and predictions for E11.2 and E11.4 over the first 11 hours (660 minutes) of the tests (during the E11.2 pre-heat period), Figure 3.59. Over the similar pre-heating periods, each test has the same steam injection mass and energy. The E11.4 pressure is lower since more long term heat sink material (concrete) is exposed to steam in E11.4 due to the uniform mixing in this test as contrasted to the E11.2 test that showed significant stratification. This figure also shows an outstanding difficulty with the E11 series of code calculations - there is very good agreement in pressure with the E11.4 test while the calculations for E11.2 show a significant over prediction. This observation has been made by analysts using other lumped parameter codes [Lee99] and even finite control volume codes employing thousands of nodes [Roy95]. Some possible reasons for this inconsistency are investigated in Section 4.

The uniform mixing resulting from the low injection is shown in Figure 3.60 where measured temperatures are plotted for the lower and upper containment. In the lower containment region two measurement locations are plotted: the measurement ct5304 is located in room 1503 away

from the staircase; measurement ct5301 is located in the equipment shaft near the staircase. The steam/gas mixture in the plume, rising up through the equipment shaft, is seen to have a slightly higher temperature than in the room adjacent to the shaft where major heat sinks are located. In the case of the calculations, also shown in the figure, we see that the temperature trends from the lower to upper containment are well predicted. The lower containment temperature is under predicted early in the transient, and less so during the late portion. Presumably this under prediction is the result of the rather coarse nodalization in the lower containment. We also see in the figure that the calculation behaves similar to the observation in measurements between the shaft and adjacent room region; where the lumping of a number of rooms on the 1500 level together amplifies the variation in temperatures at this level. In contrast, the upper containment temperature calculations are essentially within the measurement uncertainty of 1-2 degrees.

Shown in Table 3.15 are the comparisons between measured and calculated light gas concentrations in the upper and lower containment at the end of the gas mixture injection that starts at 34 hours and 44 minutes and ends 30 minutes later. The uniform mixing of the light gas is evident for the E11.4 test, and the agreement between measured and calculated light gas concentrations is shown to be very good.

The E11.4 test represents an unusually good test for an attempt to validate long term heat transfer modeling in a containment. In this respect, there are a number of reasons for emphasis:

- the test is characterized by uniform mixing such that codes, especially, lumped parameter codes are able to correctly estimate steam concentrations;
- there is relative good agreement between pressure and temperature measurements and predictions in the containment, meaning that bulk boundary conditions for condensation are nearly identical for the mass and heat transfer process;
- the extended pre-heating portion of the test is similar to the period of time, that is of interest, for the 24 hour requirements to reduce containment pressure (and temperature from an equipment qualification standpoint); and,
- there are instrumented concrete blocks that provide data on rates of heat transfer.

Unlike the separate effects type of testing that typically use cooled metal plates and relatively large bulk to wall temperature differentials (30-60 degrees, in the case of the Wisconsin flat plate tests), long term heat transfer processes are characterized by smaller temperature differentials of only a few degrees and relatively small heat transfer rates. As indicated by Green [Gre94], in plots of heat transfer coefficients, as determined with CONTAIN, small temperature differentials (i.e., vapor pressure differential) are attended by significantly reduced heat transfer coefficients as compared to the coefficients calculated at higher temperature differentials. To validate this finding we compare measured and calculated condensation coefficients for two instrumented concrete blocks in the E11.4 test, #82, and #84. The blocks are instrumented with imbedded thermocouples to allow heat transfer estimation. Green has reduced some of the data for a few of these blocks which we are comparing; the reduced data includes heat transfer coefficient and

measured bulk to wall temperature differential. The locations and instrument designation for these concrete blocks are given in Table 3.16. One of the blocks, #82, is located in a room away from the main circulation paths in the containment which is the staircase and the spiral staircase (and associated equipment shafts). One of the blocks, #84, is located along the main circulation route, adjacent to the shaft on the spiral staircase side of the containment. The two locations are shown in Figures 3.61 and 3.62.

Shown in Figures 3.63 and 3.64 are the comparison between measured and calculated heat transfer coefficients for the two instrumented concrete blocks. Two separate CONTAIN calculations are reported for blocks #82 and #84. For each block, the solid line in the figures represents the CONTAIN calculated heat transfer coefficient based on the HMTA modeling in the code using conditions for heat transfer calculated in the E11.4 test by CONTAIN. The additional calculation labeled "CONTAIN HMTA" for block #82 and #84 represents results from calculations where the measured bulk temperature, steam partial pressures, and temperature differential is input to separate CONTAIN steady state calculations to determine the heat transfer coefficients for the blocks. The error bars in the figures were generated based on assumed uncertainties in measured heat fluxes of +/-10% and uncertainties in the measured temperature differential of +/- one degree. The HDR Project did not provide uncertainties for the heat transfer coefficient measurements, nor were uncertainties mentioned in References Gre94 or Gre96, which discussed some of the heat transfer coefficient measurements with inferences to CONTAIN HMTA modeling. The estimated uncertainties in the factors (heat flux and temperature differential) required to calculate the coefficients are considered minimal values; the actual errors may be larger than shown in the figures. Clearly, as temperature differentials are reduced the error associated with the heat transfer coefficient increases as the relative uncertainty in the measured bulk to wall temperature differential increases - this is reflected in the figures.

Figure 3.63 shows that there is a good correlation between the two CONTAIN calculations that represent natural convection condensation conditions. The agreement indicates that the combination of boundary conditions (bulk temperature, steam partial pressures, and temperature differentials) represented by both calculations are consistent and in reasonable agreement for determining natural convection condensation. In comparing the CONTAIN results to the measured coefficients we see that there is an under estimation of the coefficients during the first 12000 seconds (200 minutes) of the transient. After this, the agreement between CONTAIN and measured coefficients is well within the assumed experimental measurement errors. The under prediction of heat transfer coefficient for block #84, which is located adjacent to the equipment shaft, is understandable given the measured steam/air mixture velocities in the region near the block. Measured velocities are shown in Figure 3.65. Velocity measurements near block #84 corresponds to sensor CF8401 which is located directly in the equipment shaft. Trends in the velocity measurements are evident in the heat transfer coefficients.

The model of the containment here uses the default cell velocity based on the default values for

hydraulic area A_{hd} of cell and weighting coefficients C_{in} and C_{out}.[2] These default values result in very low velocities for the nodalization used for E11.4, and through the default mixed convective correlation, produce a calculated condensation coefficient that reflects only the natural convective condensation process. The velocity measurements, of course, have significant uncertainties (perhaps +/- 0.5 m/s), and the measurements are not truly at the location of the heat transfer block; nevertheless, they indicate that there is some forced convective process occurring in this restrictive region near the main circulation pathway. To get an estimate of the increase in heat transfer that would occur had forced convective process been accounted for, a range of velocities (1 to 3 m/s) at the block location are used to determine the condensation coefficient at 4372 seconds (time of the maximum measured coefficient). In the assumed range of velocities, the coefficients values range from 100 to 244 W/m^2-K, respectively. Therefore, for the early portion of the transient, had a velocity in the 1-2 m/s range been calculated for the block the CONTAIN HMTA model would have predicted the coefficient to within the assumed measurement uncertainty.

How can we rationalize the under prediction of heat transfer coefficients with such a good estimation of pressure during the test, especially during the early transient? Part of the answer is that the amount of long-term (concrete) heat sinks in the proximity of the main circulation paths for E11.4 is small; most of the heat sinks are located in regions where the circulation currents are less than 1 m/s and therefore are well represented by a model that emphasizes natural convective condensation. We can see this in the other heat transfer block data. Block #82 is located in Room 1802 where the conditions are nearly stagnant. Figure 3.64 shows that the measured and calculated heat transfer coefficients are in very good agreement.

3.3.2.6 CVTR

A series of DBA simulation tests were conducted in a decommissioned reactor containment building in the late 1960's, as part of an effort to provide experimental information for use in developing and evaluating analytical methods for safety analyses of nuclear power plants. Three tests described in Reference Sch70 are simulated with the CONTAIN code and the results are discussed below. A summary of the key model/input options selected for the calculations are presented in Table 3.17.

3.3.2.6.1 Test #3 (no spray)

The CVTR DBA simulation test #3 has been used as a reference test for validating models in

[2] The cell velocity as calculated in CONTAIN is used in the mixed convective correlation used to determine the Nusselt number for a structure. This calculational method is described in Section 10 of the CONTAIN Code Manual [Mur97].

various containment analysis codes. In this test, steam is injected at an elevation of approximately 330 feet, slightly above the operation deck. The reference CONTAIN model of the CVTR is a 15-cell nodalization shown in Figure 3.66. As in the above calculations, the reference calculation for this test uses the default mixed convection option for the heat transfer and the default cell velocity calculation method; the result is that for the CVTR nodalization, the correlations for heat and mass transfer are the models for natural convective condensation processes. The heat sink input is based on "best-estimate" concrete areas as tabulated in the final report on the CVTR DBA simulations [Sch70] and on the upper bound estimate for exposed miscellaneous steel (this corresponds to 50% of the tabulated major-component steel area at 3/8" thickness).

A comparison of the predicted and measured pressure for CVTR test #3 is shown in Figure 3.67. The over prediction of the pressure during the injection period is believed to be the results of two causes: 1) neglect of the forced convection along the upper containment walls, and 2) the use of a nominal steam enthalpy that appeared to be slightly high. A decision to neglect forced convection along walls in the largely open upper containment region reflects on the fact that estimating forced convection in a free shear flow region is highly questionable with a lumped parameter code. However, in sensitivity studies the effect that forced convection can have on results is evaluated for various convective flows that are believed reasonable, as evidenced from some measurements taken during the test. The predicted and measured gas temperatures for CVTR test #3 are shown in Figure 3.68. The degree of temperature stratification is predicted quite well, especially at late times. The temperatures are clearly over predicted at early times, during a period in which CONTAIN predicts superheated conditions. At late times, when conditions are predicted to be saturated, the temperatures agree much better.

3.3.2.6.2 Tests #4 and #5 (sprays)

CONTAIN calculations for the CVTR facility were extended to include two spray tests, #4 and #5, using a more detailed containment nodalization scheme that added four additional cells below the operation deck, Figure 3.69. The approximate location of the spray nozzles is shown in the figure. For the tests, water at ~ 288 K and at rates of 290 gpm (test #4) and 500 gpm (test #5) were injected into the facility at an elevation of 25.9 m. The sprays followed a simulated DBA blowdown into the containment as discussed above - spray injections began at approximately 200 seconds and lasted about 12 minutes. The blowdowns for tests #3 (no sprays) and the spray tests were essentially identical.

Shown in Figure 3.70 are the pressure comparisons for tests with and without spray injections. These tests were calculated assuming no spray/wall interaction since it was specifically stated in the experimental report that spray nozzles were set at an angle to direct sprays away from the walls and toward the center of the containment. Shown in Figure 3.71 are the comparisons of gas temperatures in the upper containment (above the operating deck) below the spray nozzles.

Water from the sprays that fall onto the operation deck is directed to the basement. This "hot" water will increase evaporation in this region. Therefore, gas temperatures in the basement region will increase in the case of spray injections. This is shown in Figure 3.72 for both measurements and calculations. These test comparisons are integral test validations of the spray modeling in the CONTAIN code.

3.3.2.7 NUPEC Tests

NUPEC's Hydrogen Mixing and Distribution Test was conducted as a part of the "Proving Test on the Reliability for Reactor Containment Vessel" project [Tak91, Tak92]. A series of tests were performed to investigate hydrogen distribution phenomena in a 1/4 linearly scaled PWR containment. The intended use of the data was for evaluation and validation of containment analysis codes used to predict hydrogen concentrations for beyond DBA or SA scenarios. Four representative tests were selected (test numbers: M-4-3, M-7-1, M-8-1, and M-8-2) for analysis. Two of the tests, M–7-1 and M-8-2, include the effects of containment sprays on containment thermal hydraulics, transport, and mixing. The other two tests, M-4-3 and M-8-1, are performed without sprays. Shown in Table 3.18 are the main distinguishing features of the tests. A detailed review of the CONTAIN analyses of the NUPEC tests can be found in References Sta95, Sta98, and Mur96. In addition, since test M-7-1 was used for International Standard Problem 35 (ISP35), some additional details concerning the measurement procedures and facility description can be found in the ISP35 final report [OECD94]. In the following subsections, the tests are categorized according to whether the containment spray are activated.

The NUPEC facility was designed without incorporating long term heat sinks; therefore, the tests are of short duration, limited to the period of the hydrogen/steam injection. In this series of tests, the injection period lasts 30 minutes. For the spray tests, the test facility is pre-conditioned prior to the injection period: the initial pressure at the time of injection is approximately 140 kPa. Ambient conditions are used for the cases without spray activation.

Shown in Figures 3.73 and 3.74 are the two views of the nodalization scheme used for the CONTAIN model of the NUPEC facility. The model consists of 35 cells with various flow path connections as indicated in Figure 3.75. The operating region (cylinder and dome region) is described by cells 29-34 and cell 25 -- cell 25 is in the dome portion of the operating region. In the region below the operation deck, the containment is divided into two levels. The lowest level, includes regions that are described by cells 3-6, referred to as the lower general compartments. For the purposes of displaying the hydrogen distributions during the tests, the dome and lower general compartments are the only compartments considered here; other references mentioned above may be consulted for additional comparative analyses of distributions throughout the facility.

In terms of model options, the main model selections used in these calculations are presented Table 3.19. Since the spray modeling in the code is limited to a single cell having a water spray source, a number of pseudo pools are used in the operating region to feed a series of cascading spray sources for the cells that are directly below each other. This method is also used to model the multi-cell separate effects spray tests described in Section 3.

One important limitation of the reference NUPEC calculations presented in this section was that no spray water was assumed to contact the containment outer or inner partition walls. Water

from the upper level compartments is expected to impact the side walls of the containment, and spray water directly impacts the floor of the operation region and some other compartment walls and floors that are open to the operating region. In addition, it can be assumed that some spray water drain down from these compartments will wet other walls and floors of lower compartments. The effect of the water distributions on the containment outer and inner walls and floors is discussed below and also in Section 4; however, it should be kept in mind that the main focus of this series of tests was not atmospheric thermal hydraulics but hydrogen distribution; although, the thermal hydraulic response is important in that phenomena associated with the state of the atmosphere can influence the transport and mixing of gases in the facility.

3.3.2.7.1 M-7-1 [ISP-35] and M-8-2 (Hydrogen distribution with sprays)

Shown in Figures 3.76 and 3.77 are comparison of measured and calculated pressure and gas temperature in the dome region of the facility for tests M-7-1 and M-8-2. In general, these comparisons indicate that there are modeling difficulties with these tests in terms of the thermal hydraulic predictions. The under-estimation of pressure and temperature early in the transient for M-7-1 is believed to be related to the assumption made on input that spray water does not impact the containment outer walls. As was seen in the separate effects spray tests, spray water cooling of hot wall surfaces can have a significant affect on the containment atmosphere. Water that contacts the walls evaporates from the surfaces and adds to the vapor content of the region; this effect reduces the rate of pressure and gas temperature reduction during the early spray period when the walls are still very hot. In the reference calculations described here, heat transfer from the containment walls is assumed to be enhanced only through forced convective condensation/evaporation processes occurring along the containment walls. It is hypothesized that the interaction of the sprays generate strong updraft currents (14 m/s) along the walls and these currents are responsible for cooling of the wall surfaces [Sta95, Sta98]. Although the comparisons of the containment wall surface temperature in the dome, as shown in Figure 3.78, is reasonable given this method of wall cooling, the atmospheric temperature calculation is clearly not consistent with this modeling approach.

Later in the transient the atmospheric temperatures are in better agreement, but the pressure predictions are significantly over estimated, meaning that the calculation of energy released to the atmosphere is too high in the CONTAIN calculations soon after the start of the transient. The observation that there is too much energy released to the atmosphere in these calculations, after the early period, has been a common fault with most participating codes in the ISP35 exercise. (In fact, when the sprays are terminated at 30 minutes, these calculations show a significant increase in the gas pressure which is not observed -- further indication that too much energy remains in the structures after the spray period, and released later to the atmosphere.)

One reason for the pressure over prediction in each test has to do with the neglect, or inadequate treatment of both the containment wall and inner structure surface cooling by spray water. Shown in Tables 3.20 and 3.21 are the mass and energy balance from measurements for test

M-7-1. We see from Table 3.21 that the total condensed steam in the test is about 238 kg (including the amount of supplied steam). To condense that amount of steam requires the removal of approximately 6.43 x 10^5 kJ of energy. As spray water is added to the containment atmosphere, the spray droplets condense out steam as the droplets are heated to thermal equilibrium with the atmosphere. As seen from the mass balance table, the amount of energy change associated with the spray water is significantly higher than what could be expected based only on steam condensation. In fact, most of the energy change in the C/V walls and inner structures is due to sensible heat transfer to the spray water. That amount of sensible heat transfer is somewhat higher than the energy transferred from steam to the spray water. When the spray and condensate water drain from the C/V and inner structures, a considerable amount of sensible heat is transferred to sumps without any involvement of the atmosphere. Some energy from structures is transferred to the atmosphere by evaporation of spray water early in the transient as noted above, and then condensed out of the atmosphere. However, by neglecting the interaction of spray water with structures too much energy is left in the structures shortly after the transient begins, this energy is then transferred to the atmosphere, keeping the pressure higher than measured.

In the case of M-8-2, which has helium and steam injections located higher in the containment (injected into the pressurizer compartment, cells 22 and 35), the over estimation of pressure is greater than M-7-1. Part of the reason for this difference may be due to the lack of modeling the enhancement in mixing caused by spray dynamics (drag of spray droplets on surrounding steam/air mixtures), wherein colder gas in some lower compartments are mixed with hotter gases in the regions above the operating deck .

The low injection location for M-7-1 favors a uniform mixture of helium gas in the facility, even without the spray effect that enhances turbulent mixing and transport. Approximately 27 kg of helium are released into the containment over the 30 minute injection period. For complete mixing in the facility the final concentration (dry basis) would be 11.1%. As shown in Figure 3.79, the M-7-1 concentration measured and calculated in dome is very close to this completely mixed limit. What is even more interesting, is that for the higher injection location in test M-8-2, the complete mixing limit is also nearly met with the CONTAIN model in agreement with observation. This good agreement for M-8-2 is calculated with a model that does not account for enhanced transport (intra-compartment) as a result of spray dynamics (i.e., spray droplet drag on the gas mixture that creates turbulence). In this case, transport is only by intra-compartment flows generated by buoyancy driven forces. Evidently, the compartmental cooling effects of the sprays generate mixing currents between the compartments that are primarily responsible for the gas transport observed. Within compartments where the sprays are falling, the phenomenon of spray dynamics is believed to be mainly responsible for the highly turbulent mixing that occurs. For these compartments, the uniform mixing assumption of the lump parameter code, of course, gives similar results. The overall effect, with uniform mixing in spray compartments and buoyancy driven transport between compartments, is that the results for helium mixing and transport is in good agreement with the observations in the test M-8-2.

3.3.2.7.2 M-4-3 and M-8-1 (Hydrogen distribution without sprays)

In both tests without sprays, the facility is not pre-conditioned; therefore, the atmosphere and structure temperatures are at ambient temperature prior to the steam/helium injection. The heat transfer to the containment walls and inner structures is driven primarily by condensation. In modeling this process, it is assumed that mass transfer is by natural convection condensation. From a comparison of measured and calculated dome wall temperatures, Figure 3.80, we see that condensation in the dome region is under predicted in both tests with the rate of change in the temperatures occurring early in the transient. The tendencies to under predict condensation processes in the above deck region is likely the reason for the slight over prediction in containment pressure for each test as shown in Figure 3.81. The difference however is small. As was pointed out in Mur96, the hybrid flow solver does not model plume behavior, which early in the transient causes a stratified layer interface to work its way down from the top of the dome to the injection elevation in time. The CONTAIN hybrid flow solver will mix the region above the injection elevation faster than what could be expected had plume mixing been modeled. A higher concentration of steam in the dome region would increase condensation in the region and therefore this reasoning could explain the early disparity between the measured and calculated dome wall temperatures. Whether the cause of the under prediction in condensation is the result of errors in the steam distribution calculation (perhaps as a result of some degree of plume formation which is not modeled), or even in the HMTA condensation model, the lack of detailed thermal hydraulic instrumentation limits our ability to determine the exact reason for the slight over prediction in pressures. Based however on the variation between the two measured pressures, and on the reasoning that these two tests differ only in regards to injection location which would affect plume behavior, it is likely that the observed over prediction in pressure is the result of a initial error in the distribution of steam as calculated with CONTAIN. Even though the gas temperatures in the dome are predicted with good accuracy as shown in Figure 3.82, temperature alone is not a measure of steam concentration in a nonuniform gas/steam mixture.

One of the important observations in the tests, and predicted, is the degree that helium gas stratifies depending on the injection location. Shown in Figures 3.83 and 3.84 are the measured and calculated helium concentrations comparisons for tests M-8-1 and M-4-3. In the case of the lower injection, test M-4-3, the gas rapidly becomes completely mixed. The mass of helium injected into the containment over 30 minutes, for both tests, is 48.6 kg. A uniformly mixed gas would have a helium concentration (dry basis) of 18.3% at the end of the injection. As shown in the figures, test M-4-3 has a final helium concentration near this value. However, for the elevated injection in test M-8-1, the facility atmosphere is not well mixed. In the dome region the final helium concentration is nearly twice the concentration as measured and calculated by CONTAIN. The very good predictions of the helium gas stratification during these tests with no spray activation is verification of the hybrid flow solver modeling method for predicting stable stratification processes in PWR containments. (Of course, these tests also show that the so called

"global concentration" estimations based on an assumption of uniform mixing is not an acceptable method when the injection locations are elevated, such as when light gas is released in the pressurizer compartment, and sprays are not activated.)

Table 3.11 Key modeling/input options used in the HDR reference calculations	
Test	Model/Input Option
V44 (ISP16)	• 5 cell nodalization • default thermal properties for steel and concrete • default convective velocities • default film thickness for condensate • no thermal radiation • overflow condensate removed from facility • CFC range from 0.83 to 1.38 • water aerosols
T31.5 (ISP23)	• 33 cell nodalization • default thermal properties for steel and concrete • default convective velocities • default film thickness • with thermal radiation • overflow condensate removed from facility • CFC set to 1 • water aerosols
T31.5 (HDR benchmark)	• same as T31.5 (ISP23)
E11.2 (ISP29)	• 15 cell nodalization (including environment cell) • HDR thermal properties for steel and concrete • default convective velocities • default film thickness • with thermal radiation • film tracking on external shell • annular gas between containment shell and concrete building modeled using four cells • coolant energy extraction using code modification • overflow of condensate accumulated in sump • CFC set to 1 • water aerosols
E11.4 (HDR benchmark)	• 48 cell nodalization (includes environment cell) • default thermal properties for concrete • default convective velocities • default film thickness • with thermal radiation • coolant energy extraction using code modification • annular gas between containment shell and concrete building modeled using • overflow of condensate accumulated in sump • CFC set to 1 • water aerosols

Table 3.12 HDR facility [33 cell nodalization]			
Cell #	Volume, m^3	Elevation, m	Rooms
1	1893	-1.379	1201, 1202,1203, 1301, 1302, 1303, 1304, 1305, 1307, 1308, 1311, 1317, 1401, 1403, 1404, 1405, 1406, 1408, 1409, 1410, 1420,1421
2	655	7.354	1501, 1502, 1503, 1504, 1505, 1506, 1507, 1512, 1513
3	295	7.640	1508, 1511, 1514
4	280	15.1	1603
5	192	12.38	1611
6	303	11.851	1602, 1609, 1606
7	190	10.871	1604, 1607, 1608, 1605
8	44	15.35	1701u
9	64	21.85	1701o
10	793	18.07	1704 (breakroom)
11	90	17.6	1708
12	119	17.05	1707
13	156	17.05	1702, 1703, 1706
14	164	27.171	1803, 1904, 1905
15	343	26.05	1801
16	58	22.85	1805
17	125	22.85	1802
18	79	22.85	1804
19	38	27.6	1902
20	78	27.05	1901, 1911
21	71	27.6	1903
22	61	7.65	1327
23	40	12	1337

Table 3.12 HDR facility [33 cell nodalization] cont.			
Cell #	Volume, m^3	Elevation, m	Rooms
24	83	17.05	1347
25	68	22.85	1357
26	82	27.05	1367
27	947.98	34.35	11004*
28	947.98	34.35	11004*
29	216.3	34.35	11004*
30	216.3	41.35	11004*
31	890.62	41.35	11004*
32	890.62	41.35	11004*
33	690.19	46.85	11004*

* portion of above deck operation region designated as room 11004

Table 3.13 HDR Facility [15 cell nodalization]				
Cell #	**Volume, m^3**	**Elevation, m**	**Cooling Fraction**	**Rooms**
1	836	-4.567	0.1	1201, 1202, 1203, 1301, 1302, 1304 1305, 1307, 1308, 1311
2	2113	4.195	0.24	1405, 1406, 1407, 1403, 1409, 1401, 1410, 1408, 1404, 1317, 1327, 1501, 1506, 1507, 1512, 1513, 1502, 1520, 1503, 1504, 1505, 1508, 1511, 1514
3	1005	12.678	0.16	1603, 1611, 1602, 1609, 1606, 1604, 1607, 1608, 1605, 1337
4	574	25.0566	0.14	17010, 1902, 1804, 1902, 1803, 1904, 1905
5	202	17.05	0.02	1707, 1347
6	279	25.293	0.08	1805, 1903, 1357, 1367
7	2146.766	34.133	0.0835	33332, 33333, 1801
8	901.883	35.67	0.0351	33331
9	2094.35	45.25	0.0814	33334
10	588.16	45.25	0	2011 *
11	367.166	35.67	0	2012, 2022, 2032 *
12	654.3	22.42	0	2013, 2023, 2033 *
13	1033.58	3.34	0	2014, 2015, 2016, 2024, 2025, 2026, 2034, 2035, 2036, 2017, 2027, 2037 *
14	1083	17.77	0.06	17011, 1704, 1708, 1703, 1706, 1702
15	environ	0	0	N/A

* air gap between containment shell and concrete building

Table 3.14 HDR Facility [48 cell nodalization]				
Cell #	**Volume, m^3**	**Elevation, m**	**Cooling Fraction**	**Rooms**
1	217	-7.139	0.0612	1201, 1202, 1203, 1303
2	619	-3.665	0.0408	1301, 1302, 1304, 1305, 1307, 1308, 1311
3	445	0.839	0.0612	1405, 1406, 1407
4	113	1.15	0.0408	1403, 1409
5	359	1.539	0.0204	1401, 1410, 1317
6	59	1.0	0	1408
7	116	1.15	0	1404
8	166	8.117	0	1501, 1506, 1507, 1512, 1513
9	499	7.109	0.0612	1502, 1520, 1503, 1504, 1505
10	295	7.64	0.0408	1508, 1511, 1514
11	280	15.1	0.0204	1603
12	192	12.38	0.0612	1611
13	61	12.0	0	1602
14	59	12.38	0	1609
15	183	11.63	0.0408	1606
16	112	11.63	0.0204	1604, 1607, 1608
17	78	9.78	0	1605
18	44	15.35	0.0204	17011
19	64	21.85	0	17010
20	793	18.07	0.0612	1704

Table 3.14 HDR Facility [48 cell nodalization] cont.				
Cell #	**Volume, m^3**	**Elevation, m**	**Cooling Fraction**	**Rooms**
21	90	17.6	0.0204	1708
22	119	17.05	0.0204	1707
23	102	17.05	0.0204	1703, 1706
24	54	17.05	0	1702
25	164	27.171	0.0204	1803, 1904, 1905
26	343	26.05	0.0204	1801
27	279	25.293	0.0612	1805, 1903, 1357, 1367
28	125	22.85	0.0204	1802
29	169	25.38	0.0408	1804, 1902
30	61	7.65	0	1327
31	40	12.0	0.0204	1337
32	83	17.05	0	1347
33	588.16	45.25	0	2011
34	124.903	35.67	0	2012
35	117.36	35.67	0	2022
36	124.903	35.67	0	2032
37	218.1	22.42	0	2013
38	218.1	22.42	0	2023
39	218.1	22.42	0	2033
40	232.43	6.871	0	2014, 2015, 2016

Table 3.14 HDR Facility [48 cell nodalization] cont.				
Cell #	**Volume, m^3**	**Elevation, m**	**Cooling Fraction**	**Rooms**
41	384.3	7.014	0	2024, 2025, 2026
42	235.6	6.961	0	2034, 2035, 2036
43	384.3	-2.75	0	2017, 2027, 2037
44	901.883	35.67	0.0408	33331
45	901.883	35.67	0.0204	33332
46	901.883	35.67	0.0612	33333
47	2094.35	45.25	0.0816	33334
48	environ	0	0	N/A

Table 3.15 Gas concentration [%] comparisons for HDR test E11.4 (t=2175 min.)			
Room (sensor elev.)	Cell #	Measured	Calculated
33334 (40.5 m)	47	5.6	5.53
1503 (6.8 m)	9	5.9	5.99
1704 (avg 17.6, 23.3, and 28.0 meter measurements)	20	5.79	5.87

Table 3.16 Concrete heat transfer block data			
Block #	Elevation, m	HDR Room	Internal TC's
82	22.6	1802	ct8201-8202
84	23.5	1804	ct8401-8402

Table 3.17 Key modeling/input options used in the CVTR reference calculations	
Test	Model/Input Options
#3	• 15 cell nodalization • specified thermal properties for steel and concrete • default convective velocities • default paint heat transfer coefficient • film thickness = 0.0001 meters for condensate • overflow condensate to sump • flooding of lower concrete structures in contact with sump • atmospheric radiation to structures • CFC set to 1 • upper bound estimate misc. steel mass - 50% measured large structure steel
#4	• 19 cell nodalization • sprays modeled with pseudo pools for cascading spray sources • default spray droplet diameter • default convective velocities • default paint heat transfer coefficient • film thickness = 0.0001 meters for condensate • overflow condensate to sump • flooding of lower concrete structures in contact with sump • atmospheric radiation to structures • CFC set to 1 • upper bound estimate misc. steel mass - 50% measured large structure steel
#5	• same as #4, except for adjustment in the spray source rate

Table 3.18 Comparison of the differences that had the largest effect on the thermal hydraulics amoung the test analyzed for the NUPEC series by the CONTAIN code		
Release Location	No Sprays	Sprays
Low-elevation	M-4-3	M-7-1
Mid-elevation	M-8-1	M-8-2

Table 3.19 CONTAIN modeling/input options for NUPEC tests.	
Test	Model/Input Options
M-7-1	• spray model for cells 29-34, 25 (with pseudo pools to feed lower cell spray source) • forced convective heat and mass transfer along the above deck C/V walls (14 m/s for 30 minutes) • atmospheric to wall radiation • condensate drain from walls to lower compartment sump using overflow keyword • default film thickness calculation • C/V wall and partitions modeled with conducting heat slabs • insulation modeled/outside wall heat transfer coefficient set to 6.28 W/m^2-K • no spray water/structure modeling or draining effect (pool on first floor level drained to sump directly) • injection into cell 8
M-8-2	• same as above, except injection into cells 22 and 35
M-4-3	• no spray source or pseudo pools in the upper containment • natural convective condensation modeling • atmospheric to wall radiation • condensate drain from walls to lower compartment sump using overflow keyword • default film thickness calculation • C/V wall and partitions modeled with conducting heat slabs • insulation modeled/outside wall heat transfer coefficient set to 6.28 W/m^2-K • injection in cell 8
M-8-1	• same as M-4-3, except injection into cells 22 and 35

Table 3.20 Energy balance for NUPEC test M-7-1 [OECD94]		
Component	Supplied energy kJ	Energy change during test kJ
He	$4.02\pm0.21 \times 10^4$	$4.50\pm0.09 \times 10^4$
Steam	$2.67\pm0.15 \times 10^5$	$-3.69\pm0.75 \times 10^5$ *)
Spray water	$5.85\pm0.33 \times 10^6$	$7.22\pm0.36 \times 10^6$ **)
Air		$-3.63\pm2.16 \times 10^4$
Inner structures		$-3.14\pm0.42 \times 10^5$
C/V walls		$-3.68\pm0.66 \times 10^5$

*) Calculated assuming saturated steam

**) Including condensed water

Table 3.21 Mass balance for NUPEC test M-7-1 [OECD94]			
Component	Supplied mass kg	Mass existed in the containment kg	
		Start of test	End of test
He	$2.70\pm0.15 \times 10^1$	0.0	$2.74\pm0.06 \times 10^1$
Steam	$9.90\pm0.54 \times 10^1$	$2.19\pm0.27 \times 10^2$	$7.99\pm0.72 \times 10^1$
Spray	$3.49\pm0.18 \times 10^4$	0.0	$3.52\pm0.18 \times 10^4$

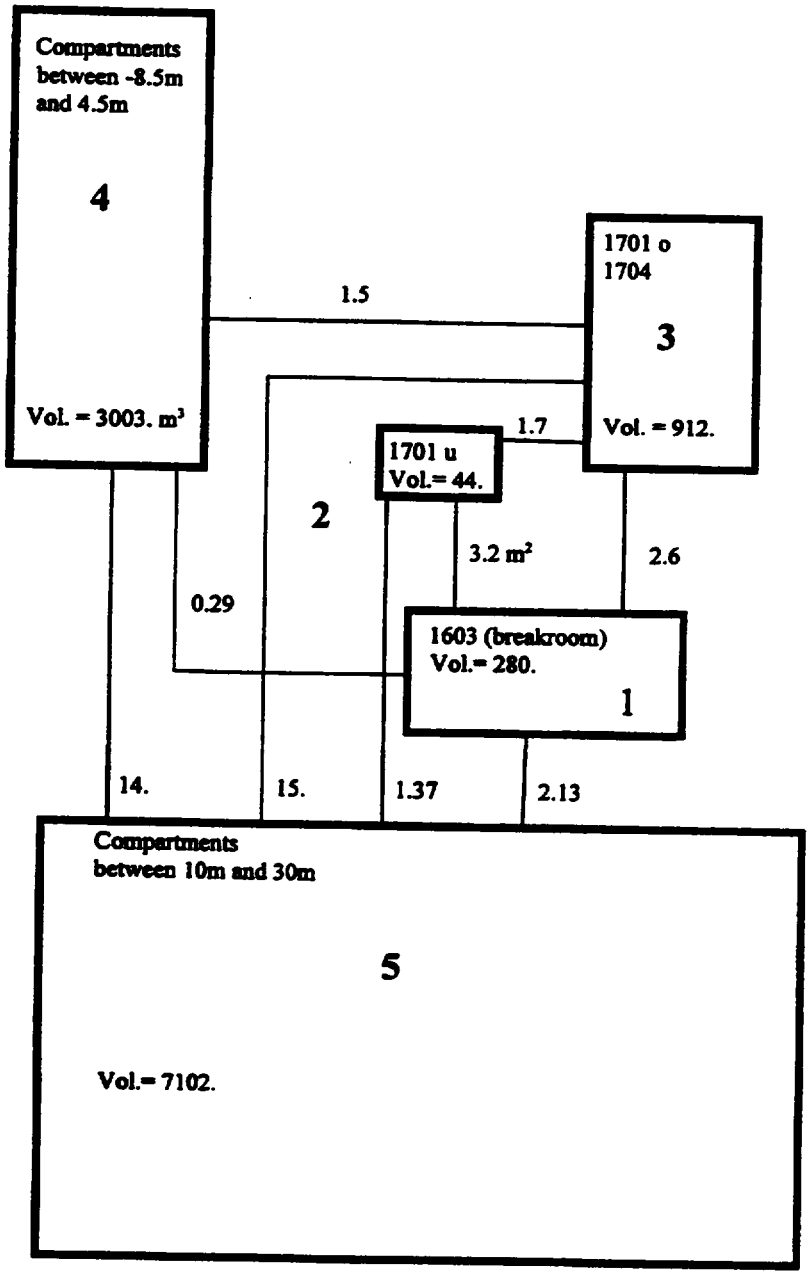

Figure 3.31 CONTAIN nodalization for the HDR 5 cell V44 reference calculation.

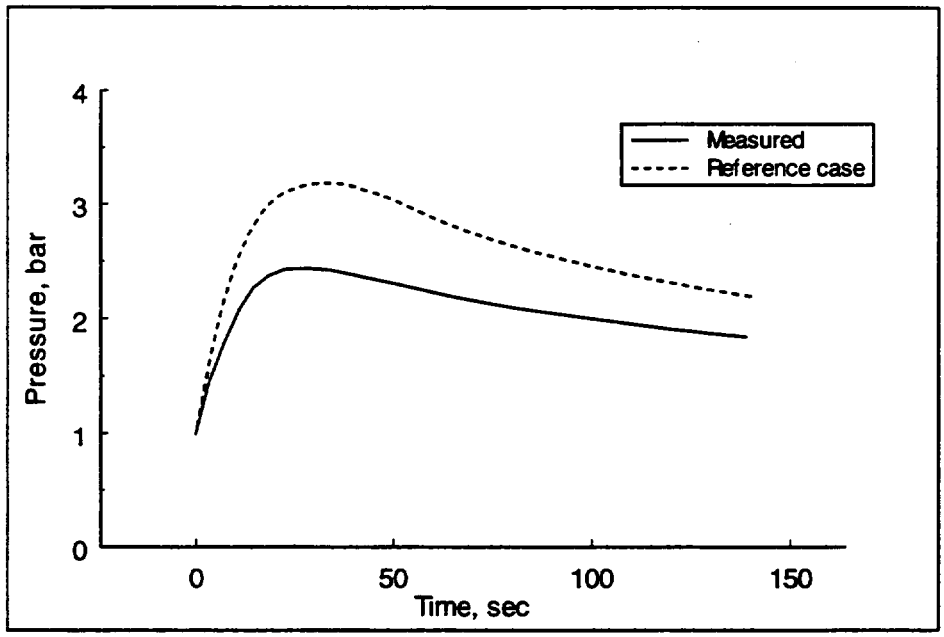

Figure 3.32 Comparison of measured and CONTAIN calculated containment pressures for HDR test V44.

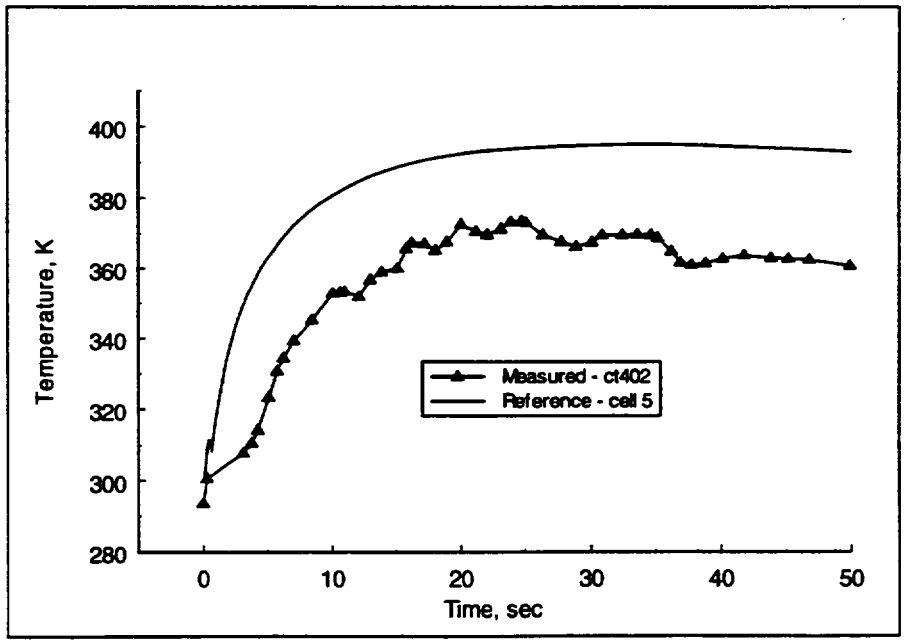

Figure 3.33 Comparison of measured and CONTAIN calculated containment temperature for HDR test V44. The measurement is at an elevation of 30.8 meters.

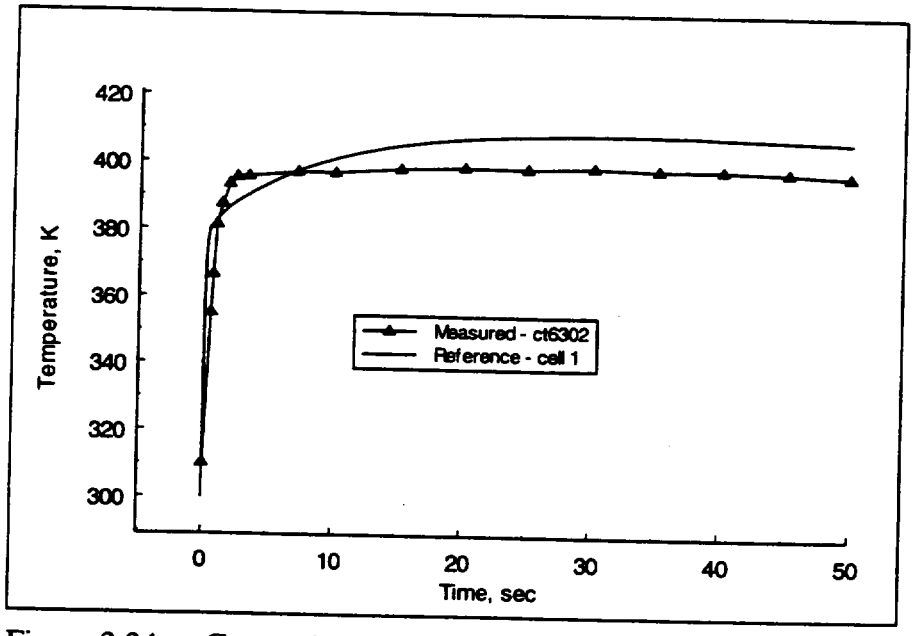

Figure 3.34 Comparison of measured and CONTAIN calculated breakroom temperature for HDR test V44

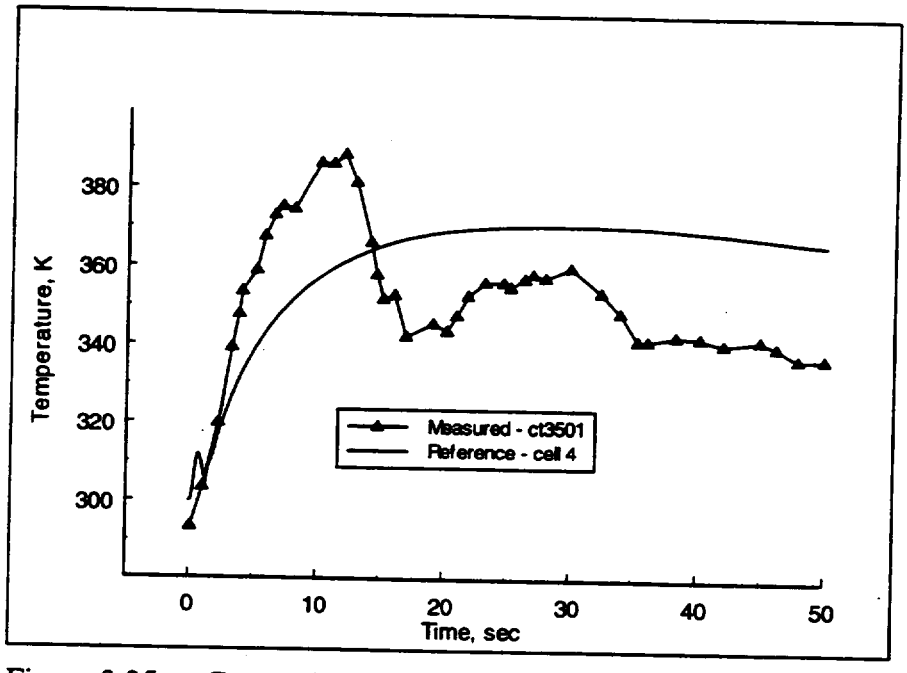

Figure 3.35 Comparison of measured and CONTAIN calculated temperature in the lower containment for HDR test V44. The measurement location is at an elevation of -4.8 meters.

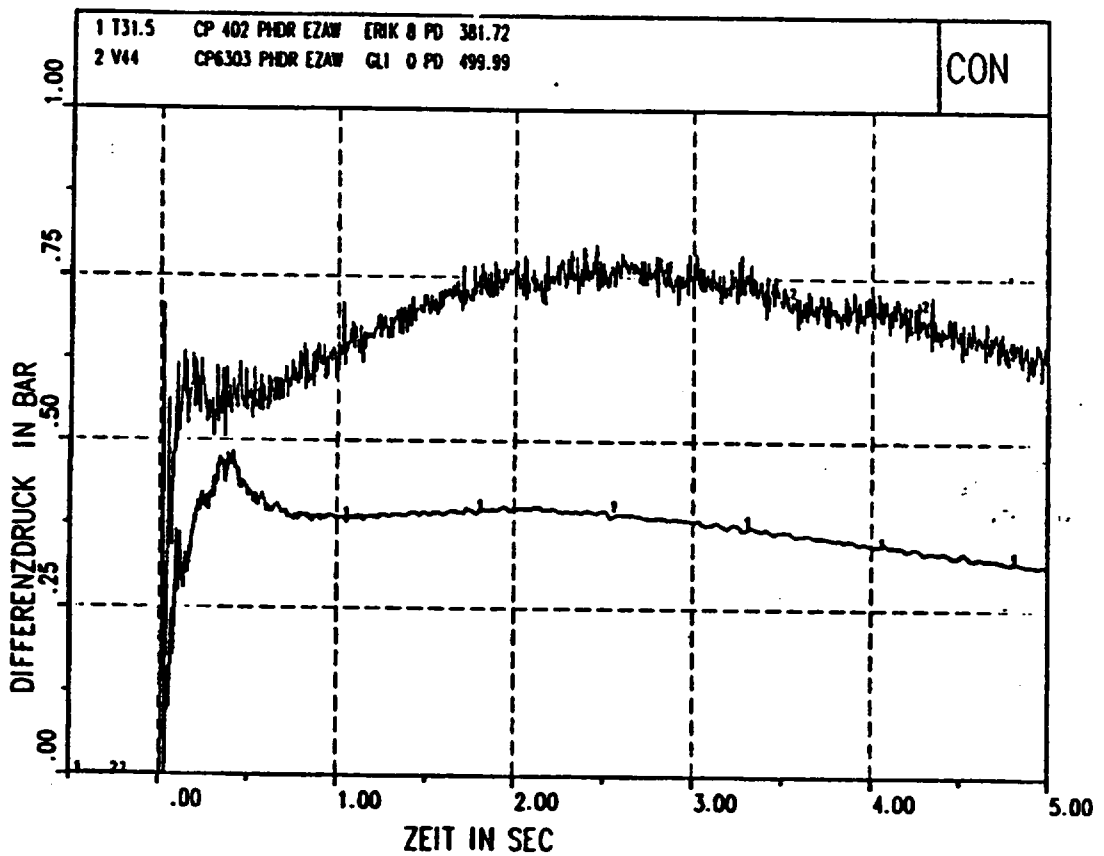

Figure 3.36 Pressure difference between compartment of rupture and adjacent compartments for ISP16 (V44) and ISP23 (T31.5) [Kar89].

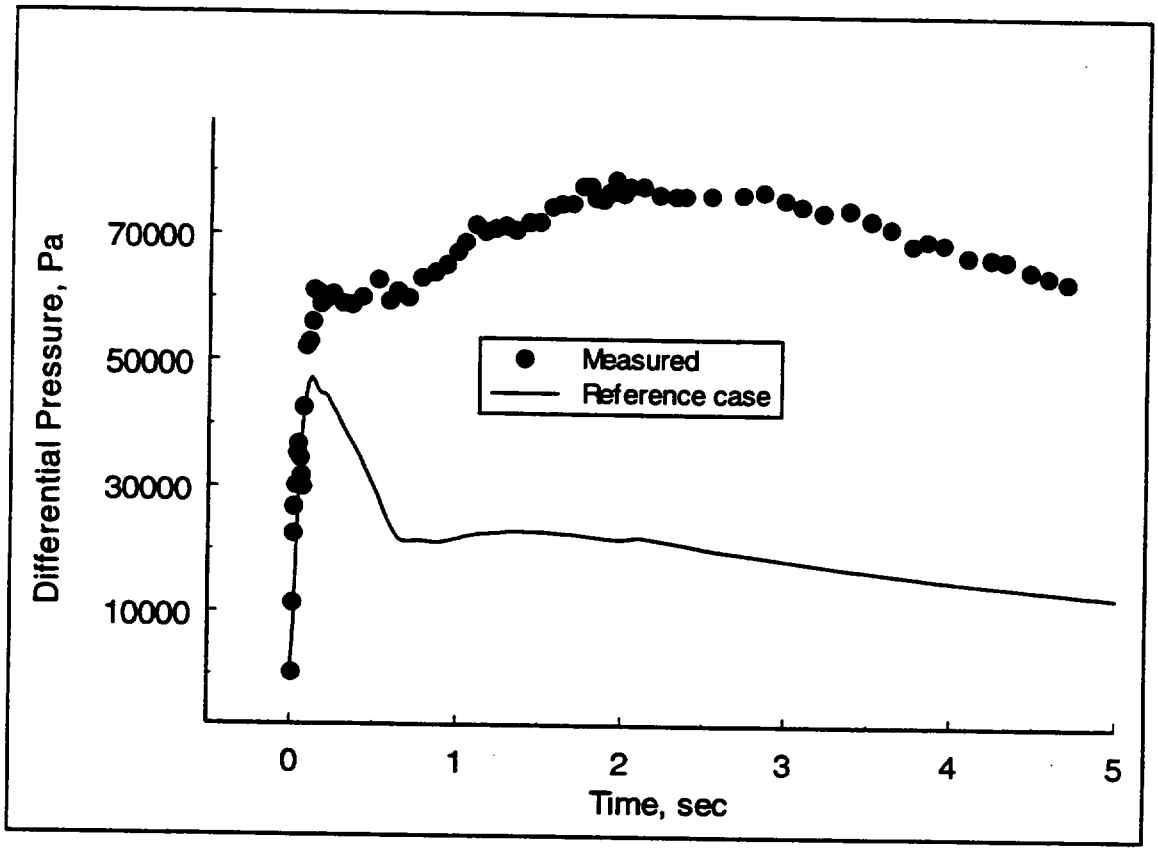

Figure 3.37 Comparison of measured and CONTAIN calculated differential pressures between the breakroom and an adjacent room (1708) for HDR test V44.

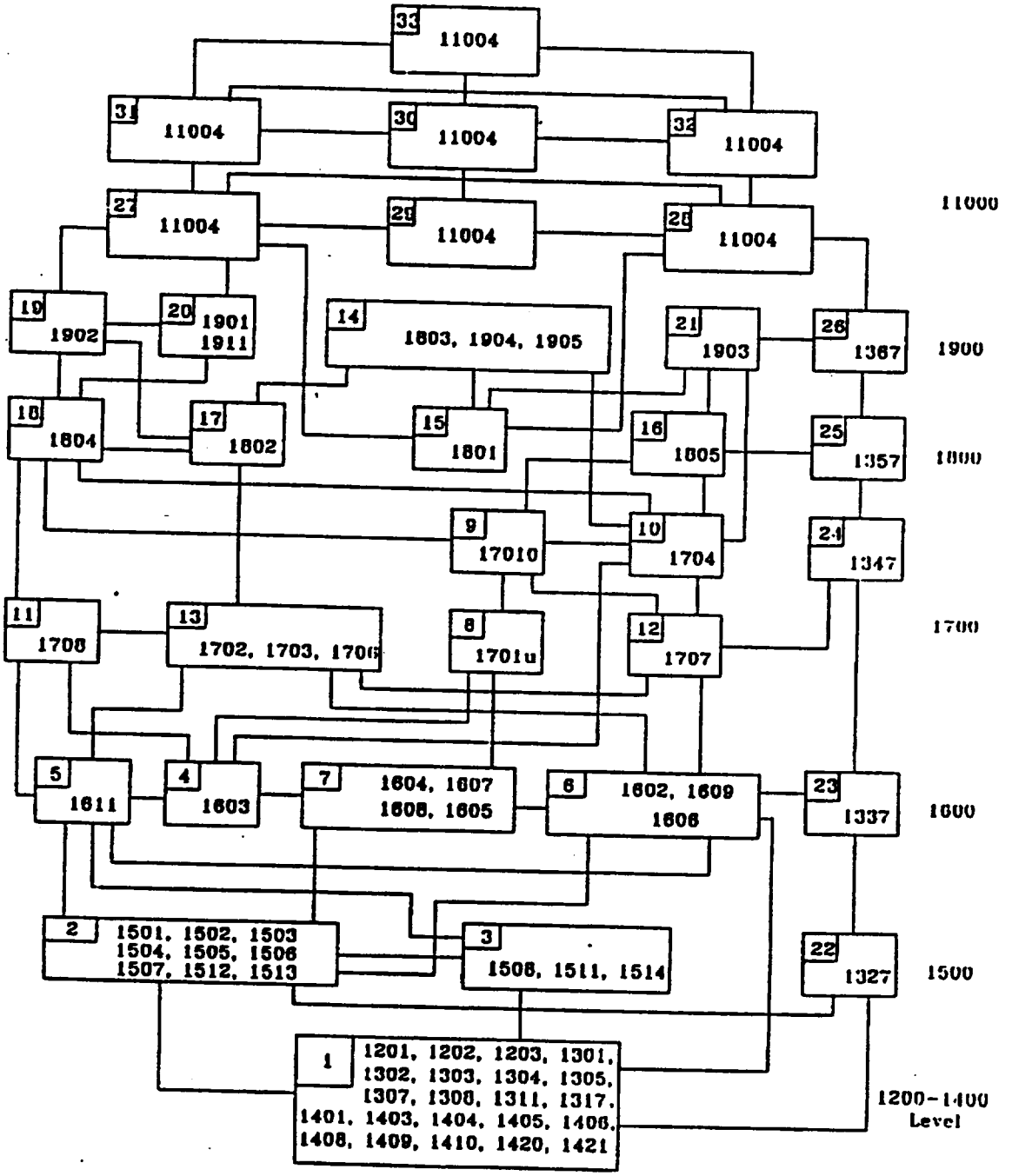

Figure 3.38 CONTAIN nodalization of the HDR facility for ISP23

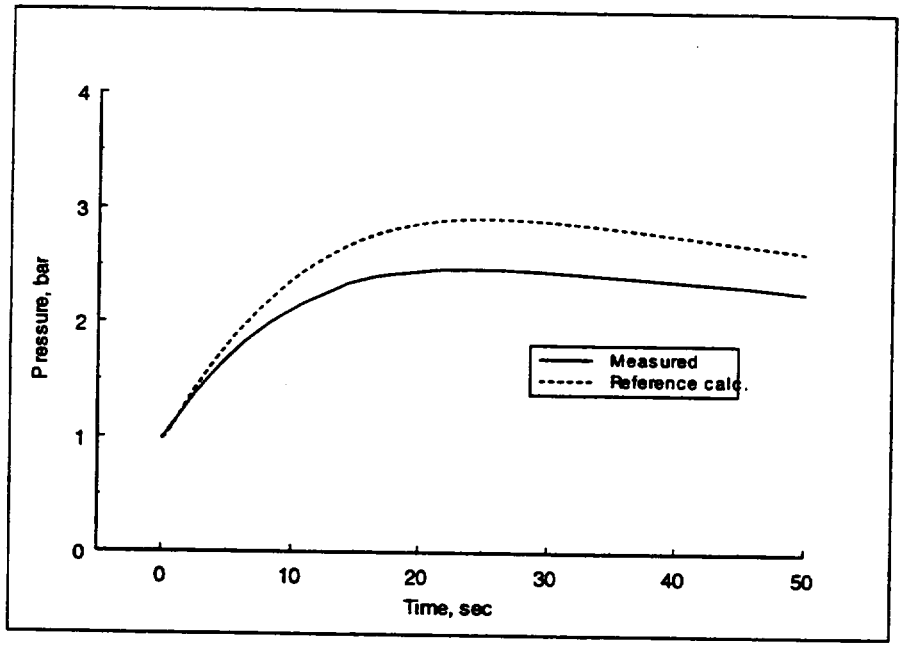

Figure 3.39 Comparison of the T31.5 test containment pressures for the CONTAIN reference calculation and measurement.

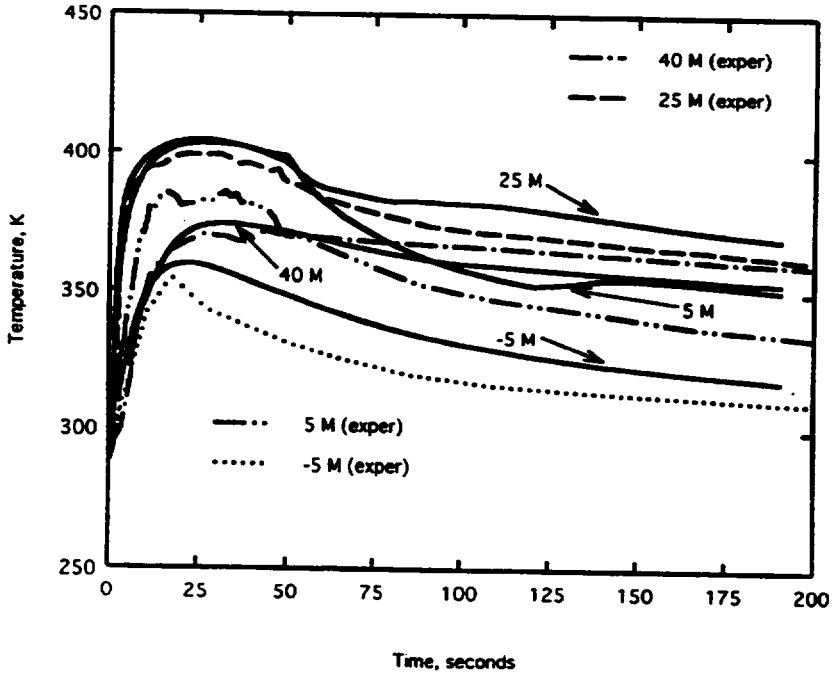

Figure 3.40 Comparison of the T31.5 test containment temperatures for the CONTAIN reference calculation and measurement.

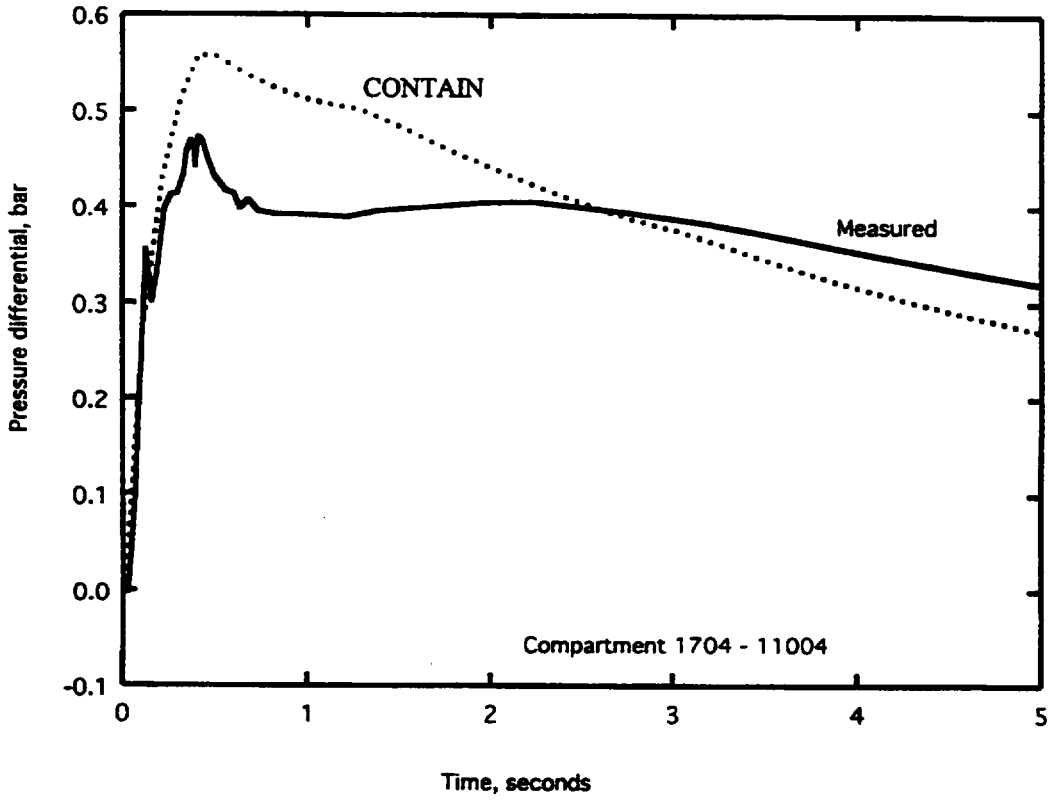

Figure 3.41 Comparison of the T31.5 test pressure differential for the CONTAIN reference calculation and measurement.

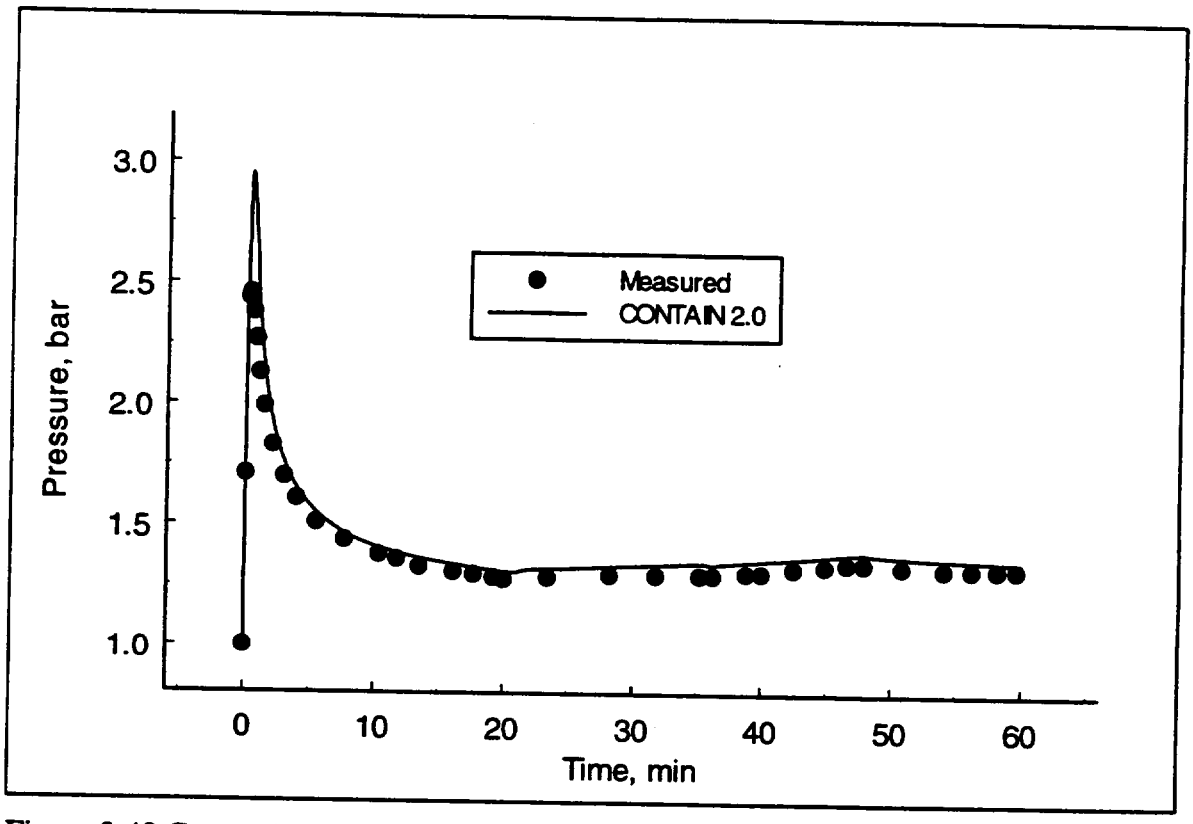

Figure 3.42 Comparison of measured and calculated gas pressure for the T31.5 benchmark exercise.

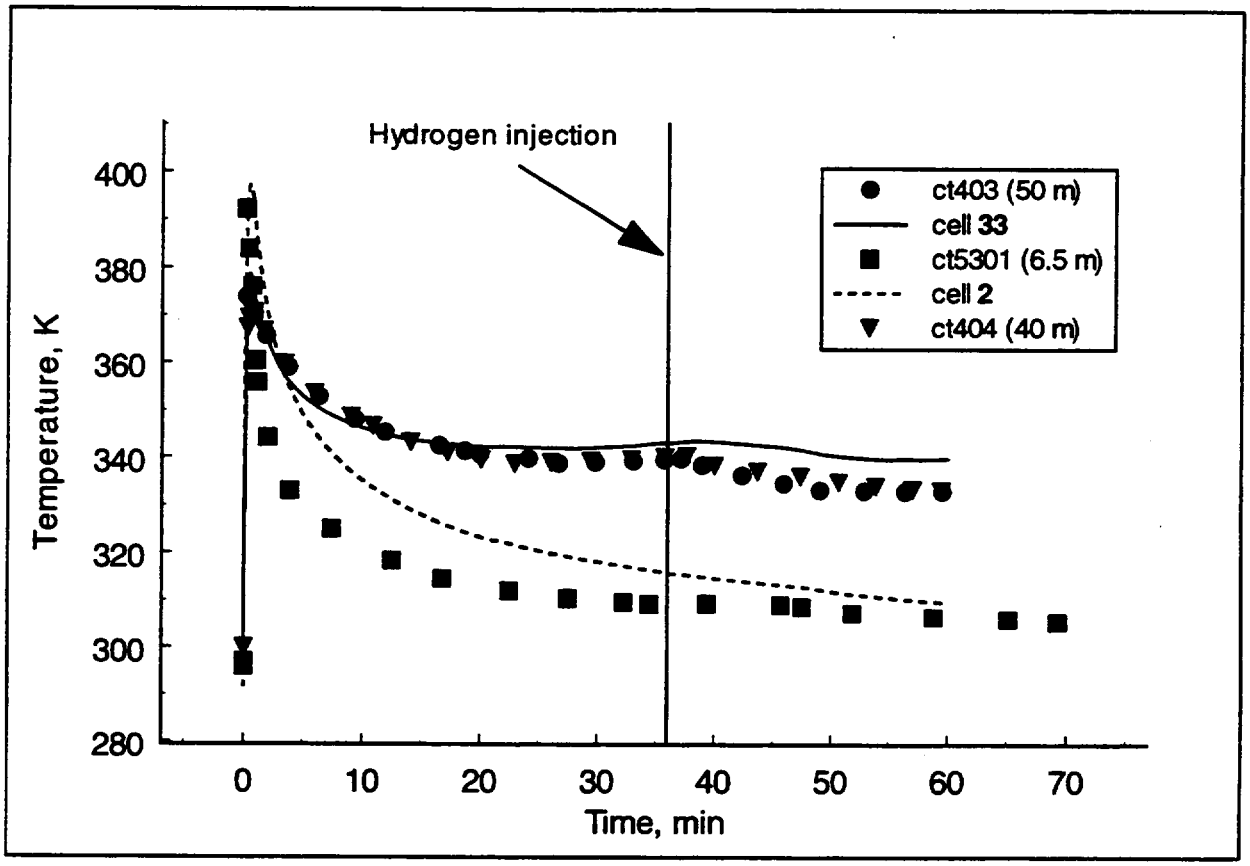

Figure 3.43 Comparison of measured and calculated upper and lower containment temperatures for the T31.5 benchmark exercise.

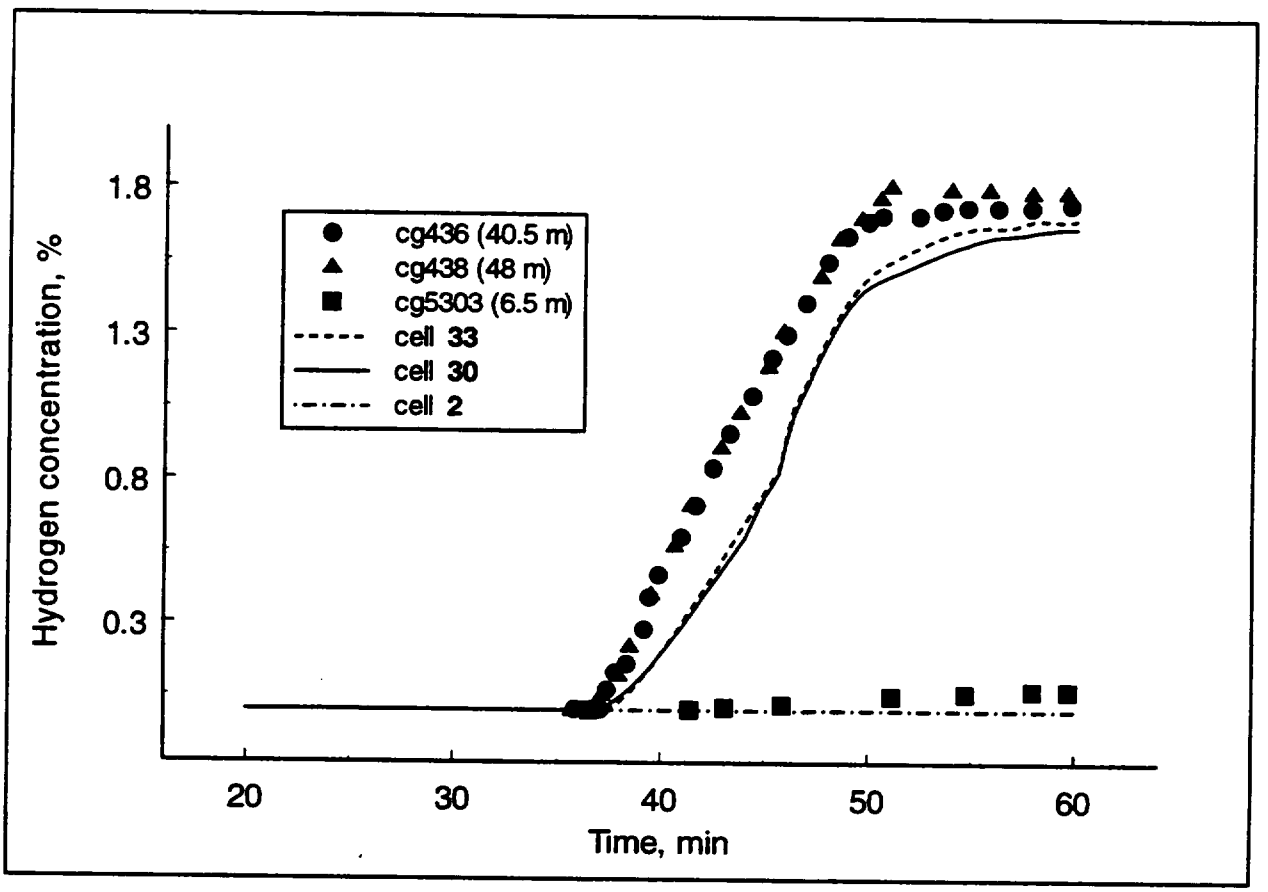

Figure 3.44 Comparison of measured and calculated hydrogen concentration in the upper and lower containment for the T31.5 benchmark exercise.

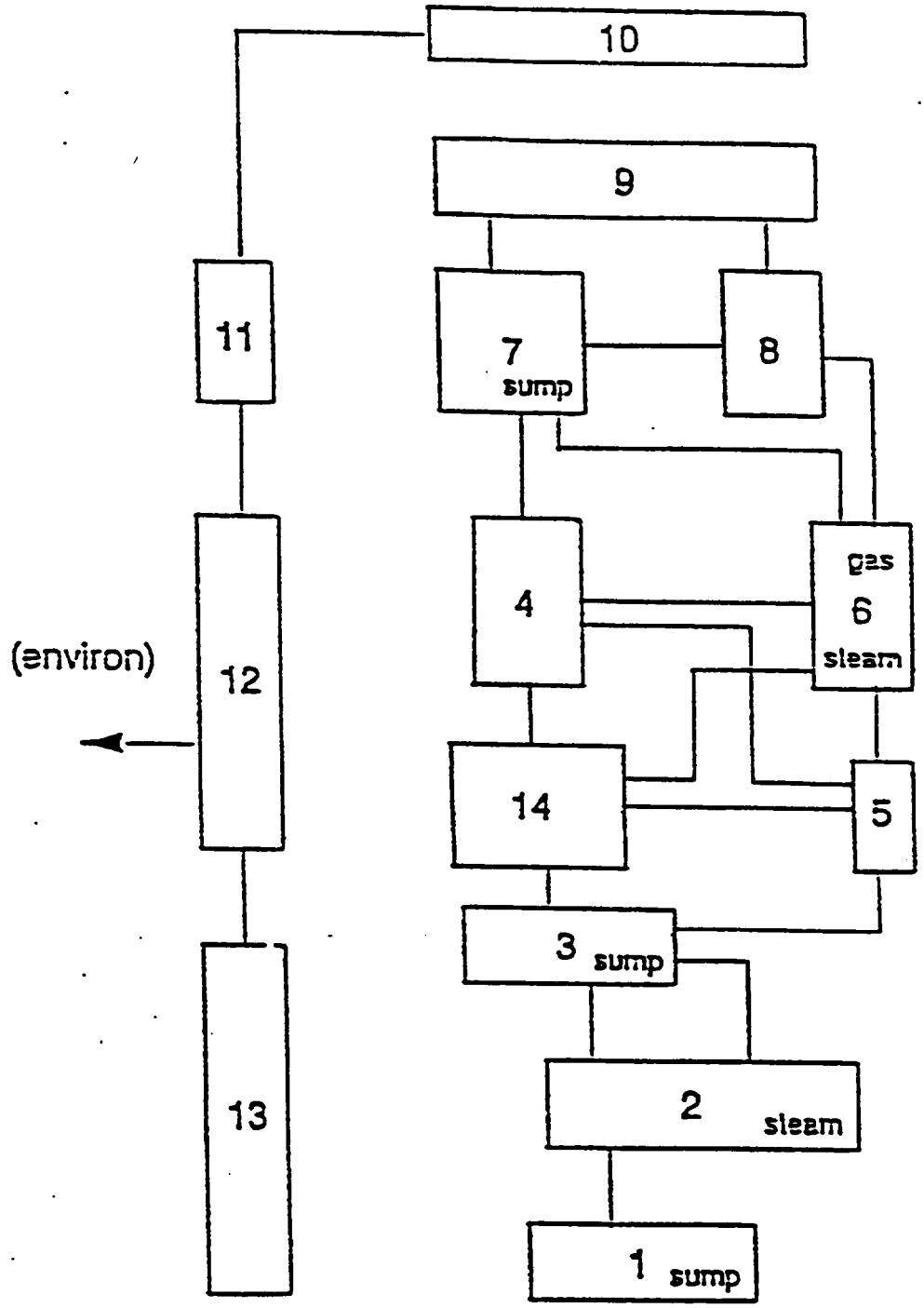

Figure 3.45 Schematic of the HDR 15-cell deck

Test No.:	E11.1	E11.2
Geometry:	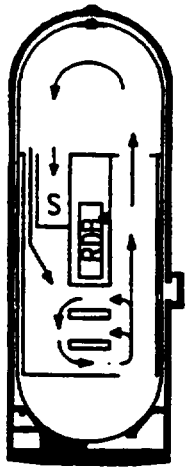	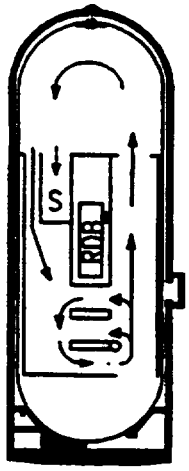
Characterization:	Small break +23m Loop-Geometry Dead end room 1802	Small break +23m Loop-Geometry Dead end room 1802

● Position of break and injection, BS

○ 2. position of injection

S Dead end room closed at its lower end

Course of experimental procedure:

	E11.1	E11.2
steam injection at BS	~11.17h	~11.5h
steam + H_2-injection at break position, BS	1.33h	1.37h
steam injection at BS	~0.67h (at BS)	~3.12h (2. injection pos.)
natural cooldown	~ 2.58	~ 0.27h
inside spray	2.55h	
external spray		3.08h
natural cooldown	10.73h	~ 4.75h
venting	till depressurization	till depressurization

Related to: Begin of KSU-ND*-path

Figure 3.46 Test setup for experiments E11.1 and E11.2.

Figure 3.47 Experimental procedure for E11.2

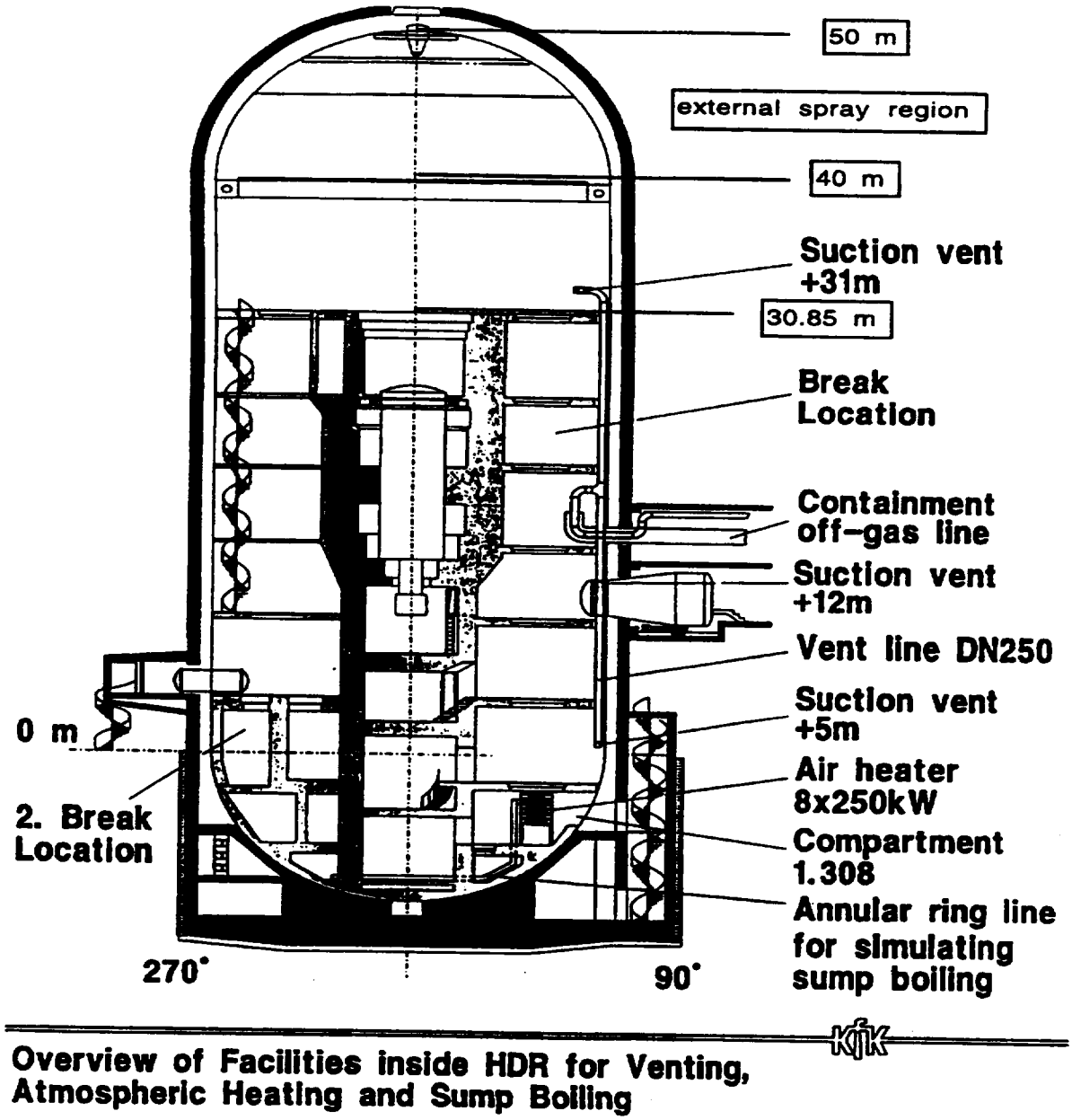

Figure 3.48 HDR facility showing the configuration for the E11.2 test.

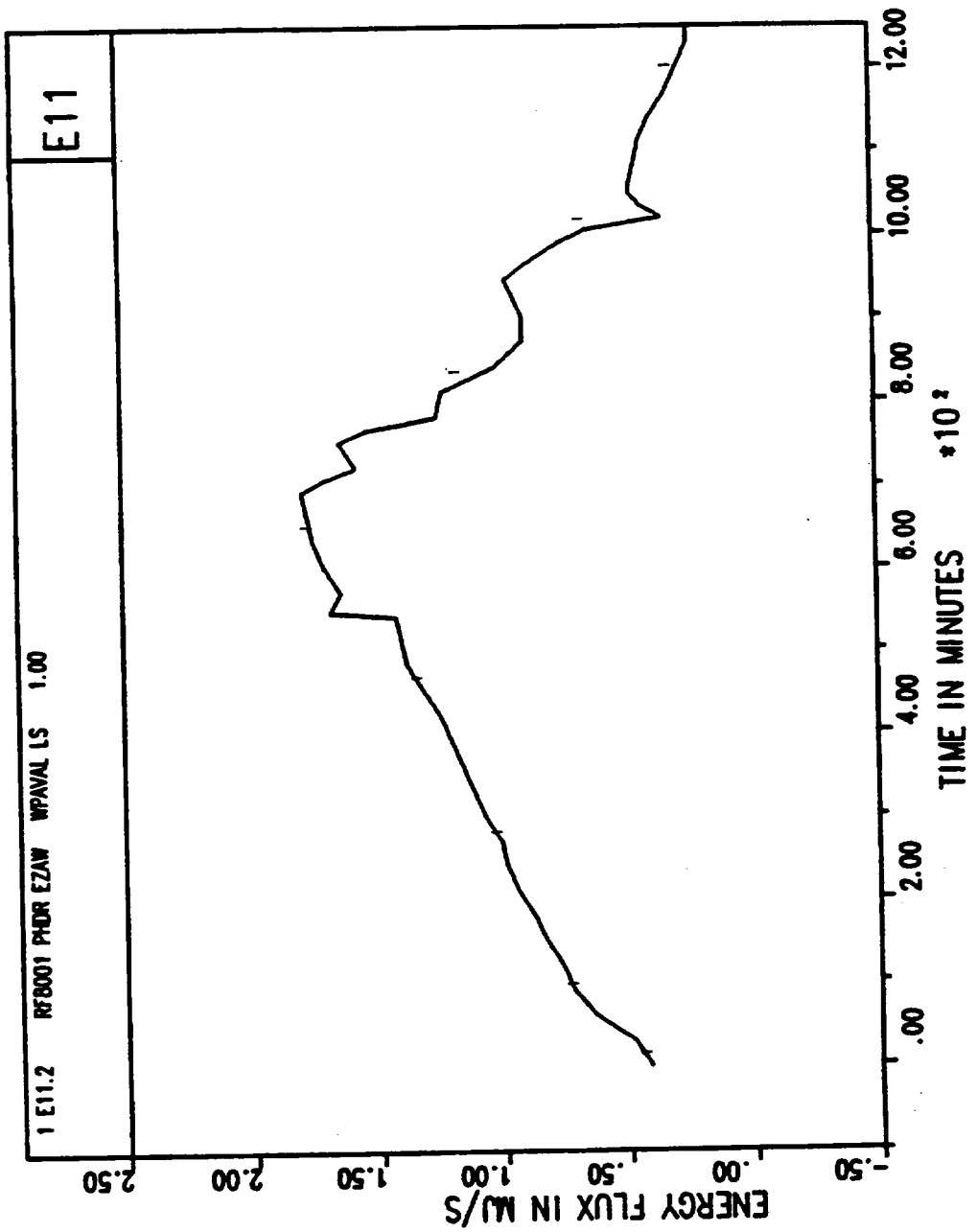

Figure 3.49 Cooling water energy rate for experiment E11.2

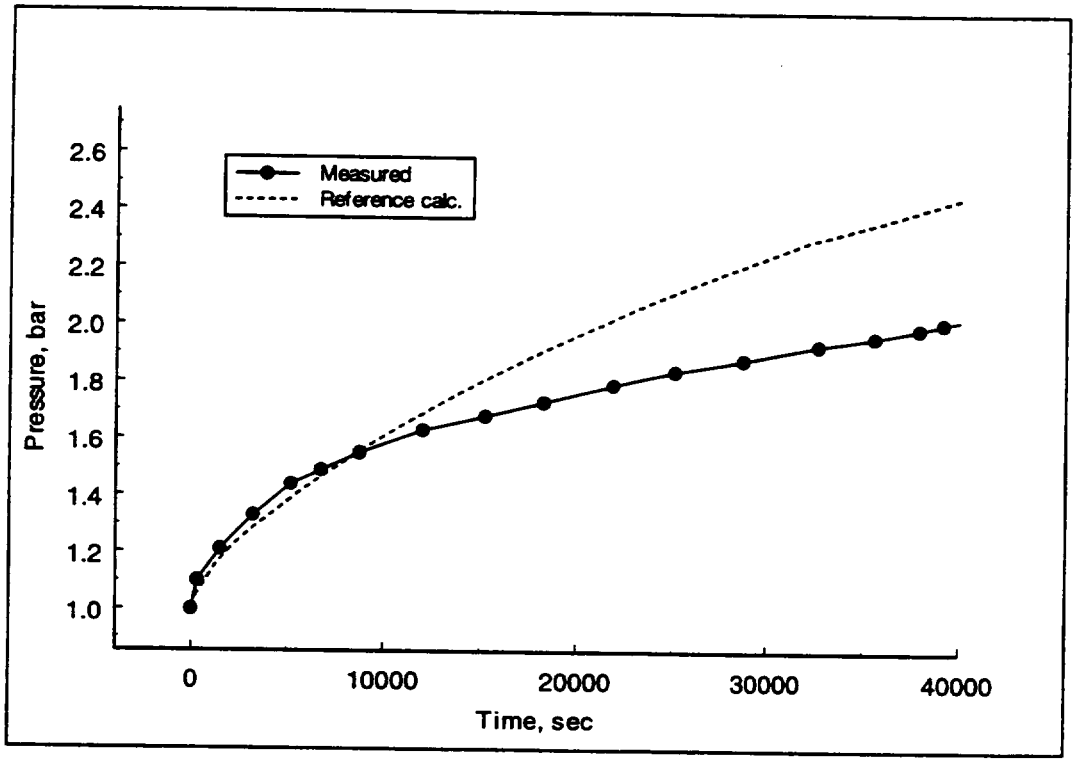

Figure 3.50 Comparison of the measured containment pressure for the E11.2 test and CONTAIN reference calculation.

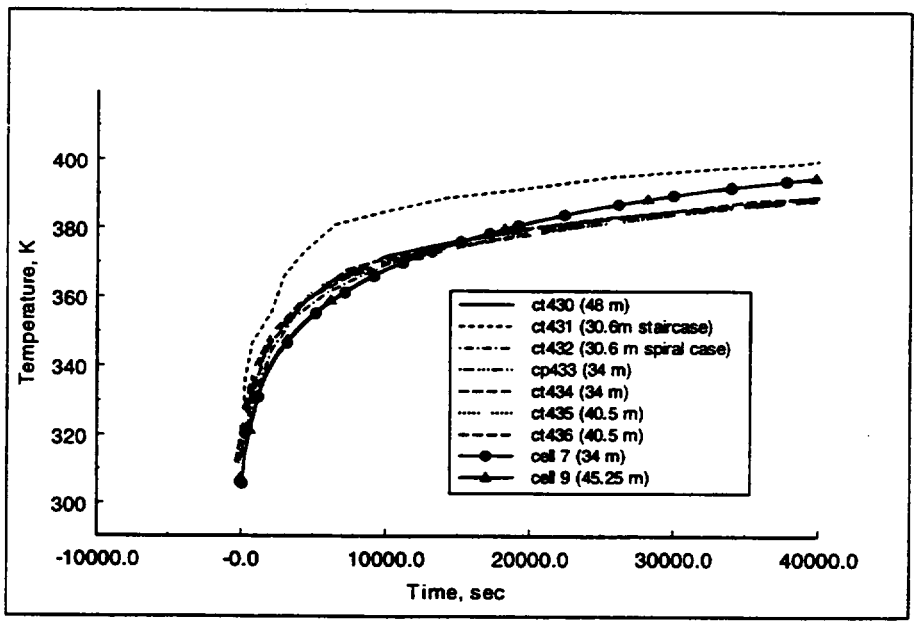

Figure 3.51 Comparison of the measured and CONTAIN reference calculation for local temperatures above the operation deck for the E11.2 test. (Location ct431 measures the temperature of the steam plume entering the above region and therefore is elevated compared to other regional measurements.)

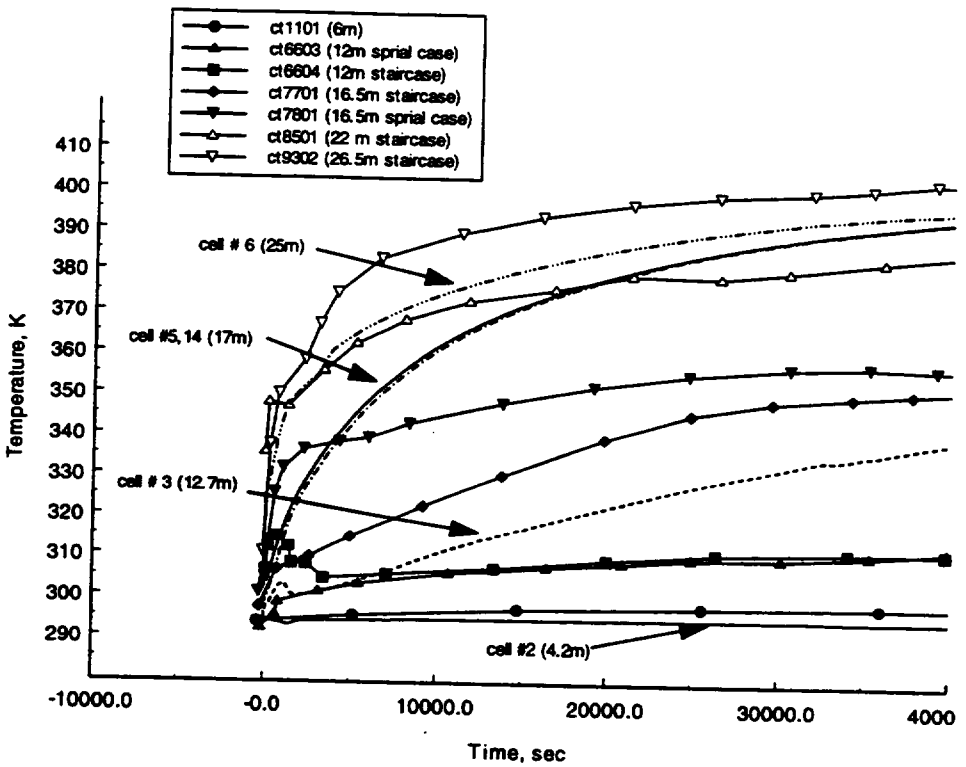

Figure 3.52 Comparison of below operation deck local temperature measurement with the CONTAIN reference calculation for the E11.2 test.

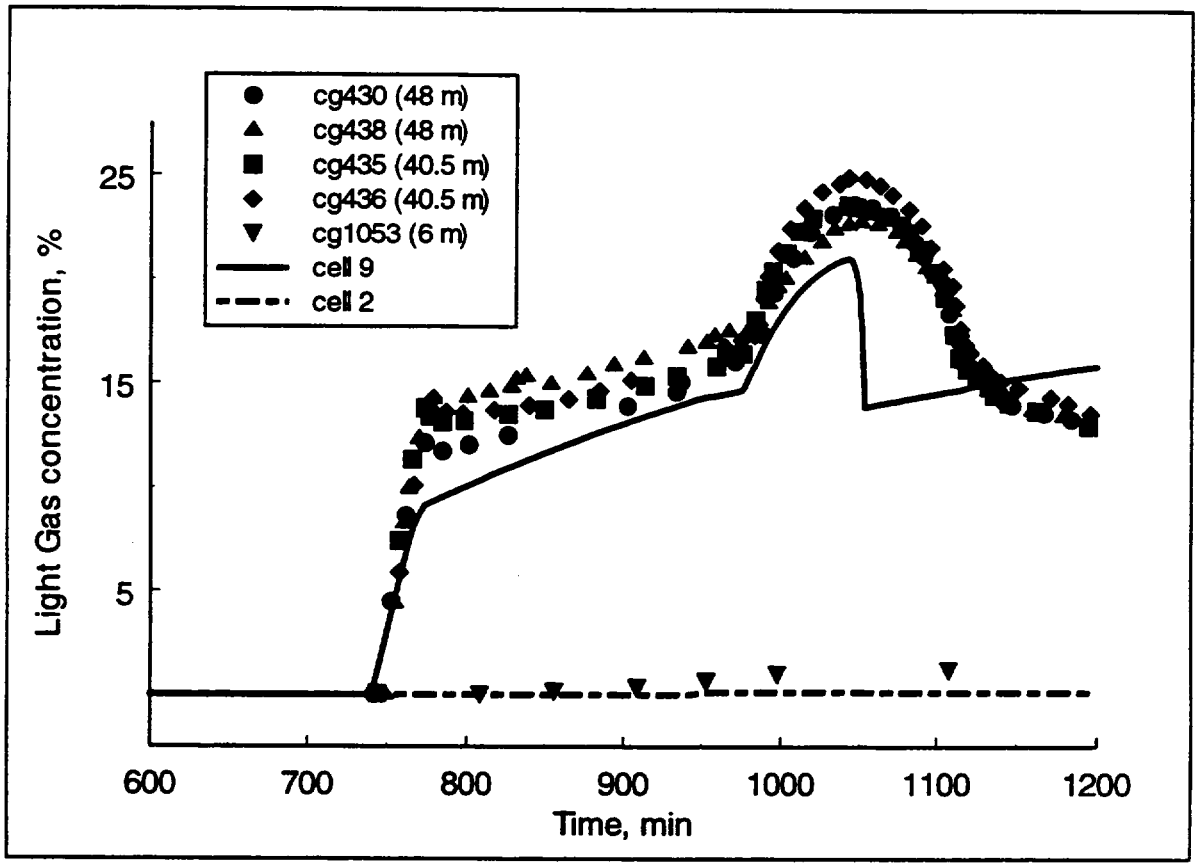

Figure 3.53 Comparison of measured and calculated light gas concentrations for test E11.2. (Cell #9 is at an elevation of 45.25 meters; whereas, cell #2 is at an elevation of 4.2 meters.)

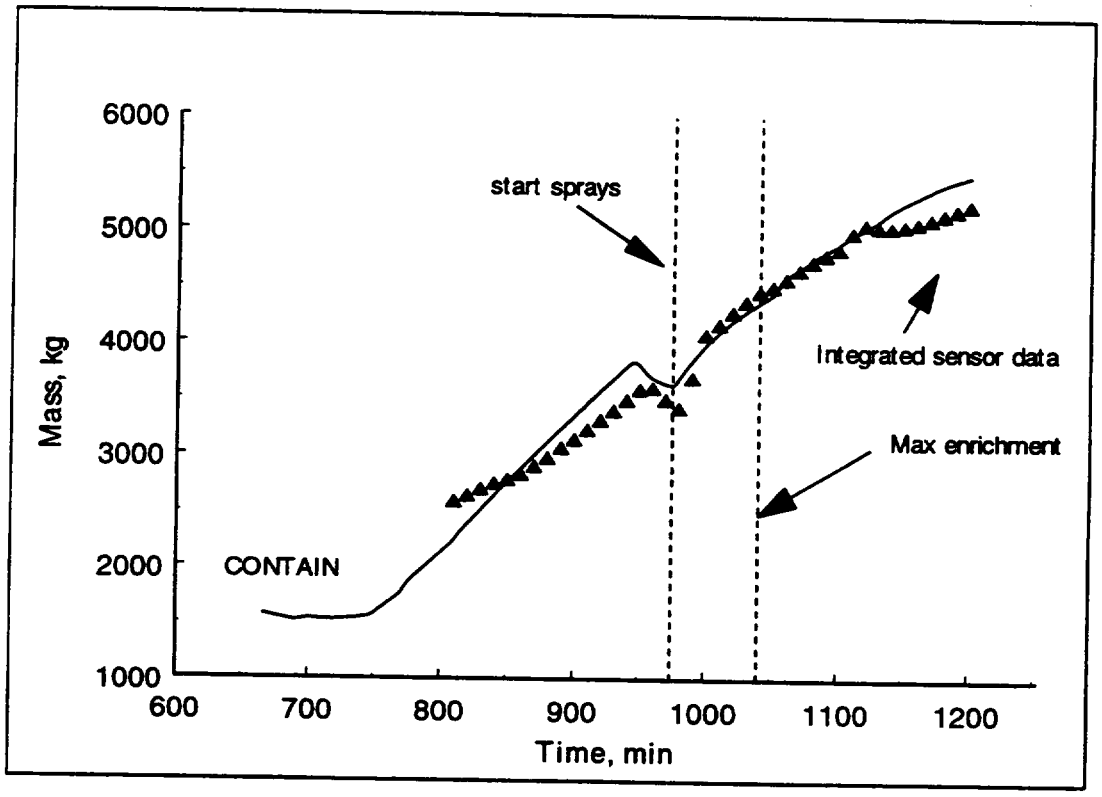

Figure 3.54 Total air mass above the operation deck for test E11.2

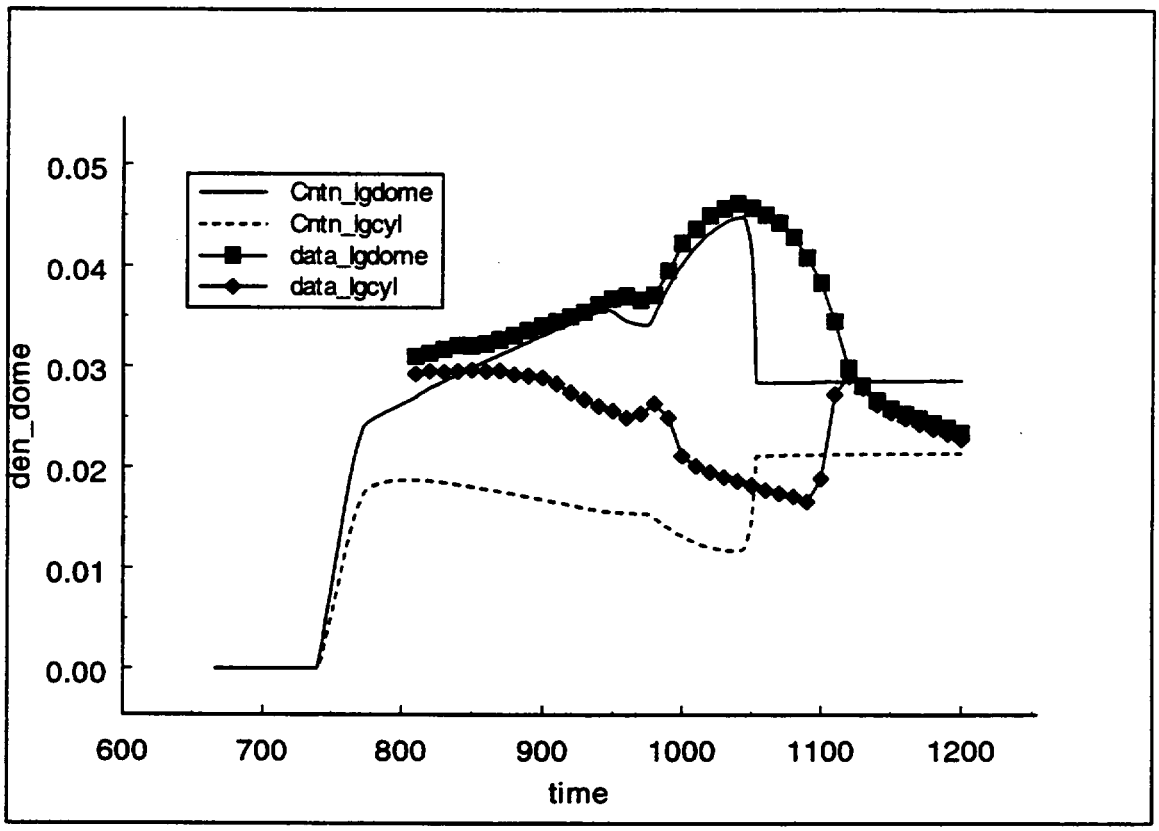

Figure 3.55 Comparison of light gas average densities in the cylinder and dome portions of the above deck region of HDR for test E11.2.

Test No.:	E11.3	E11.4
Geometry:	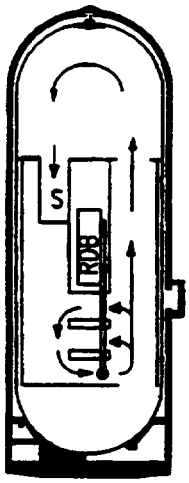	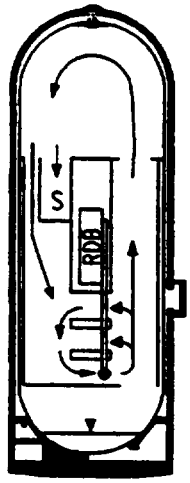
Characterization:	Small break ±0m no Loop-Geometry Dead end room 1802	Small break ±0m Loop-Geometry Dead end room 1802
Course of experimental procedure:		
steam injection at BS	20h•	33.92h
steam + H_2-injection at break	1.62h	1.33h
steam injection at BS	3h	1h
add. of dry energy + H_2-injection + superh. steam		6.2h
steam injection at BS		1h
boiling sump		3h
natural cooldown	23.7h	0.17h
external spray		3.53h
natural cooldown		3.52h
venting	till depressurization	till depressurization
Related to:	Begin of KSU-ND•-path	KSU-ND•-path, with sump water break in

- ● Position of break; injection position, BS
- S Dead end compartment
  Note: stair case (left) closed

Figure 3.56 Test setup for experiments E11.3 and E11.4.

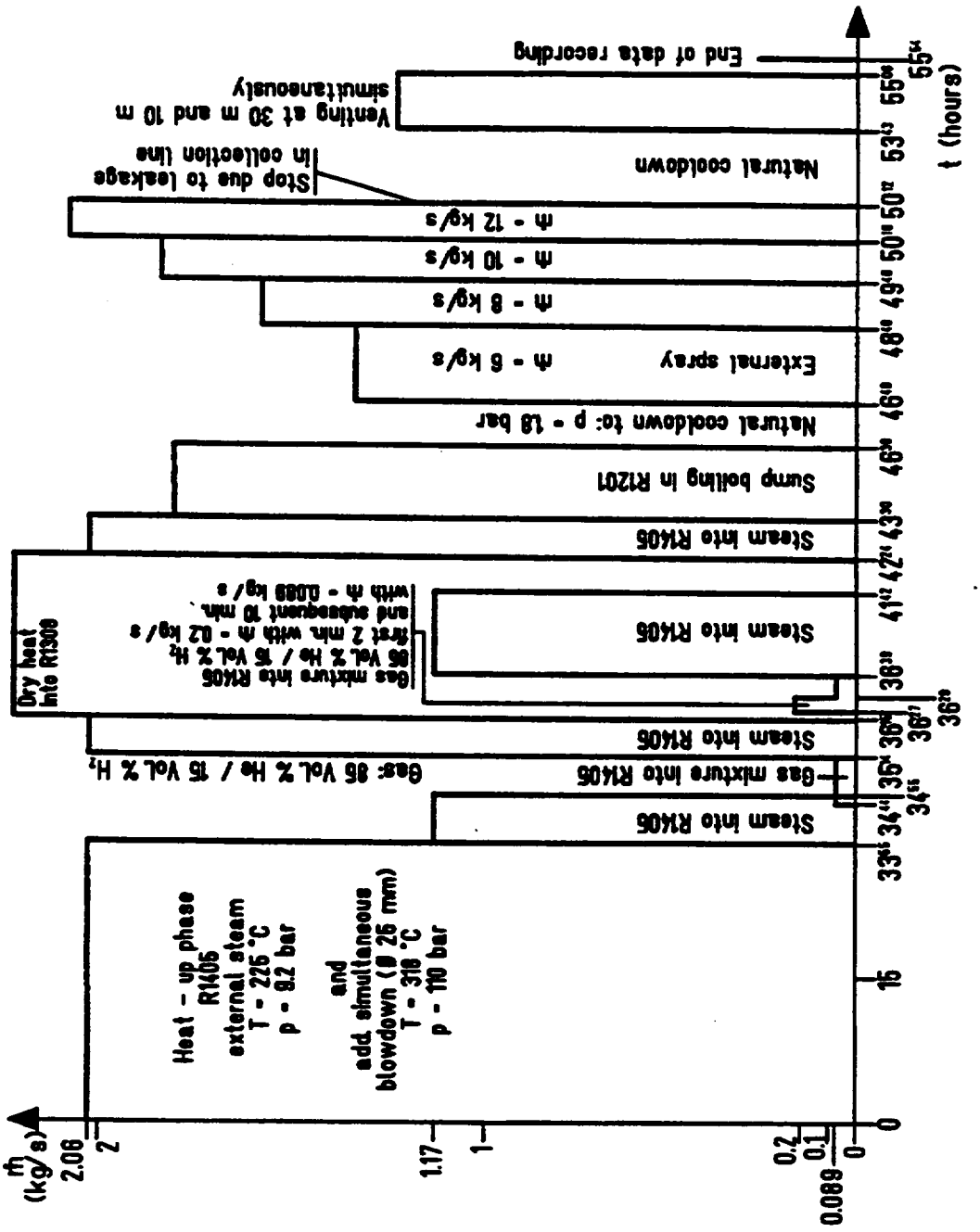

Figure 3.57 Experimental procedure for E11.4

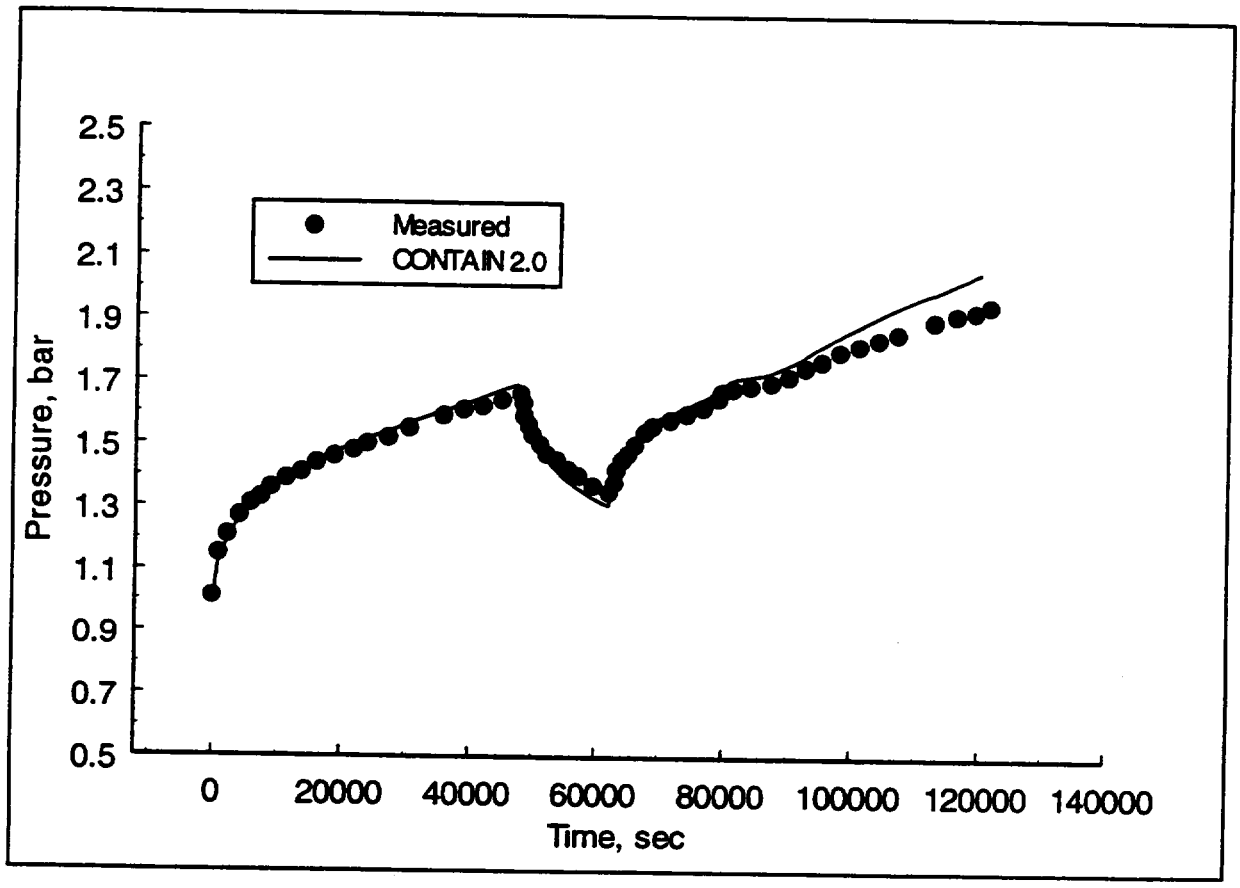

Figure 3.58 Comparison of measured and calculated containment pressure for E11.4

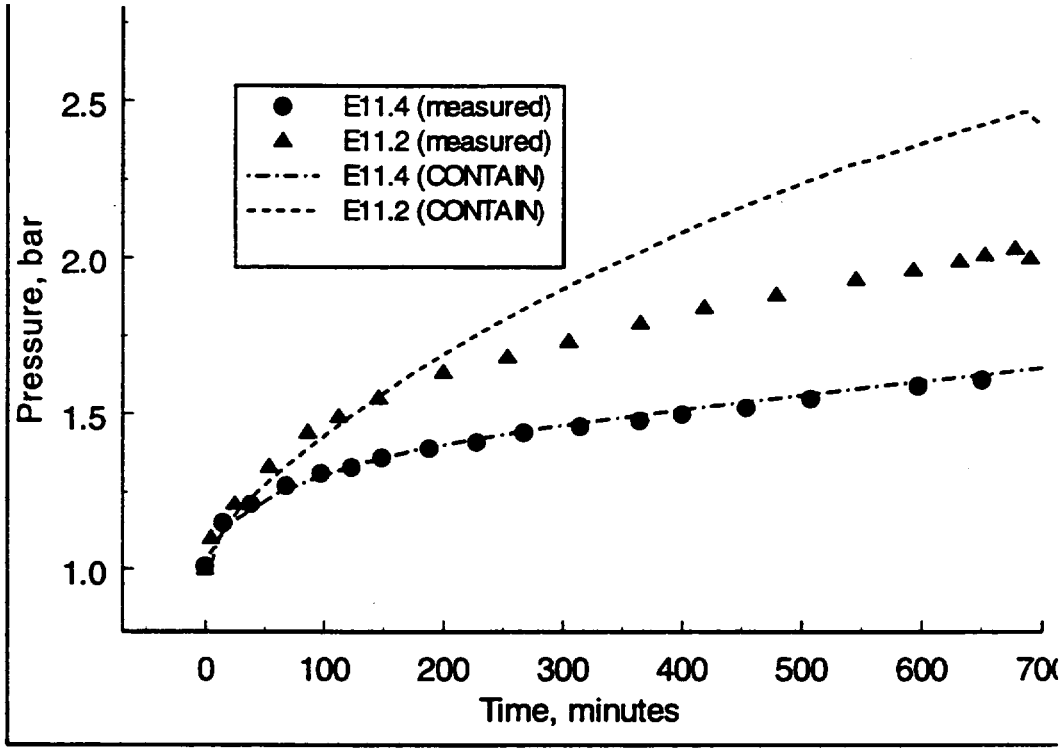

Figure 3.59 Comparison of measured and calculated containment pressure for E11.2 and E11.4 tests, showing an inconsistency in an ability to predict containment pressure.

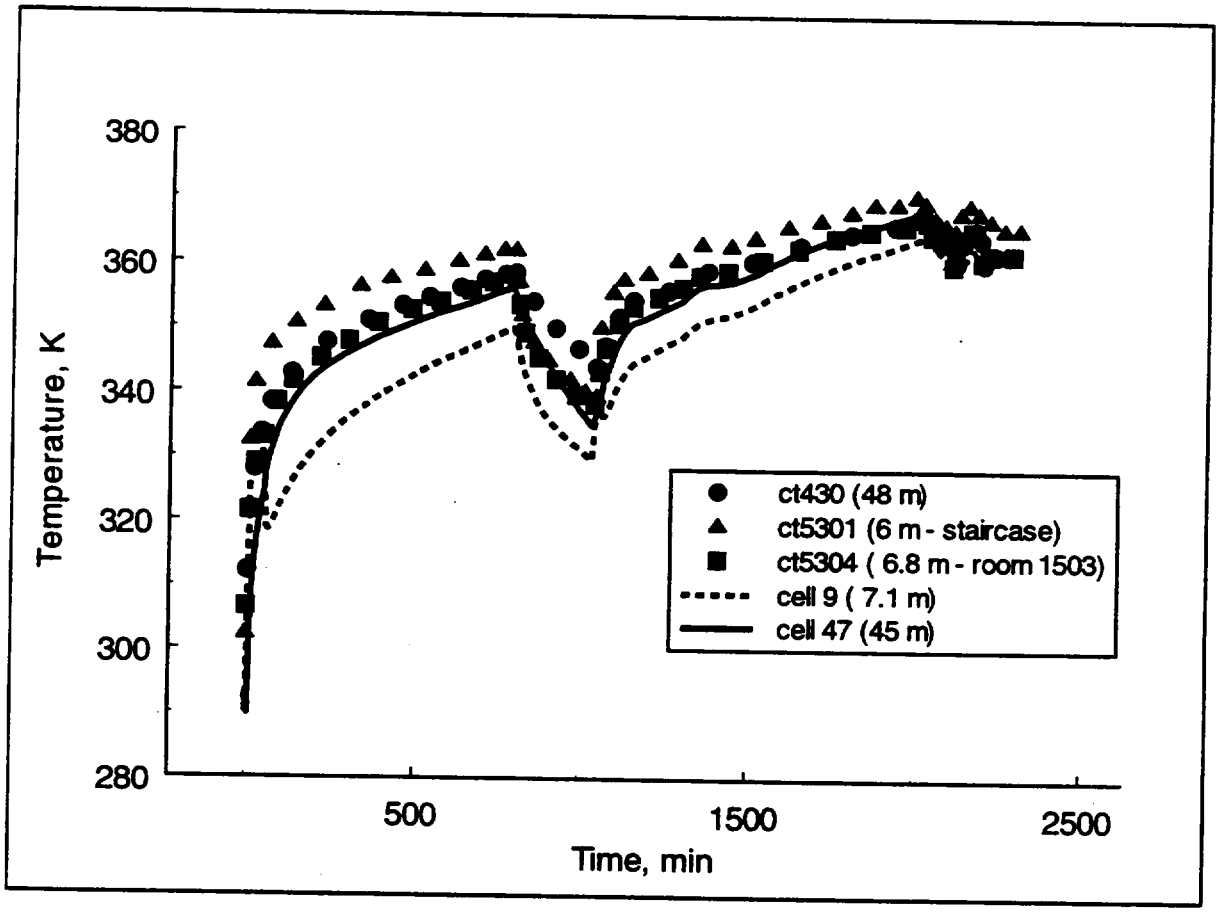

Figure 3.60 Comparison of measured and calculated upper and lower containment gas temperatures for E11.4

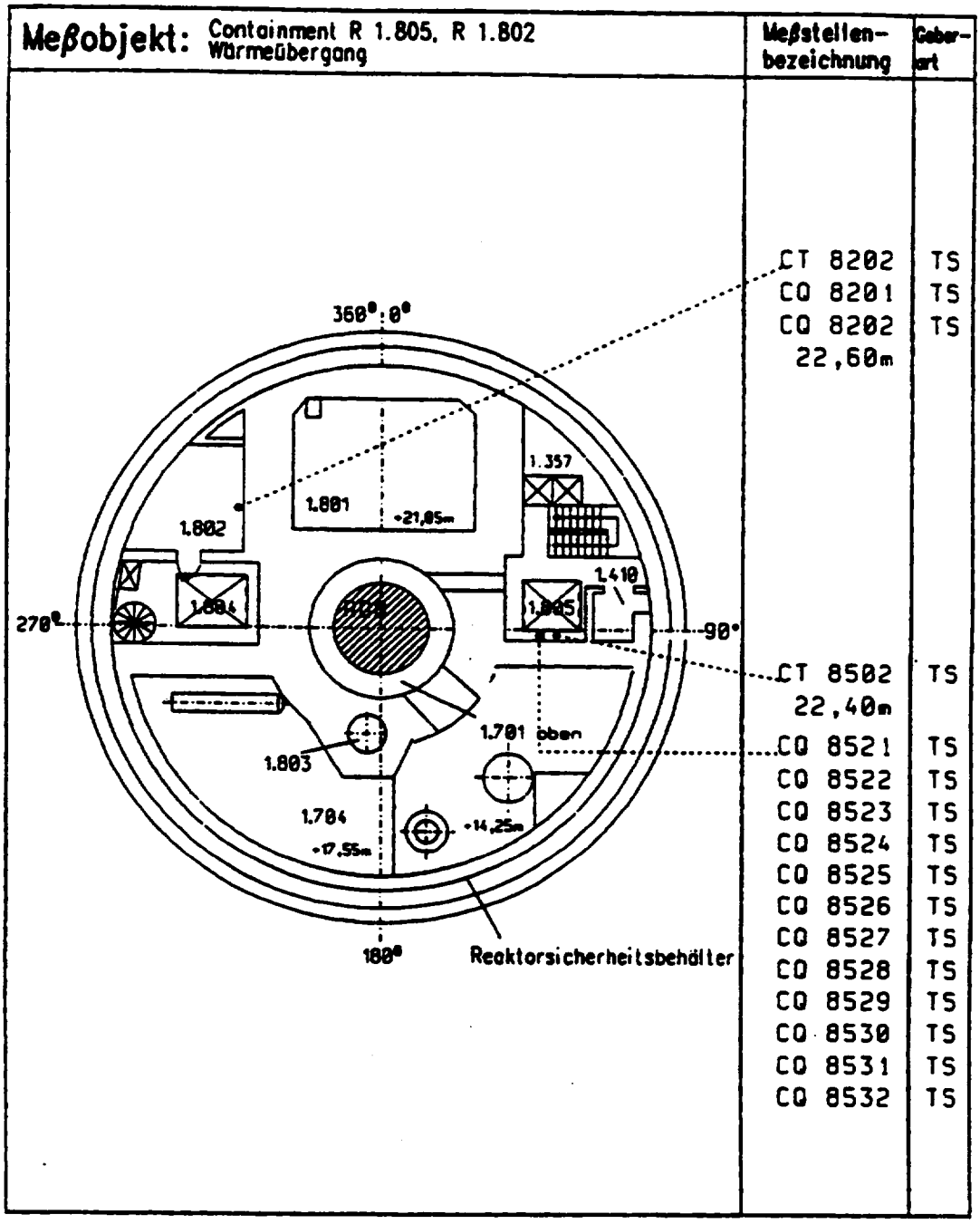

Figure 3.61 Measurement plan at the 1800 level showing the location of concrete block #82, indicated by TC's CQ8201-8202 at elevation 22.6 meters.

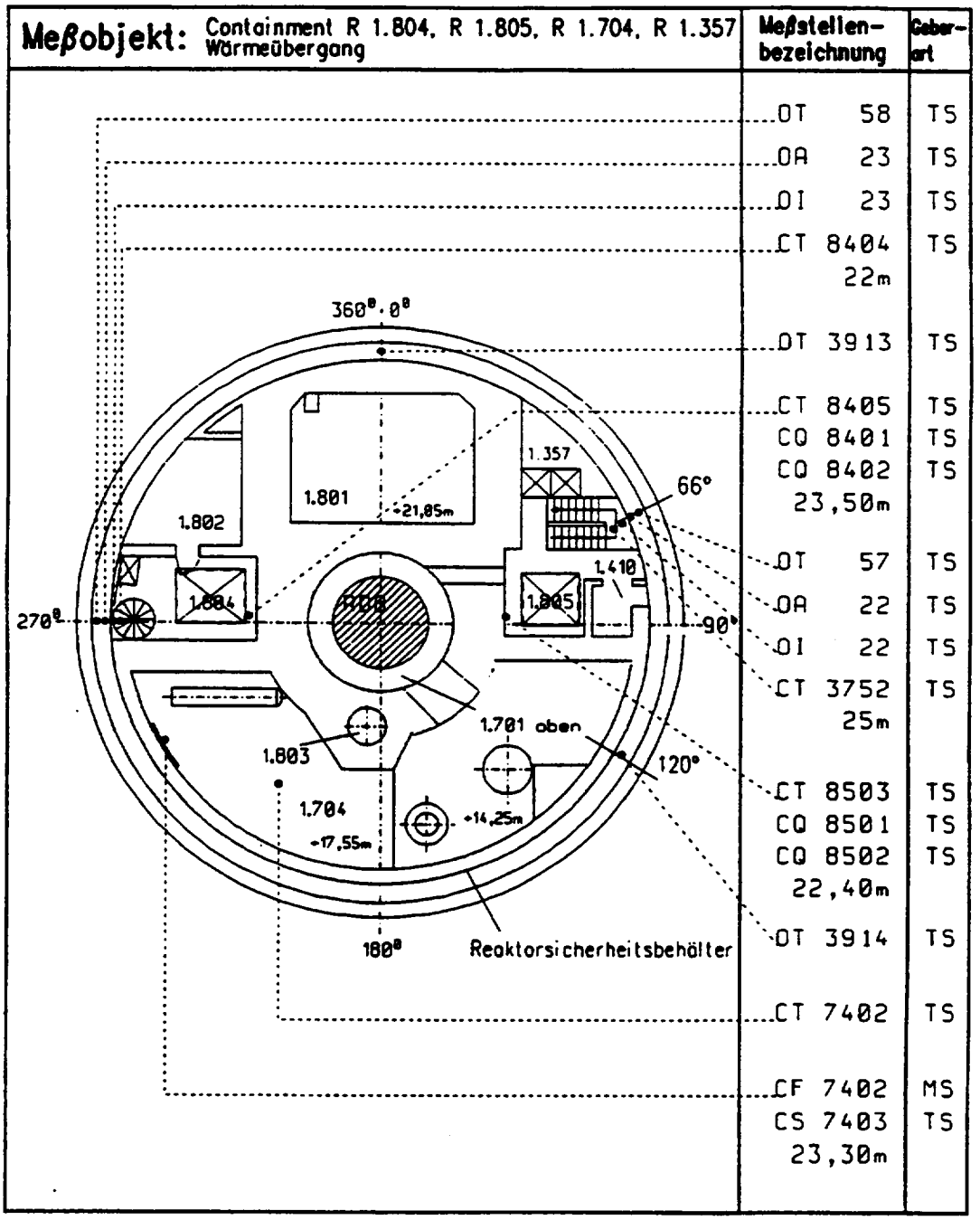

Figure 3.62 Measurement plan for the 1800 level showing the location of concrete block #84, indicated by TC's CQ8401-8402 at elevation 23.5 meters.

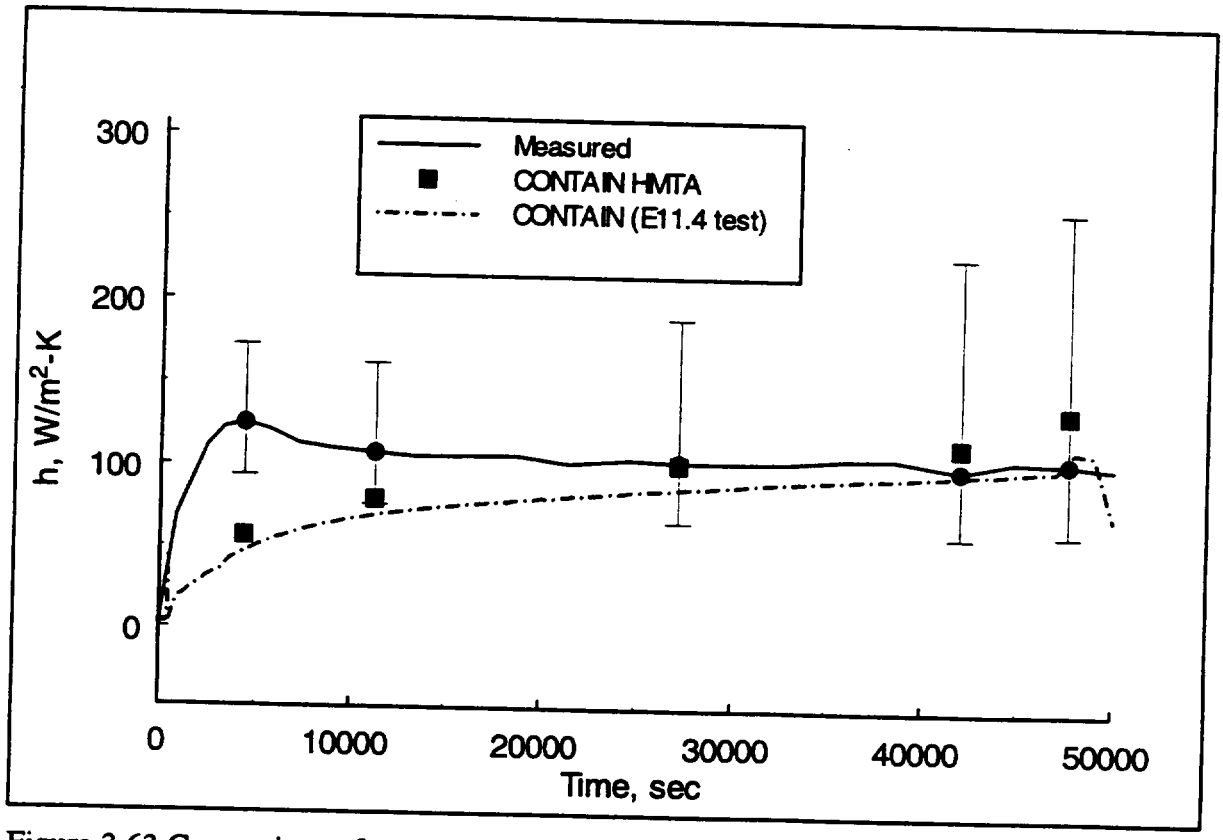

Figure 3.63 Comparison of measured and calculated condensation heat transfer coefficients during E11.4 for concrete block #84, located in Room 1804 at elevation 23.5 meters

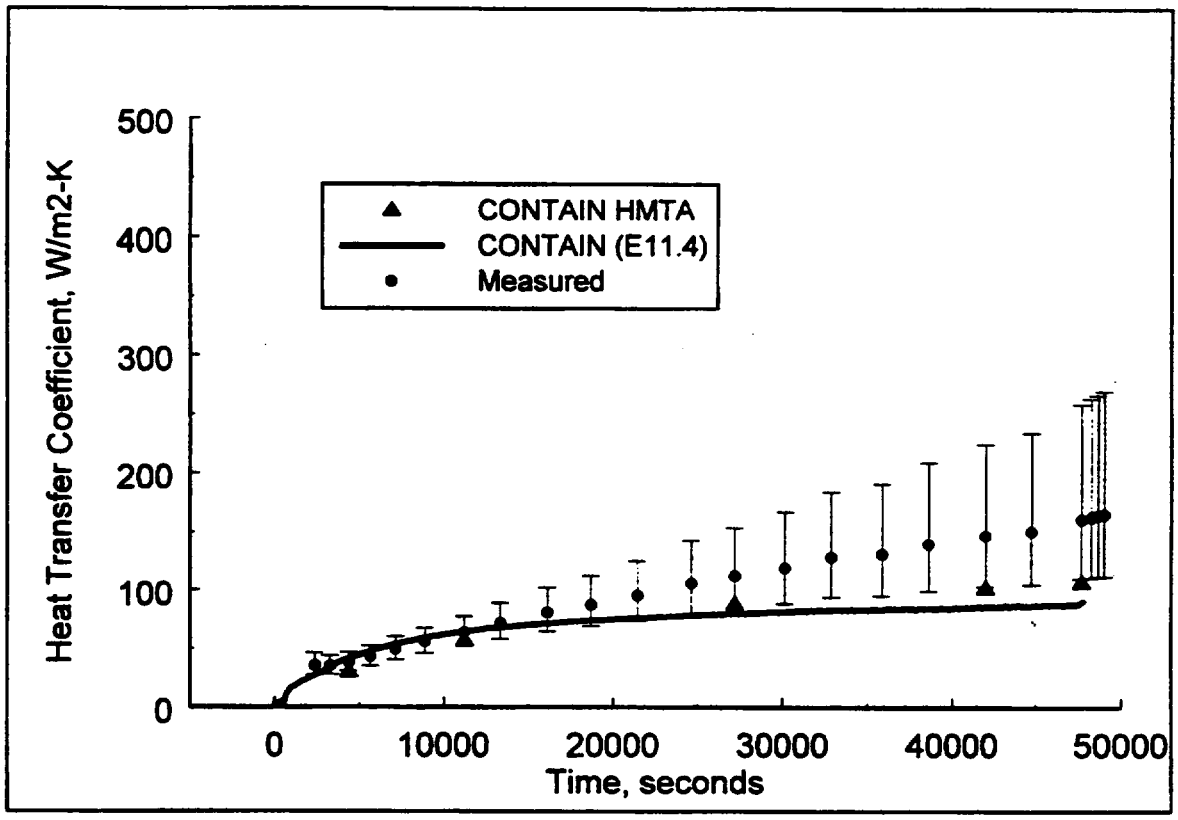

Figure 3.64 Comparison of measured and calculated condensation heat transfer coefficients during E11.4 for concrete block #82, located in Room 1802 at elevation 22.6 meters.

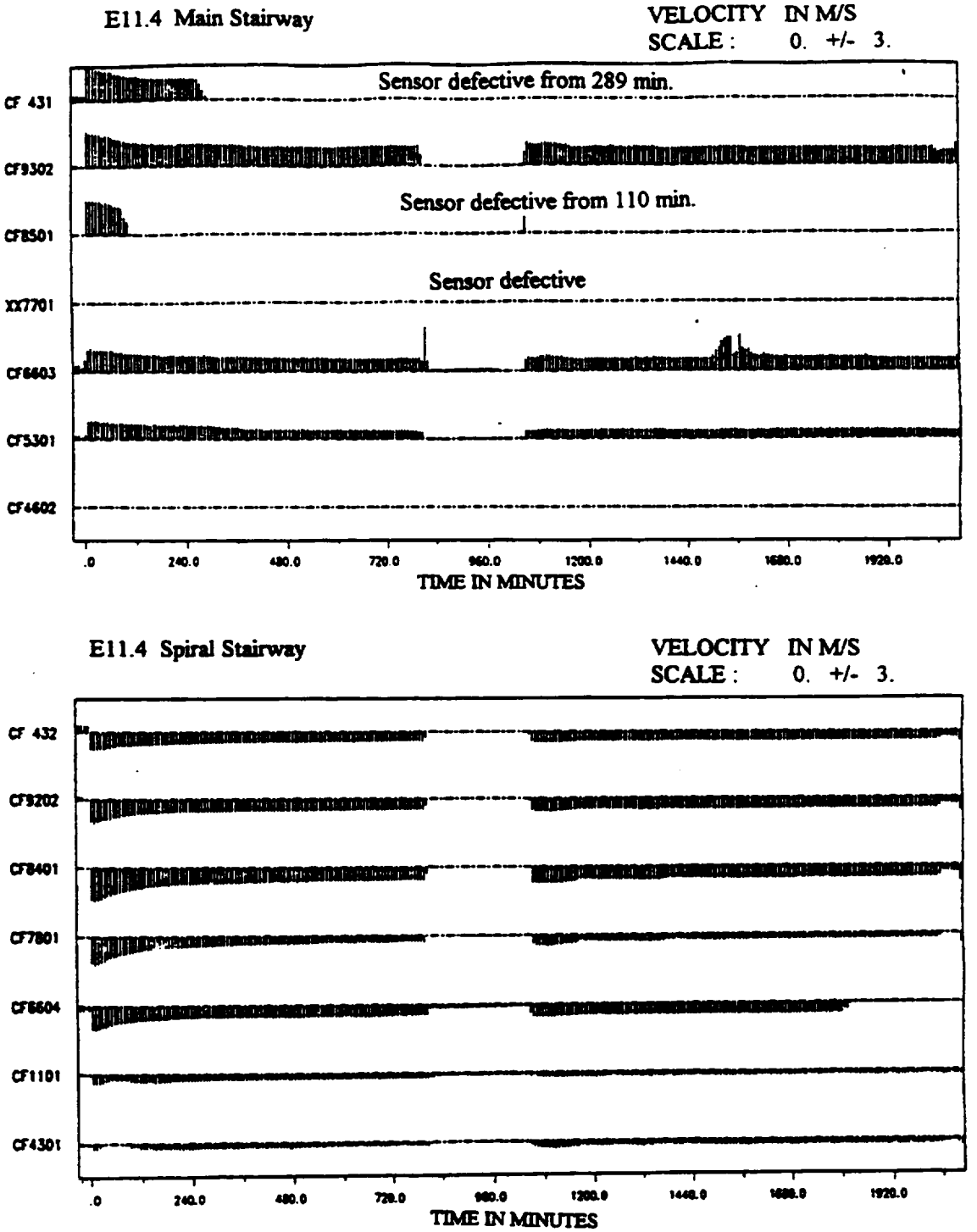

Figure 3.65 Measured velocities along the two main circulation pathways for E11.4.

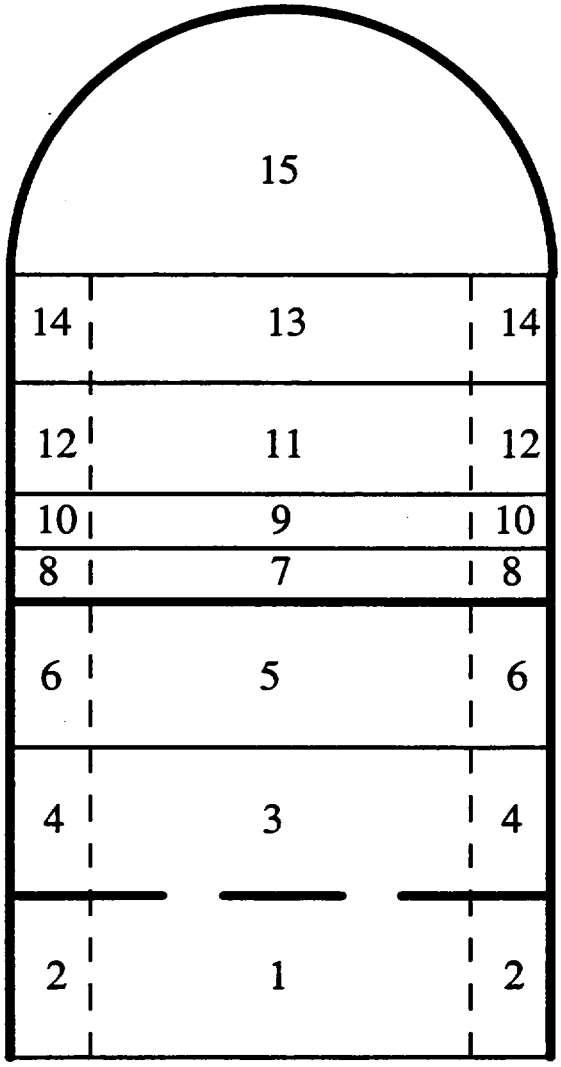

Figure 3.66 Nodalization for CVTR multi-cell CONTAIN deck

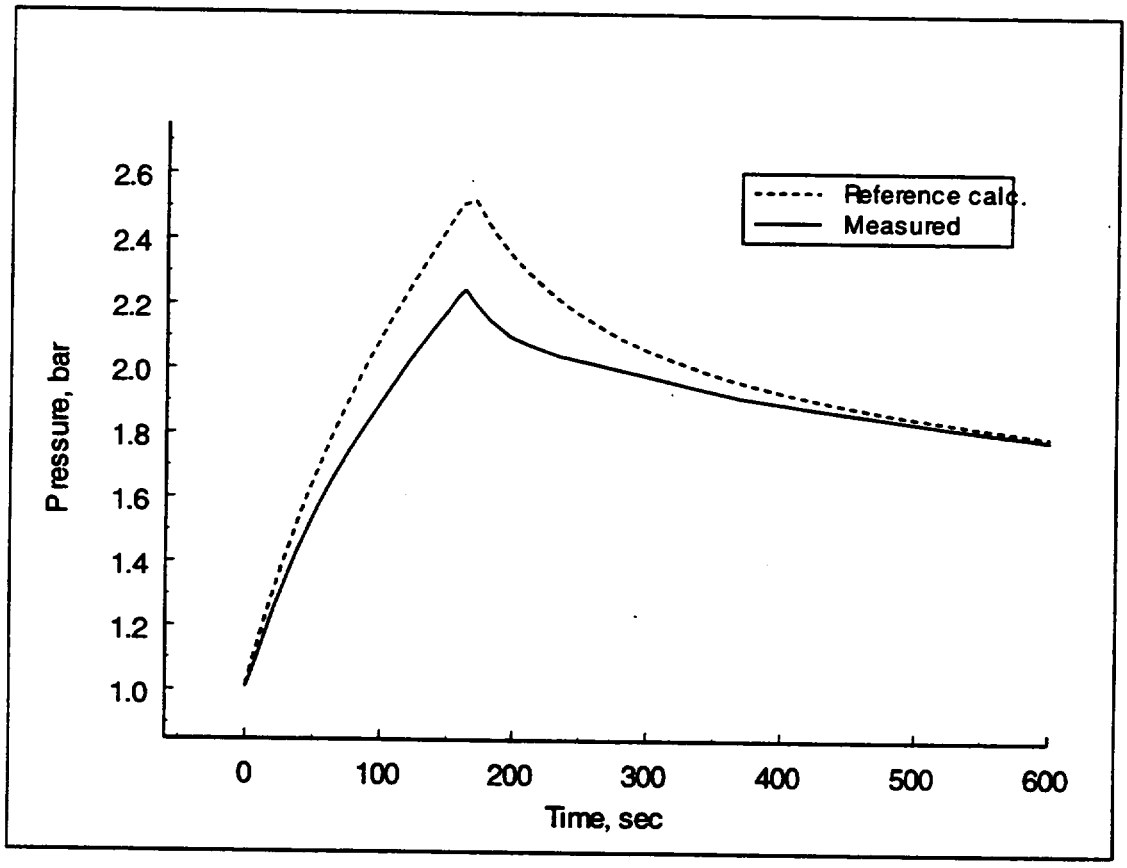

Figure 3.67 Comparison of CVTR test #3 containment pressures for the CONTAIN reference calculation and measurement.

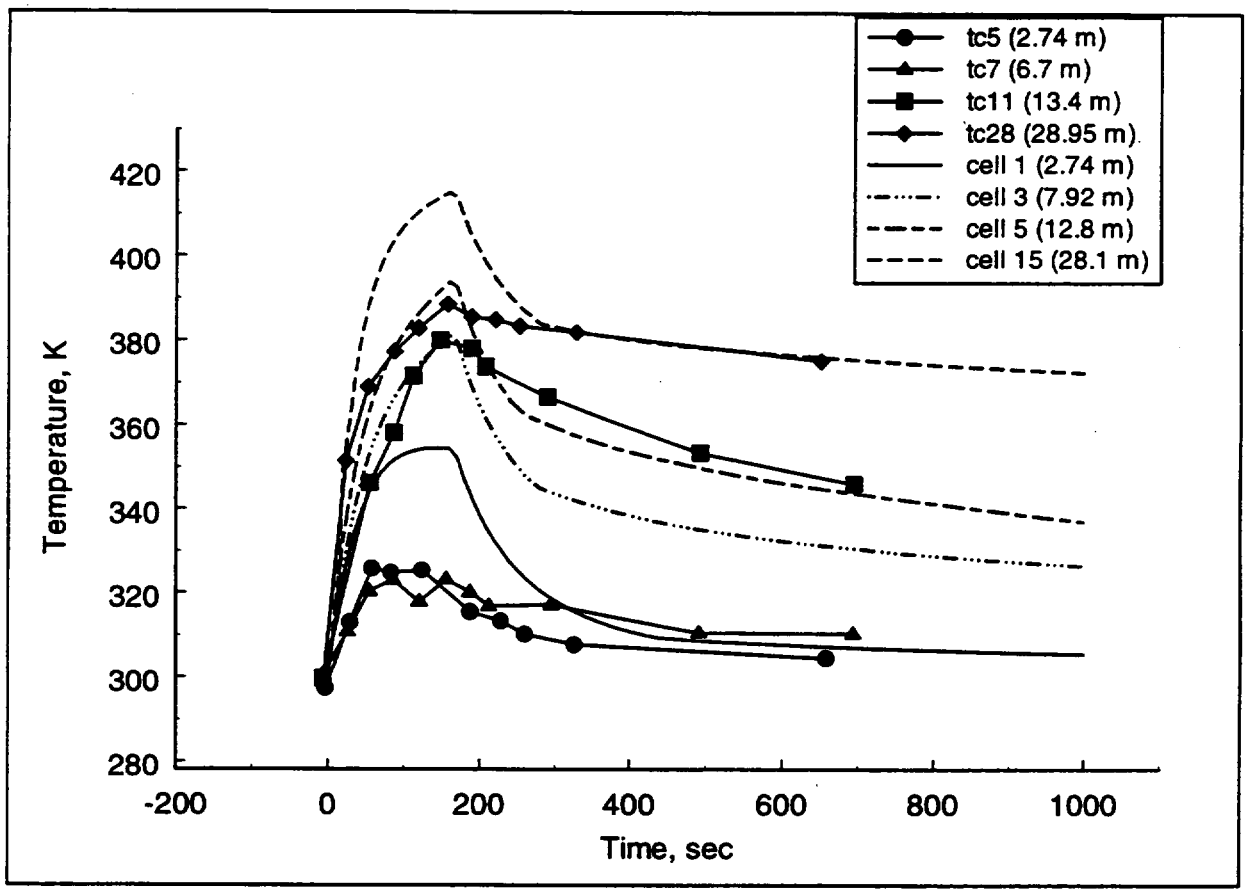

Figure 3.68 Comparison of measured and calculated local temperatures for CVTR test #3 using the CONTAIN reference input deck.

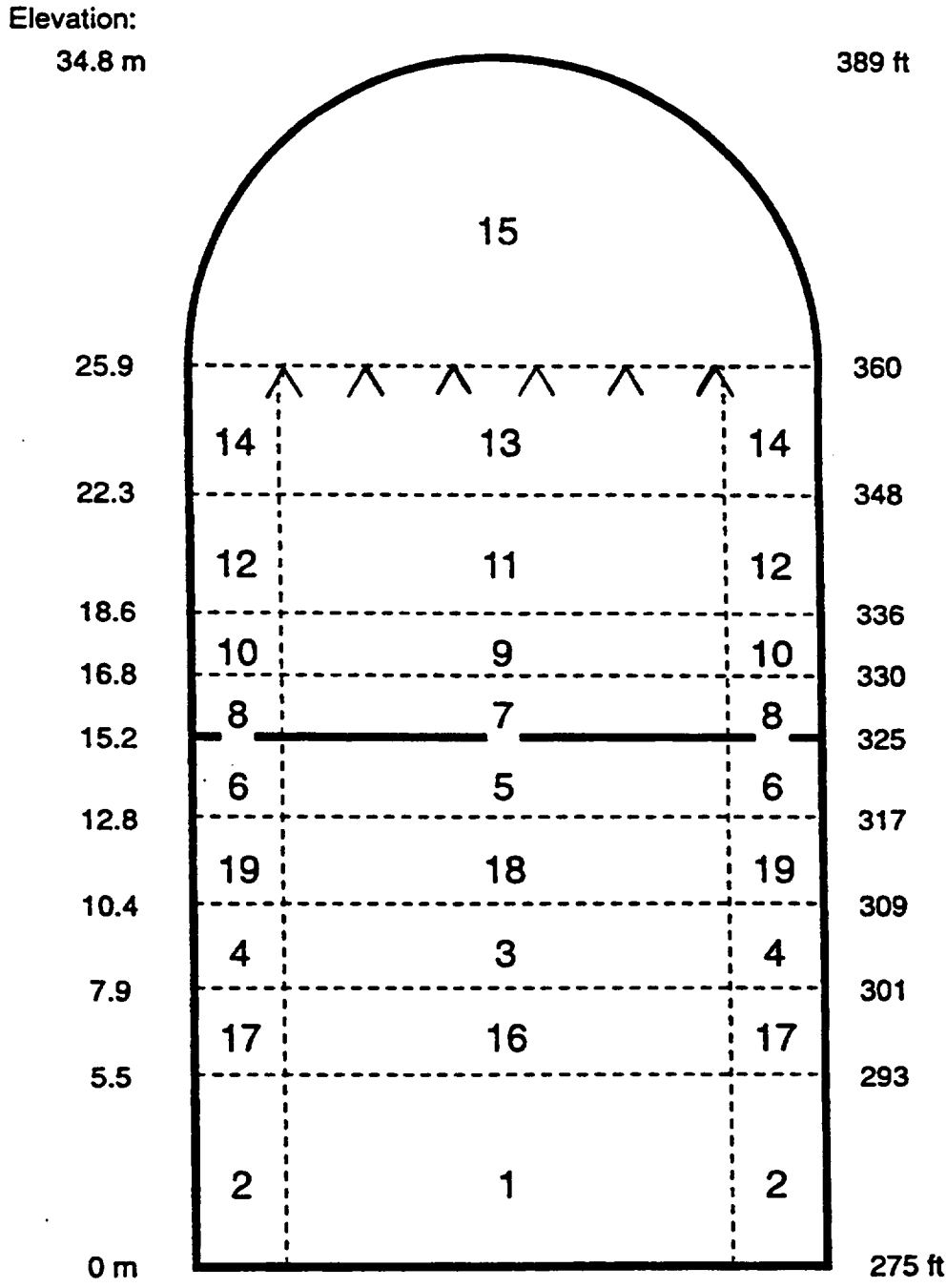

Figure 3.69 CONTAIN 19 cell model of the CVTR facility - showing sprays at the 25.9 m elevation

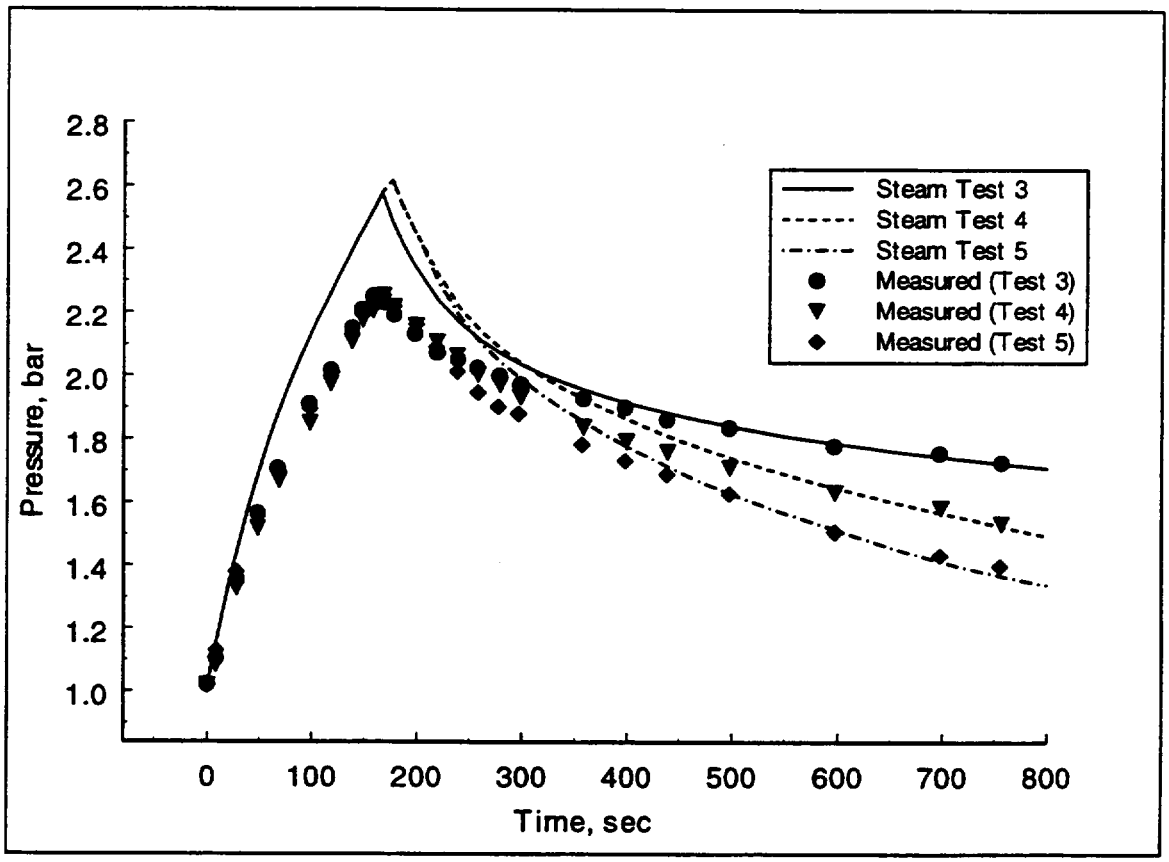

Figure 3.70 Comparison of measured and calculated containment pressures for CVTR tests #3, #4, and #5. Tests #4 and #5 included pressure suppression by internal sprays of 290 and 500 gpm.

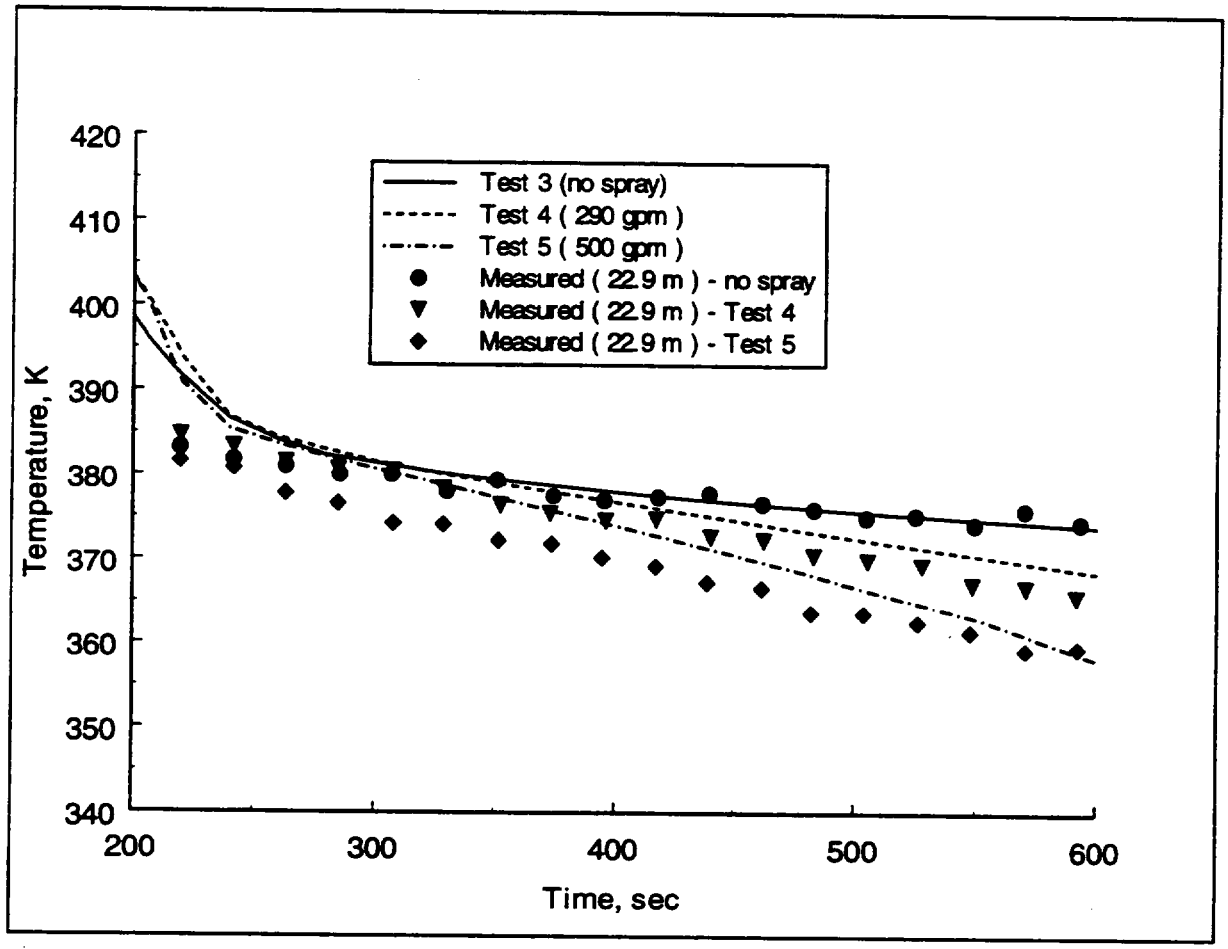

Figure 3.71 Comparison of measured and CONTAIN calculated (average of cell #11 and #12) gas temperature below upper containment sprays system.

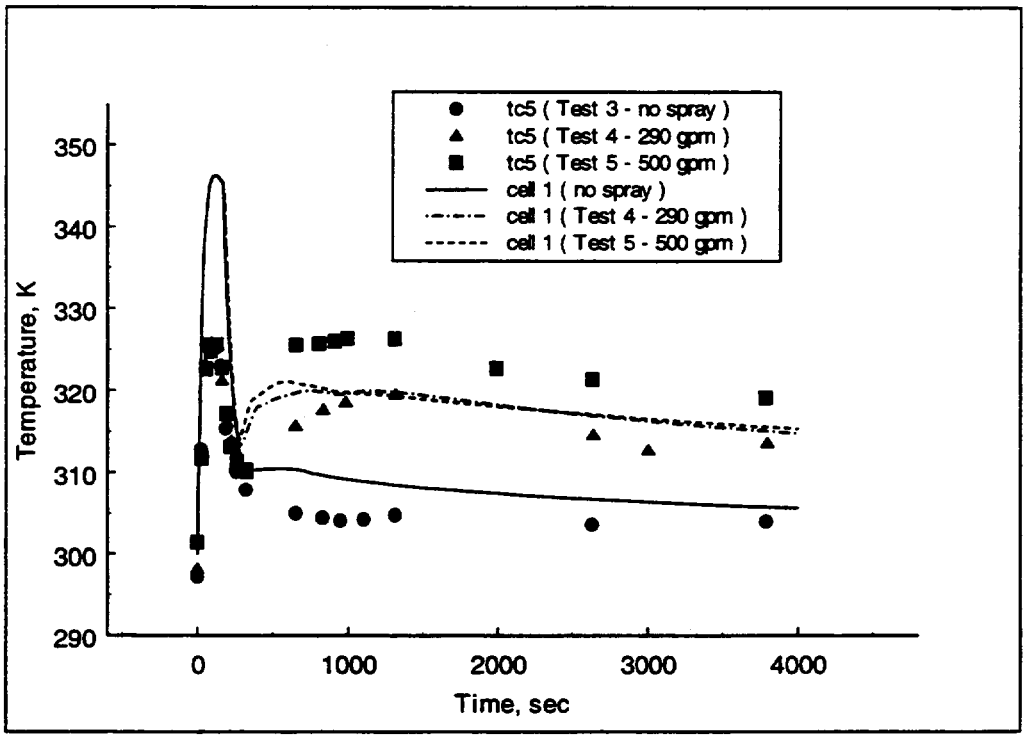

Figure 3.72 Comparison of measured and CONTAIN calculated gas temperature in the basement region of the CVTR facililty - showing the effect of sprays for increasing gas temperatures in this region due to sump water evaporation.

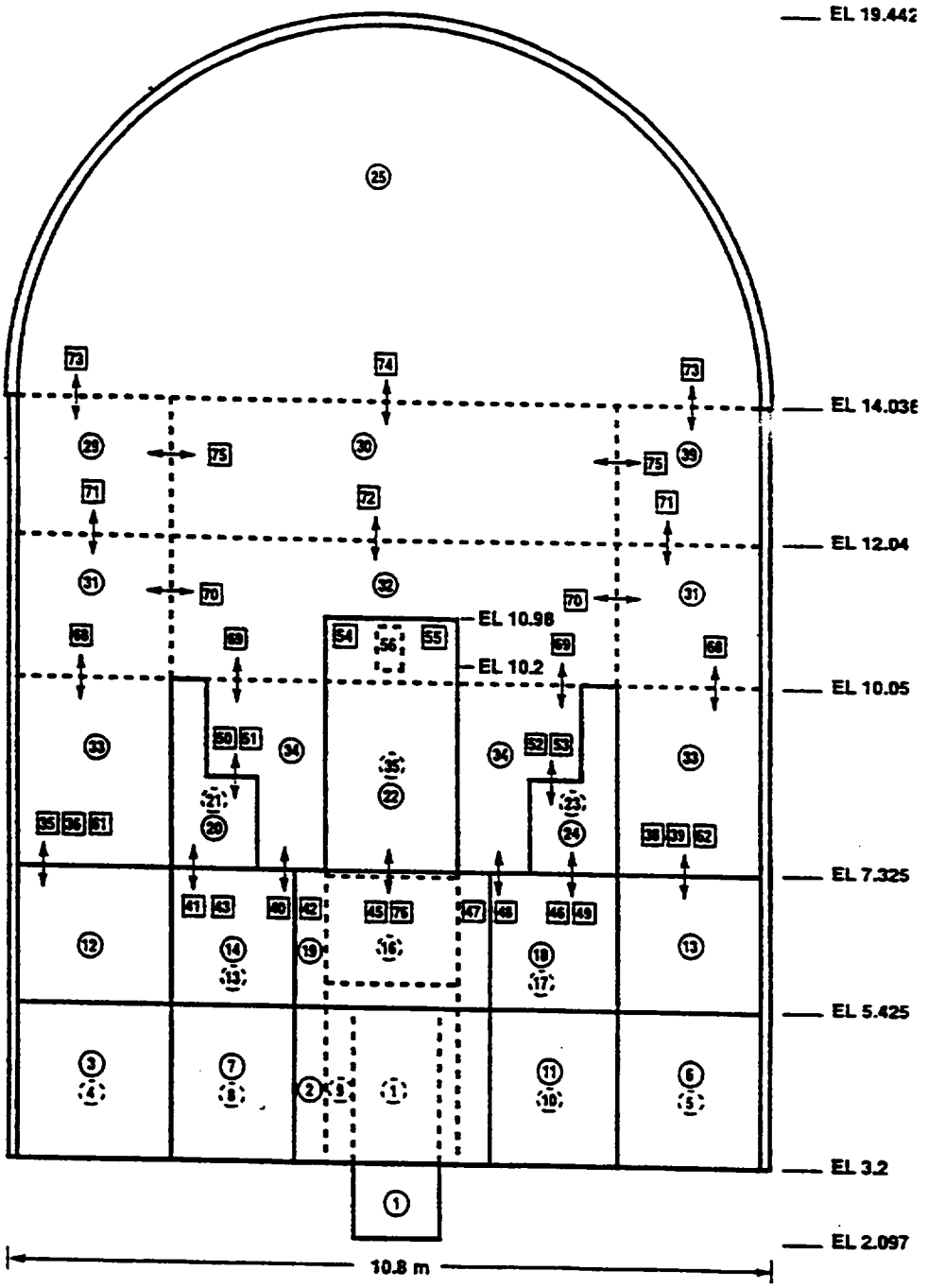

Figure 3.73 Vertical cross-sectional view of the CONTAIN 35-cell nodalization for the NUPEC facility.

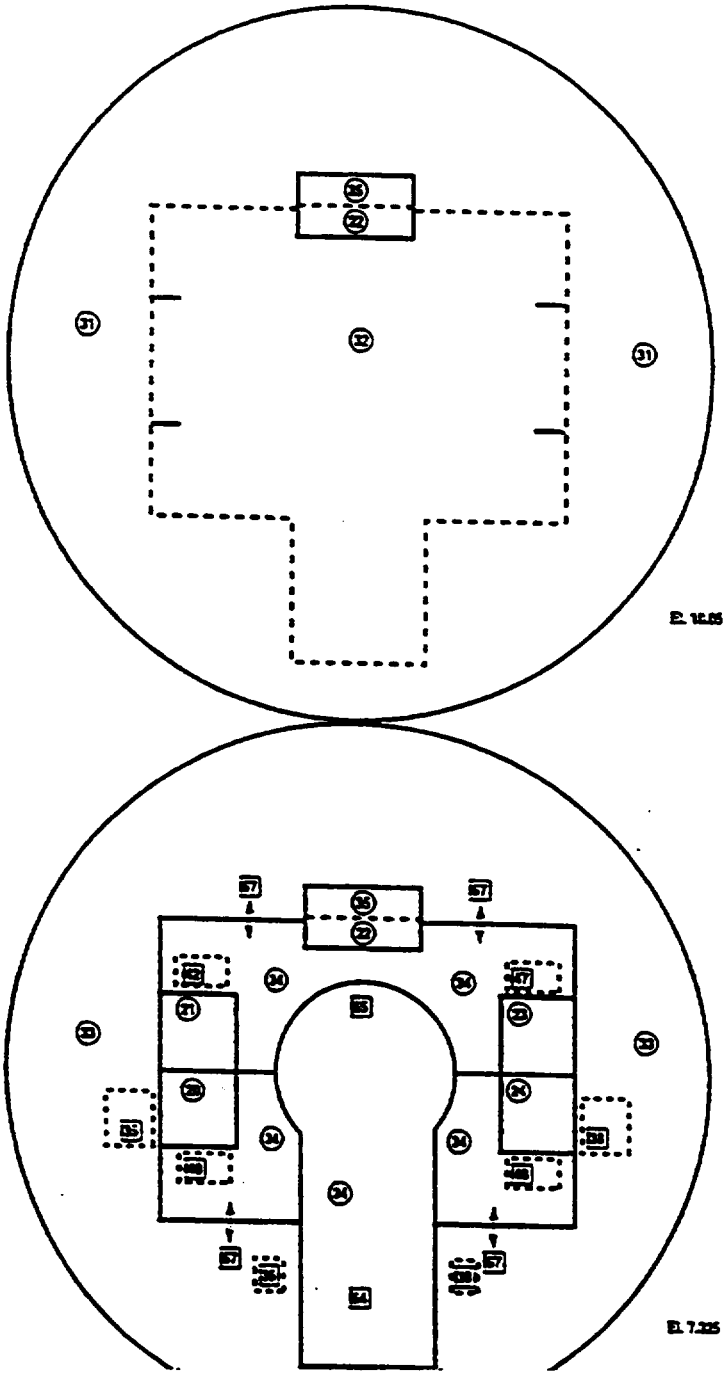

Figure 3.74 Horizontal cross-sectional view of the CONTAIN 35-cell nodalization for the NUPEC facility at (a) the 10.05 m elevation and (b) the 7.325 m elevation.

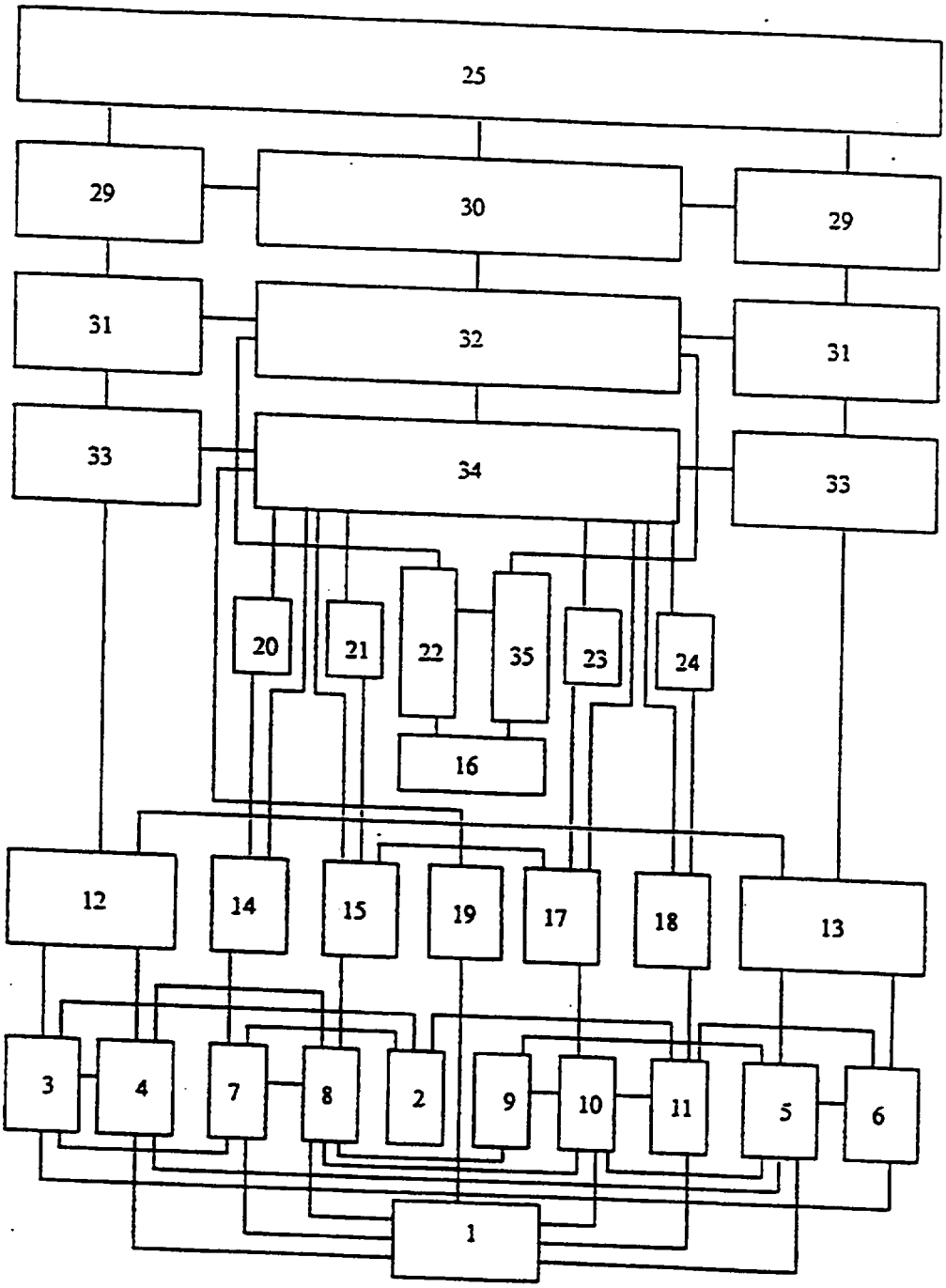

Figure 3.75 Block schematic of the 35-cell nodalization for the NUPEC facility showing cells and flow paths.

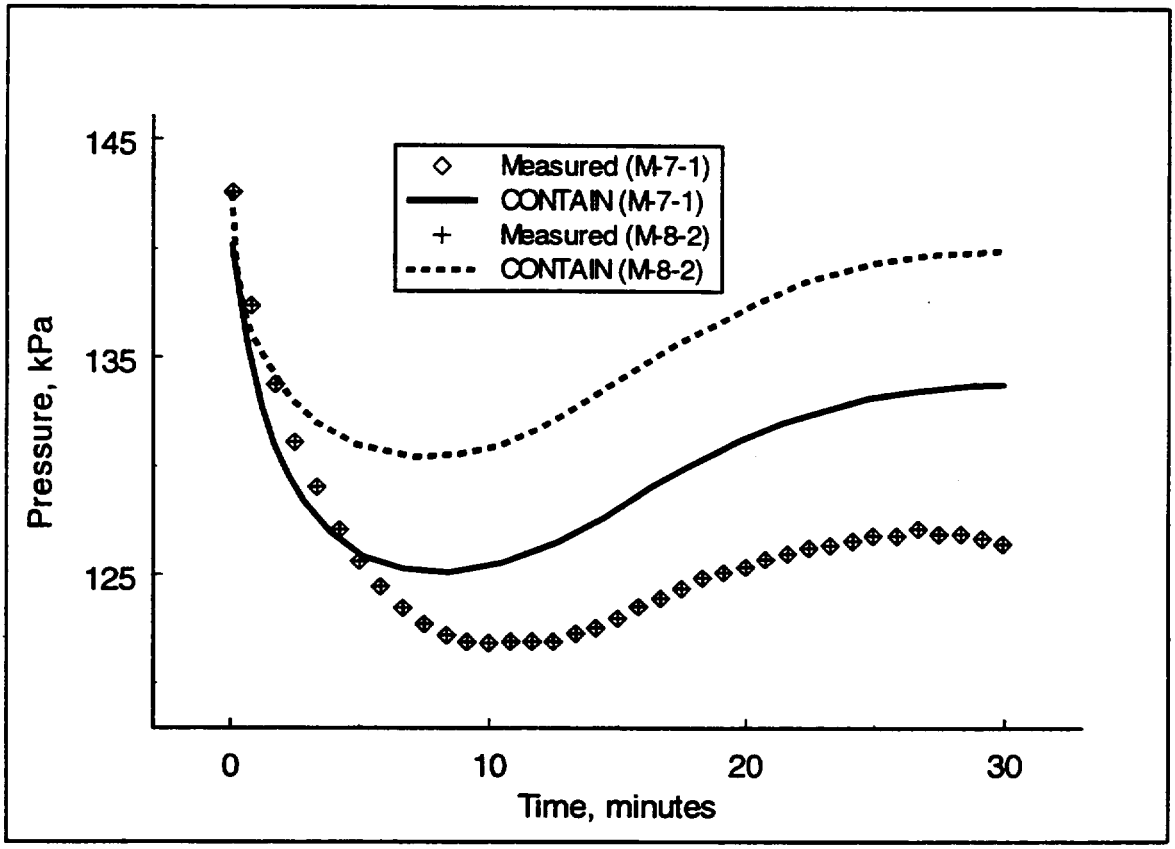

Figure 3.76 Comparison of measured and calculated pressures for NUPEC tests M-7-1 and M-8-2 (with sprays)

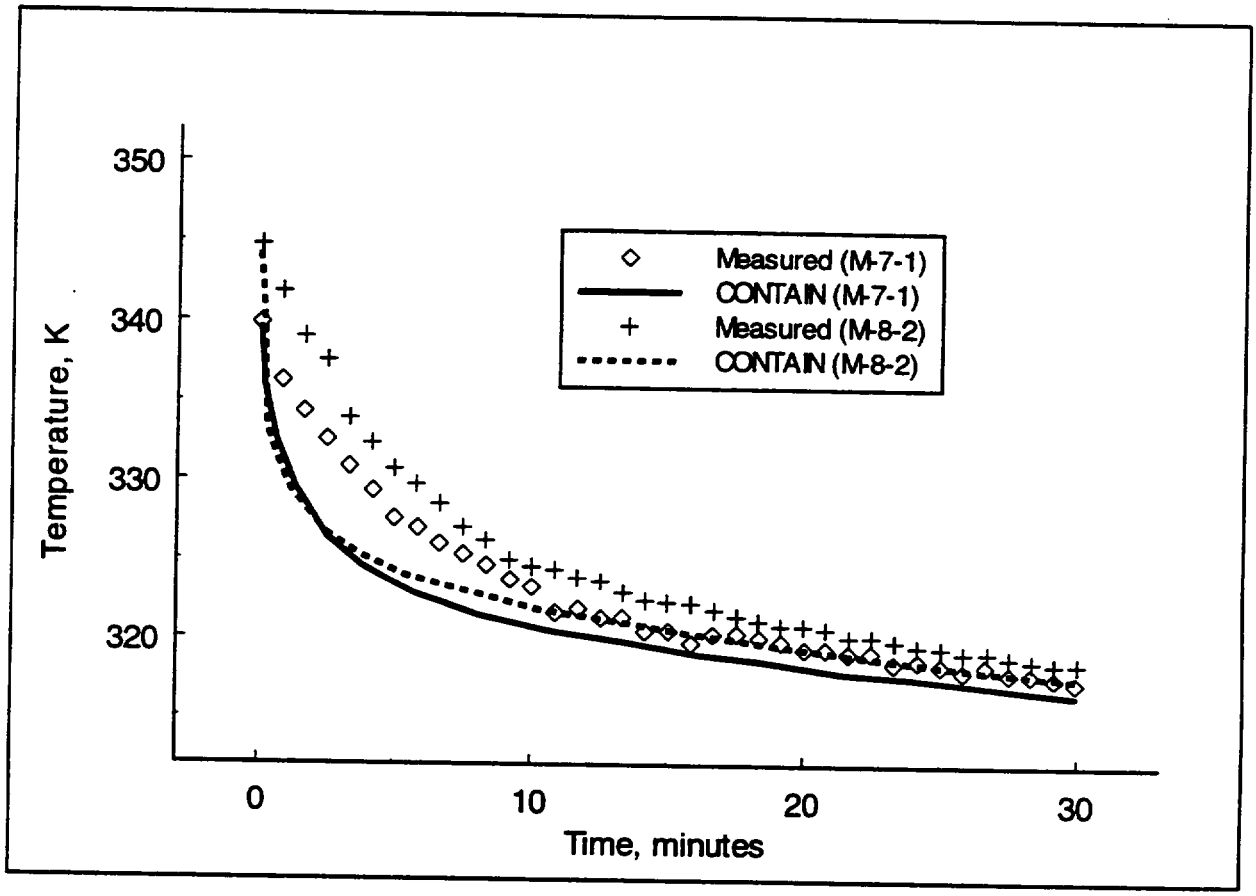

Figure 3.77 Comparison of measured and calculated gas temperatures in the dome of the NUPEC facility for tests M-7-1 and M-8-2 (with sprays).

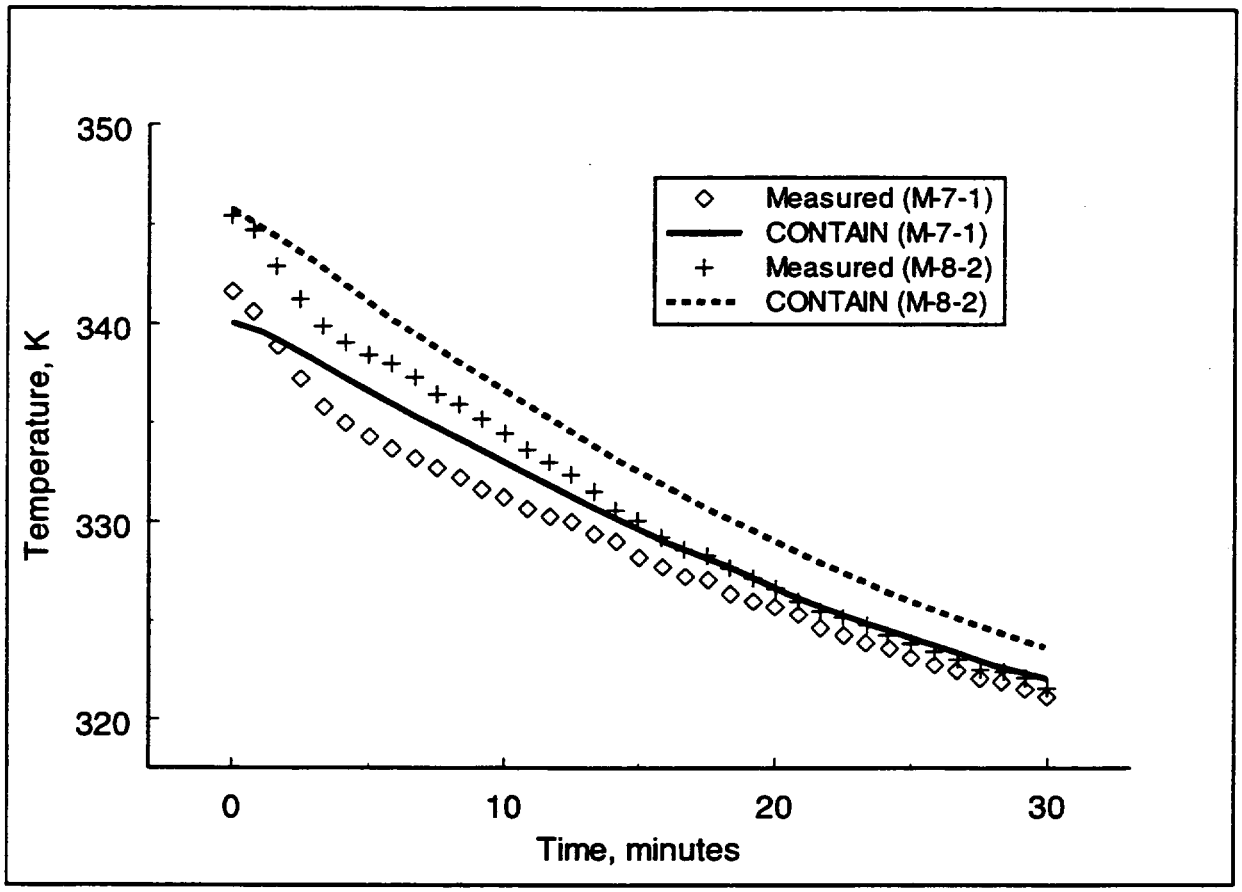

Figure 3.78 Comparison of measured and calculated dome wall temperatures for NUPEC test M-7-1 and M-8-2.

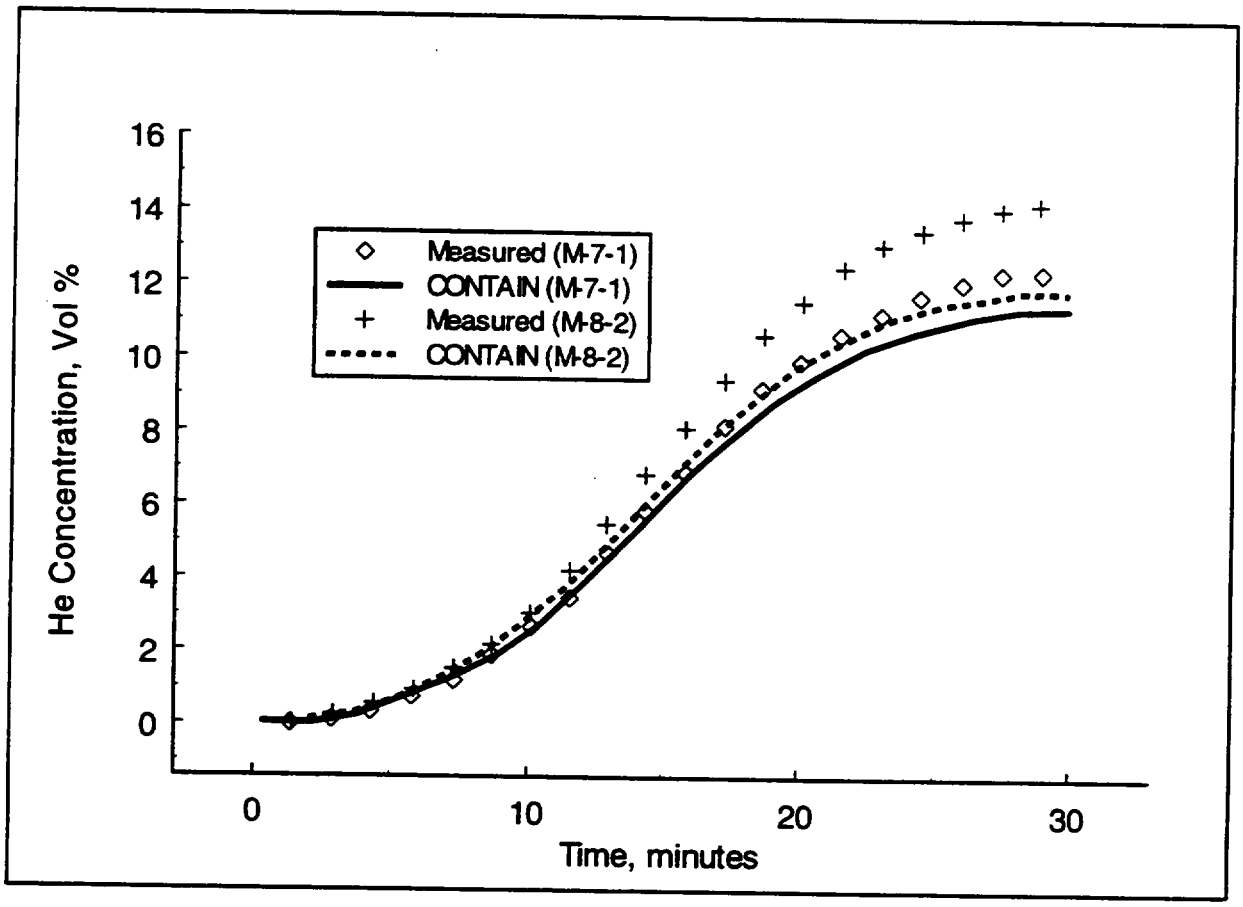

Figure 3.79 Comparison of measured and calculated helium concentrations in the dome for NUPEC tests M-7-1 and M-8-2 (with sprays).

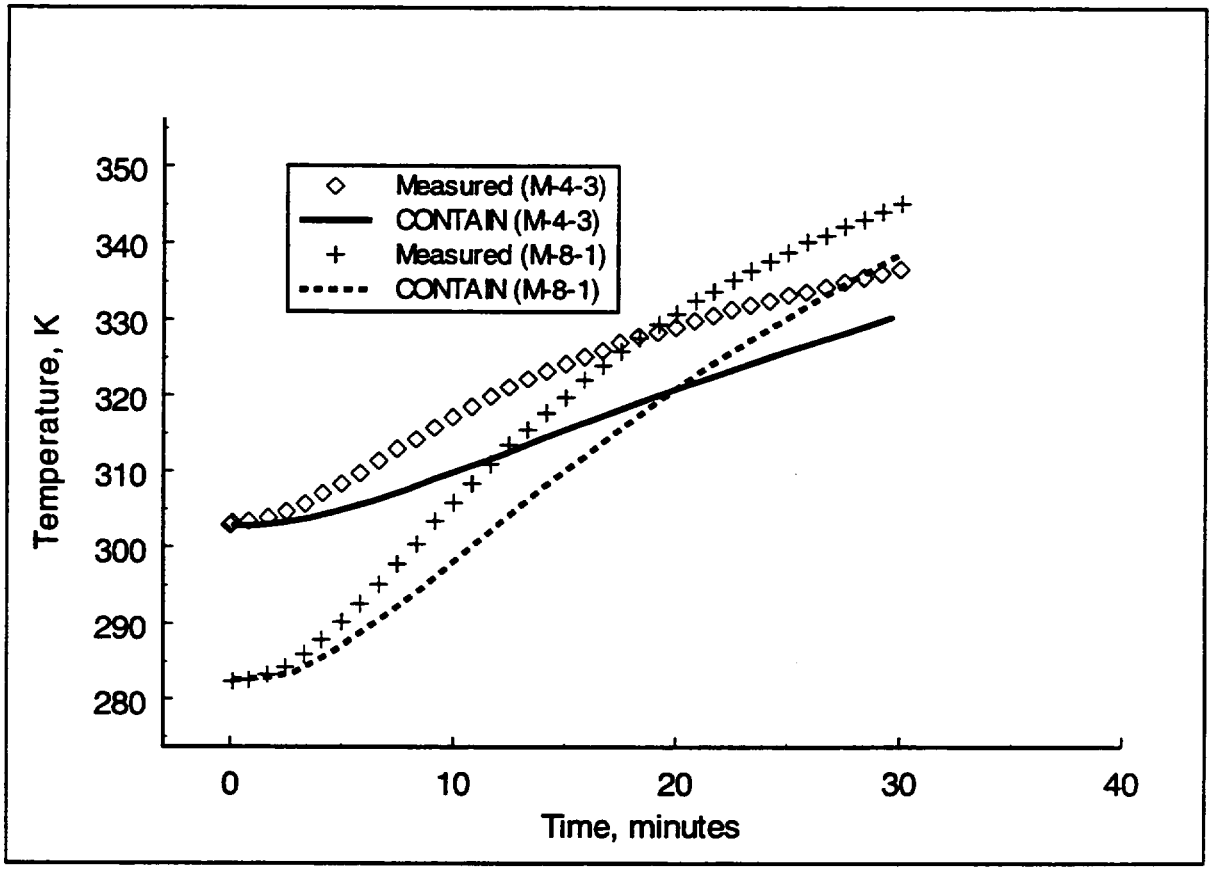

Figure 3.80 Comparison of measured and calculated dome wall temperature for NUPEC tests M-4-3 and M-8-1 (no sprays).

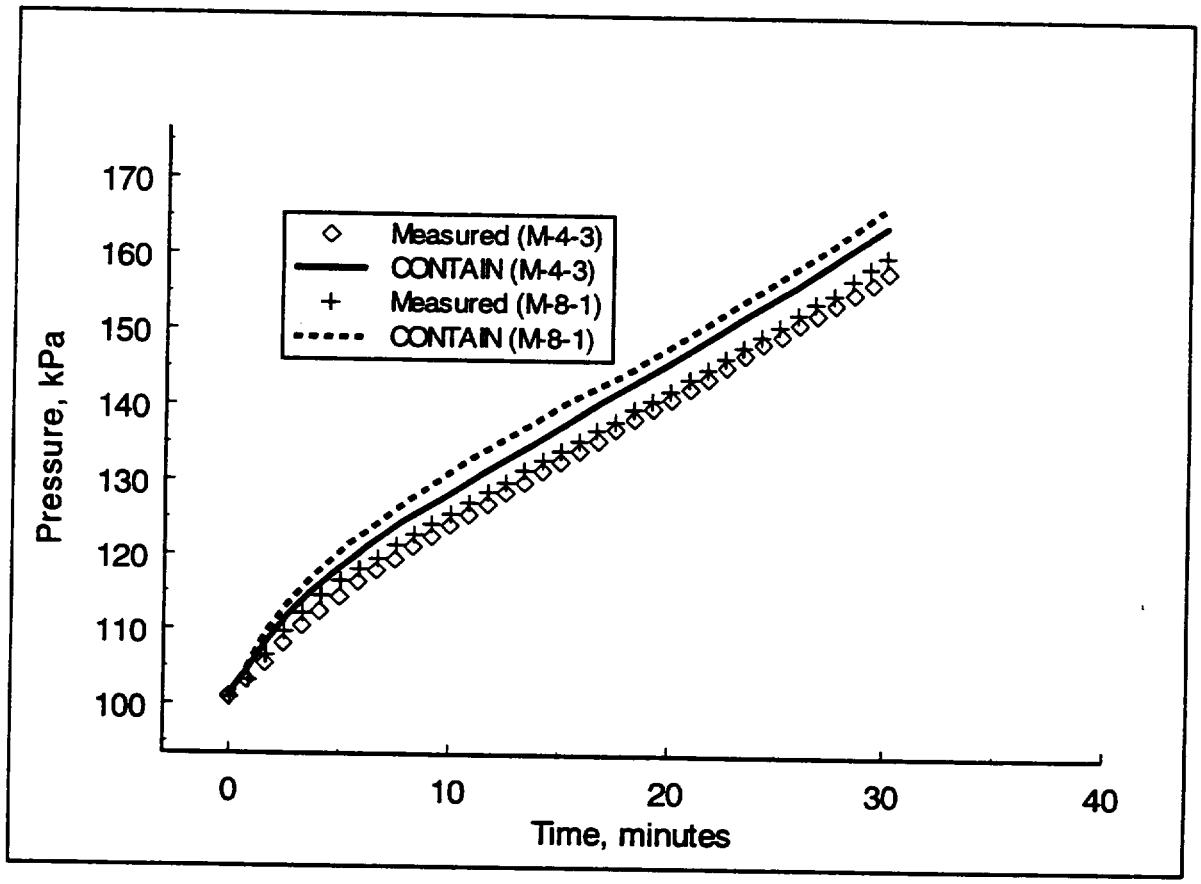

Figure 3.81 Comparison of measured and calculated containment pressure for NUPEC tests M-4-3 and M-8-1 (no sprays).

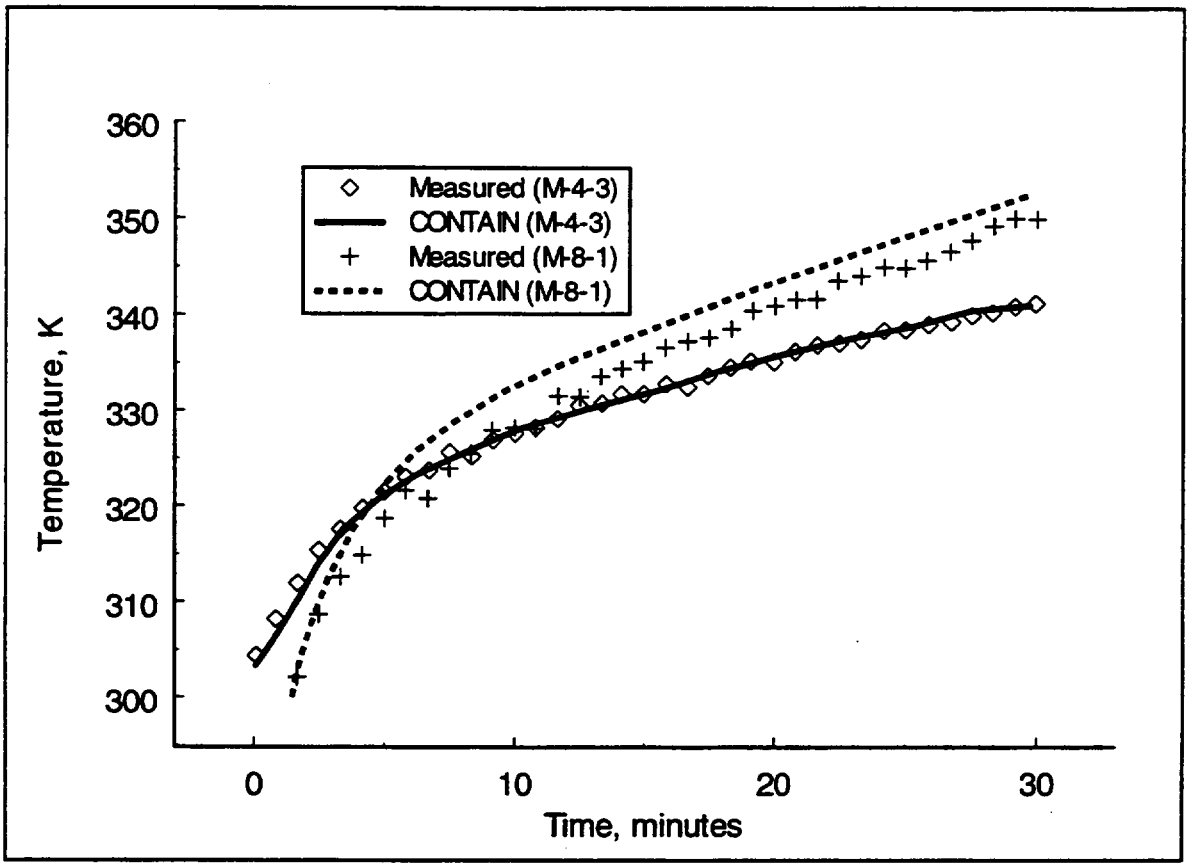

Figure 3.82 Comparison of measured and calculated dome gas temperature for NUPEC tests M-4-3 and M-8-1 (no sprays).

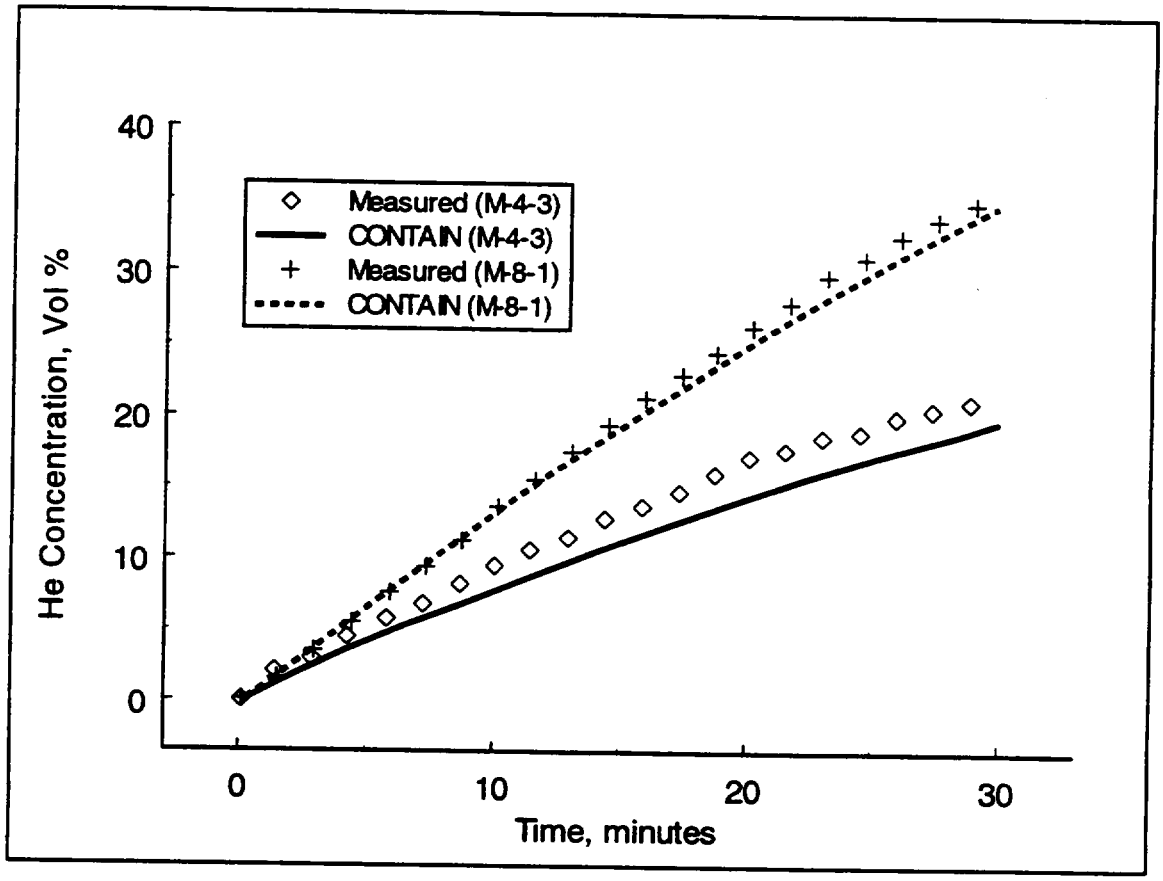

Figure 3.83 Comparison of measured and calculated helium concentrations in the dome of the NUPEC facility for tests M-4-3 and M-8-1(no sprays).

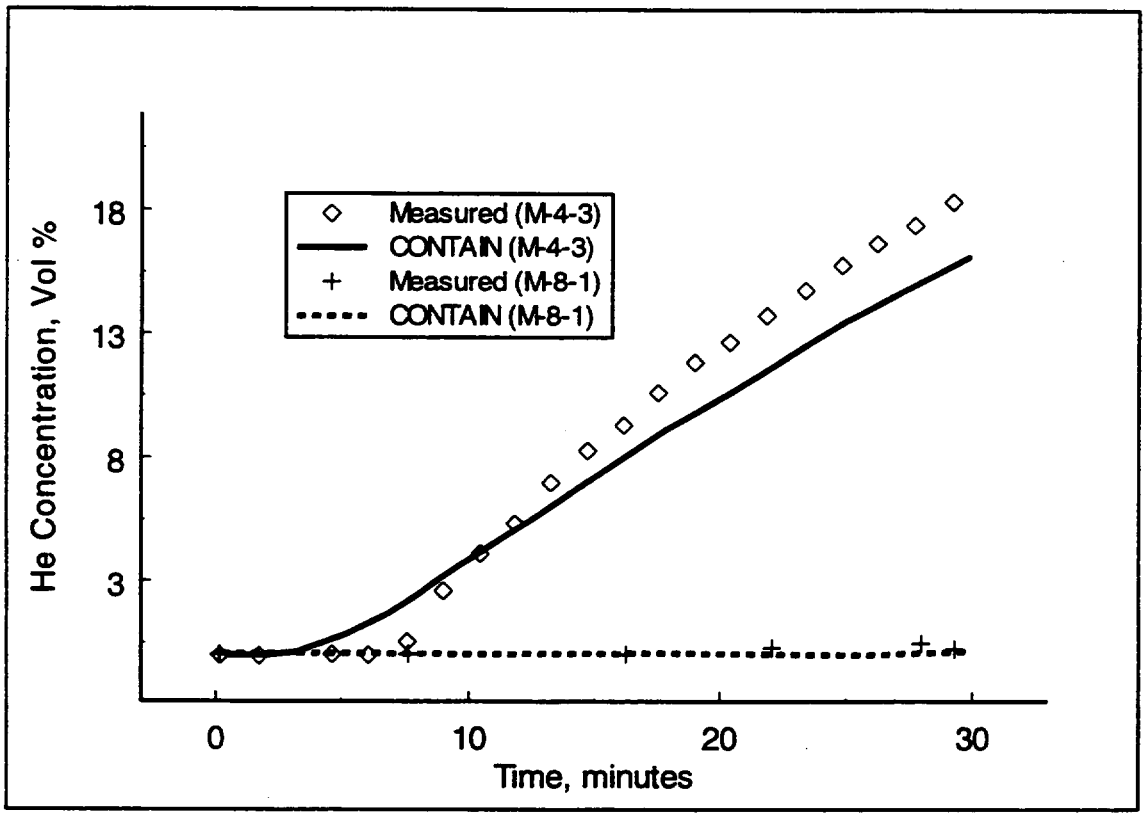

Figure 3.84 Comparison of measured and calculated helium concentrations in the lower general compartment of the NUPEC facility for tests M-4-3 and M-8-1 (no sprays).